UNIVERSITY OF CYPRUS

FACULTY OF ENGINEERING
DEPRATMENT OF MECHANICAL AND MANUFACTURING ENGINEERING

« DESIGN, MOTION PLANNING AND CONTROL OF A MODULAR RECONFIGURABLE BUILDING STRUCTURE »

M.Sc. Dissertation

Konstantinos Petrou

NICOSIA
MAY 2021

Konstantinos Petrou

Konstantinos Petrou

Dedicated to my family
© Konstantinos Petrou
Konstantinos Petrou

Konstantinos Petrou

« Design, Motion Planning and Control of a Modular Reconfigurable Building Structure »

by

Konstantinos Petrou

Konstantinos Petrou

Thesis supervisor:

Dr. Eftychios Christoforou, Assistant Professor

Department of Mechanical and Manufacturing Engineering, University of Cyprus

Examination committee:

Dr. Eftychios Christoforou, Assistant Professor

Department of Mechanical and Manufacturing Engineering, University of Cyprus

Dr. Marios C. Phocas, Professor

Department of Architecture, University of Cyprus

Dr. Loucas Louca, Associate Professor

Department of Mechanical and Manufacturing Engineering, University of Cyprus

May 2021

Konstantinos Petrou

Special Thanks

It is a genuine pleasure to express my deep gratitude to my thesis supervisor, Dr. Eftychios Christoforou, Assistant Professor at the Department of Mechanical and Manufacturing Engineering of the University of Cyprus. His prompt inspirations, timely advice and constant encouragement have been of substantial importance for the development of this thesis. His guidance, ideas and feedback have been invaluable.

I am also very grateful to Dr. Marios C. Phocas, Professor at the department of Architecture, University of Cyprus, for the valuable advices give to me for successful development of the thesis. I would also like to thank Constantina Theokli, M.Sc. student at the Department of Architecture, University of Cyprus, for the fruitful cooperation in the last year.

Finally, I would like to thank my family and friends for providing me with constant support and continuous encouragement throughout my years of study.

Konstantinos Petrou

ABSTRACT

The overall aim of the project is the design and control of a reconfigurable structure, achieving symmetrical and non-symmetrical forms with minimum actuation requirements. The structure is also required to provide flexibility in regard to motion planning and energy efficiency. Most buildings are designed as fixed-shape structures. During the design process future conditions and needs are uncertain and may change throughout use and time. Technological advances that took place in recent years have enabled kinematics to be implemented and tested in functioning prototypes for reconfigurable structures, which can adjust their shape. Moreover, reconfigurability of structures establishes a framework that enables customization and optimization. Compared to traditional fixed-shape structures, reconfigurable buildings provide unique opportunities, including: optimization of occupants' comfort by adjusting ventilation and lighting conditions, reduction of aerodynamic loads on structure, optimization of space utilization to serve different functional needs, optimization of performance of a photovoltaic roof, shaking snow off the roof, and provision of unique aesthetic effects.

The research focuses on the design and control of a proposed multilink, articulated reconfigurable structure and the investigation of its morphological and kinematic behavior. Control is based on the dual 'Effective Crank–Slider' reconfiguration approach, namely a kinematics approach that practically reduces a planar system to an externally actuated 1-DOF system, through selective application of brakes installed on the system's joints. Two different actuation configurations are proposed related to a horizontal and a vertical motion of a linear actuator, respectively. The structural body of the system consists of aluminum bars, connected via rotational joints and one slider associated with a linear actuator.

Initially, concepts and typologies of deployable and lightweight structures are discussed in comparison with the case of non-reconfigurable structures. Kinematics analysis focuses on the articulated system's degrees-of-freedom to define the actuation requirements. The study also includes the analysis of the singular configurations of the mechanisms which impose constraints on motion planning and control. The analysis of the system starts from the selection of appropriate forms for the structure, the analysis

Konstantinos Petrou

of the construction design and proceeds to numerical studies. Main parameters that influence the design refer to the ground supports of each linkage, the members and their joint connections, as well as the actuation components that are integrated on the system. In motion planning the alternative reconfiguration sequences are generated and their feasibility is examined, also considering spatial constraints and singularities. Each sequence involves the selective application of joint brakes and a corresponding motion of the slider block via the linear actuator. Subsequently, the construction design of the proposed structure is presented and simulation studies provide the required brake torques and actuator effort. The methodology allows selecting an optimal sequence on the basis of different criteria (brake torques, required actuated joints motion, etc.).

An alternative actuation method is proposed based on specially-designed aerodynamic profiles installed on the proposed structure to exploit wind energy while realizing a reconfiguration. A system is designed that adjusts the orientation of the profiles according to the required control action. The feasibility of this concept is briefly examined by considering the wind conditions in different geographical locations.

The selection of an appropriate building shape can be on the basis of external conditions. The solar gain and lighting condition inside the building are factors that may drive reconfigurations. The analysis of the solar gain and lighting condition in relation to the motion of the sun will be investigated using software simulations in relation to the proposed reconfigurable structure and its reconfiguration capabilities.

Konstantinos Petrou

ΠΕΡΙΛΗΨΗ

Ο στόχος της μελέτης αυτής είναι η ανάπτυξη και ο έλεγχος μιας αναδιαμορφώσιμης κατασκευής, επιτυγχάνοντας συμμετρικές και μη συμμετρικές μορφές με ελάχιστες απαιτήσεις ενεργοποίησης. Η δομή απαιτείται επίσης να παρέχει ευελιξία όσον αφορά τον προγραμματισμό κίνησης και την ενεργειακή απόδοση. Τα περισσότερα κτίρια έχουν σχεδιαστεί ως δομές σταθερού σχήματος. Κατά τη διάρκεια της διαδικασίας σχεδιασμού, οι μελλοντικές συνθήκες και οι ανάγκες είναι αβέβαιες και ενδέχεται να αλλάξουν κατά τη διάρκεια της χρήσης και του χρόνου. Οι τεχνολογικές εξελίξεις που σημειώθηκαν τα τελευταία χρόνια επέτρεψαν την εφαρμογή και δοκιμή της κινηματικής σε λειτουργικά πρωτότυπα για αναδιαμορφώσιμες δομές, οι οποίες μπορούν να προσαρμόσουν το σχήμα τους. Η αναδιαμόρφωση των δομών δημιουργεί ένα πλαίσιο που επιτρέπει την προσαρμογή και βελτιστοποίηση. Σε σύγκριση με τις παραδοσιακές κατασκευές σταθερού σχήματος, τα αναδιαμορφώσιμα κτίρια παρέχουν μοναδικές ευκαιρίες, όπως: βελτιστοποίηση της άνεσης των χρηστών προσαρμόζοντας τις συνθήκες αερισμού και φωτισμού, μείωση των αεροδυναμικών φορτίων της δομής, βελτιστοποίηση της χρήσης χώρου για την εξυπηρέτηση διαφορετικών λειτουργικών αναγκών, βελτιστοποίηση της απόδοσης σε μία φωτοβολταϊκή οροφή, απομάκρυνση του χιονιού από την οροφή και παροχή μοναδικών αισθητικών αποτελεσμάτων.

Η έρευνα επικεντρώνεται στο σχεδιασμό και τον έλεγχο μίας προτεινόμενης αναδιαμορφώσιμης δομής πολλαπλών ράβδων με αρθρωτές συνδέσεις και τη διερεύνηση της μορφολογικής και κινηματικής της συμπεριφοράς. Ο έλεγχος βασίζεται σε μία κινηματική προσέγγιση που ουσιαστικά μειώνει ένα επίπεδο αρθρωτό σύστημα σε ένα σύστημα ενός βαθμού ελευθερίας όπου ενεργοποιείται εξωτερικά, μέσω εφαρμογής φρένων εγκατεστημένων στις αρθρώσεις του συστήματος. Προτείνονται δύο διαφορετικές διαμορφώσεις ενεργοποίησης που σχετίζονται με μια οριζόντια και κάθετη κίνηση γραμμικού ενεργοποιητή, αντίστοιχα. Το δομικό σώμα του συστήματος αποτελείται από ράβδους αλουμινίου, που συνδέονται μέσω περιστροφικών αρθρώσεων και ένα σύστημα ελέγχου που συνδέεται με έναν γραμμικό ενεργοποιητή.

Konstantinos Petrou

Αρχικά, οι έννοιες και οι τυπολογίες των διαμορφώσημων και ελαφριών δομών συζητούνται σε σύγκριση με τις μη αναδιαμορφώσιμες δομές. Η ανάλυση της κινηματικής επικεντρώνεται στους βαθμούς ελευθερίας του αρθρωτού συστήματος για τον καθορισμό των απαιτήσεων ενεργοποίησης. Η μελέτη περιλαμβάνει επίσης την ανάλυση των ιδιόμορφων θέσεων των μηχανισμών που επιβάλλουν περιορισμούς στον σχεδιασμό και τον έλεγχο της κίνησης. Η ανάλυση του συστήματος ξεκινά από την επιλογή των κατάλληλων μορφών της δομής, την ανάλυση του κατασκευαστικού σχεδιασμού και στη συνέχεια σε αριθμητικές μελέτες. Οι κύριες παράμετροι που επηρεάζουν το σχεδιασμό αναφέρονται στα γειωμένα στηρίγματα κάθε συνδέσμου, τις ράβδους και τις αρθρώσεις τους, καθώς και τα στοιχεία ενεργοποίησης που είναι ενσωματωμένα στο σύστημα. Κατά τον προγραμματισμό κίνησης δημιουργούνται όλοι οι πιθανοί συνδυασμοί των ακολουθιών επαναδιαμόρφωσης και εξετάζεται η σκοπιμότητά τους, λαμβάνοντας επίσης υπόψη τους χωρικούς περιορισμούς και άλλες ιδιαιτερότητες. Κάθε ακολουθία περιλαμβάνει την επιλεκτική εφαρμογή των φρένων στις άρθρωσεις και μια αντίστοιχη κίνηση του γραμμικού ενεργοποιητή. Στη συνέχεια, παρουσιάζεται ο κατασκευαστικός σχεδιασμός της προτεινόμενης δομής και οι μελέτες προσομοίωσης που παρέχουν τις απαιτούμενες ροπές, καθώς επίσης και τις μετακινήσεις του ενεργοποιητή. Η μεθοδολογία επιτρέπει την επιλογή της βέλτιστης ακολουθίας με βάση διαφορετικά κριτήρια (ροπές, απαιτούμενη κίνηση ενεργοποιημένων φρένων κ.λ.π.).

Στη συνέχεια, προτείνεται μια εναλλακτική μέθοδος ενεργοποίησης που βασίζεται σε ειδικά σχεδιασμένα αεροδυναμικά προφίλ εγκατεστημένα στην προτεινόμενη δομή για την εκμετάλλευση της αιολικής ενέργειας, καθώς πραγματοποιεί μια αναδιάρθρωση. Έχει σχεδιαστεί ένα σύστημα που προσαρμόζει τον προσανατολισμό των προφίλ σύμφωνα με την απαιτούμενη ενέργεια ελέγχου. Η σκοπιμότητα αυτής της ιδέας εξετάζεται λαμβάνοντας υπόψη τις συνθήκες ανέμου σε διαφορετικές γεωγραφικές τοποθεσίες.

Η επιλογή ενός κατάλληλου σχήματος κτιρίου μπορεί να γίνει βάσει εξωτερικών συνθηκών. Το ηλιακό κέρδος και η κατάσταση φωτισμού στο κτίριο είναι παράγοντες που μπορεί να οδηγήσουν σε αναδιαμόρφωση. Η ανάλυση της κατάστασης ηλιακού κέρδους και φωτισμού σε σχέση με την κίνηση του ήλιου διερευνάται χρησιμοποιώντας προσομοιώσεις λογισμικού σε σχέση με την προτεινόμενη αναδιαμορφώσιμη δομή και τις δυνατότητες που παρέχει.

Konstantinos Petrou

Contents

Konstantinos Petrou

FIGURES

Konstantinos Petrou

Konstantinos Petrou

TABLES

Konstantinos Petrou

Konstantinos Petrou

GRAPHS

Konstantinos Petrou

APPENDIX

Konstantinos Petrou

Chapter 1

1 INTRODUCTION

1.1 Reconfigurable and Fixed Buildings

Most architectural theories and practices aim at designing unique, fixed and ideal buildings solutions. The general goal is that the final shape of a building can be achieved by analyzing present situations, and meet clients' stated needs, demands and desires. Likewise, this approach is based on descriptions and assumptions, which consider future situations as invariable (Rosenberg 2010).

During the design process future situations are uncertain, since not only buildings face unprecedented and unexpected situations, but also these situations evolve and change through use and time. Suggest an indeterminate architecture, where in the building remains in an open-ended process of definition and redefinition of the shape according to clients' needs. So, that defines two complementary design considerations: "Designing the Range" and "Enabling the Choice". While Designing the Range refers to transformable buildings able to offer a variety of states, Enabling the Choice refers to the users' selection of states, within the range and according to emergent situations. This intriguing architecture was envisioned from the Archigram movement in the sixties, and aims at radicalizing the inventive and technical kinetic architecture proposed by William Zuk and Roger H. Clark in the seventies (Rosenberg 2010; Αθηνή 2017; Zakou 2016).

Figure 1.1: A structure case example shown in two possible target positions following deployment and reconfiguration (Dimitriou, Phocas & Christoforou 2020)

Konstantinos Petrou

More and more architects, engineers and designers endorse to the notion of flexibility and transformability, the belief that nothing stays fixed through time, that everything evolves and changes. Unexpected events can change the future demands and functions of a building. The sharp technological progress in mechanics, electronics and robotics has been the main cause of the increasing growth of practical applications of adaptive structures over the past years. The integration of all these technologies has led to changes in the design approach, while it pushed the limits of structural feasibility further. Reconfigurable architecture may be the answer to these concerns, as it's an open-ended process that offers the possibility of designing a range of situations and enabling a variety of choices (Anastasiadou 2018).

The significance of buildings with variable geometry that adapt in response to external loading, functional and environmental conditions, has been widely acknowledged. At the same time, technological advances that took place in recent years have enabled kinematics to be implemented and tested in functioning prototypes for reconfigurable structures, which can adjust their shape. Reconfigurability of structures establishes a framework that enables customization and optimization. In general, reconfigurable structures combine two elements: the structural system that may assume different geometrical configurations and the control system that implements the specified transformations an example is shown in Fig. 1.2 (Matheou, Phocas & Christoforou 2015; Dimitriou, Phocas & Christoforou 2020).

Figure 1.2: The concept of a regonfigurable building, as a variable geometry structure (Matheou et al. 2013)

Konstantinos Petrou

One problem in reconfigurable structures arises in case of natural loads including the snow, temperature changes and wind, which can lead to extensive deformations. Nevertheless, these structures have important characteristics that may contribute towards a sustainable built up environment. Compared to traditional fixed-shape structures, reconfigurable buildings provide opportunities, including: optimization of occupants' comfort by adjusting ventilation and lighting conditions, reduction of aerodynamic loads on the structure, optimization of space utilization to serve different functional needs, optimization of performance of a photovoltaic roof, shaking snow off the roof, provision of unique aesthetic effects (Zakou 2016; Dimitriou, Phocas & Christoforou 2020).

Problems such as natural load of snow can be treated by changing the shape of the building. This is achieved with the drive mechanisms that they are integrated into the joints of the structures to allow movement. This will modify the shape of structure so that no snow loads are created and the structure is burdened. In a similar way can be treated the temperature and wind problems. The structure may take different shapes depending on the weather positions, so that, there is a constant temperature and proper ventilation in the building and they do not cause deformations in the structural elements.

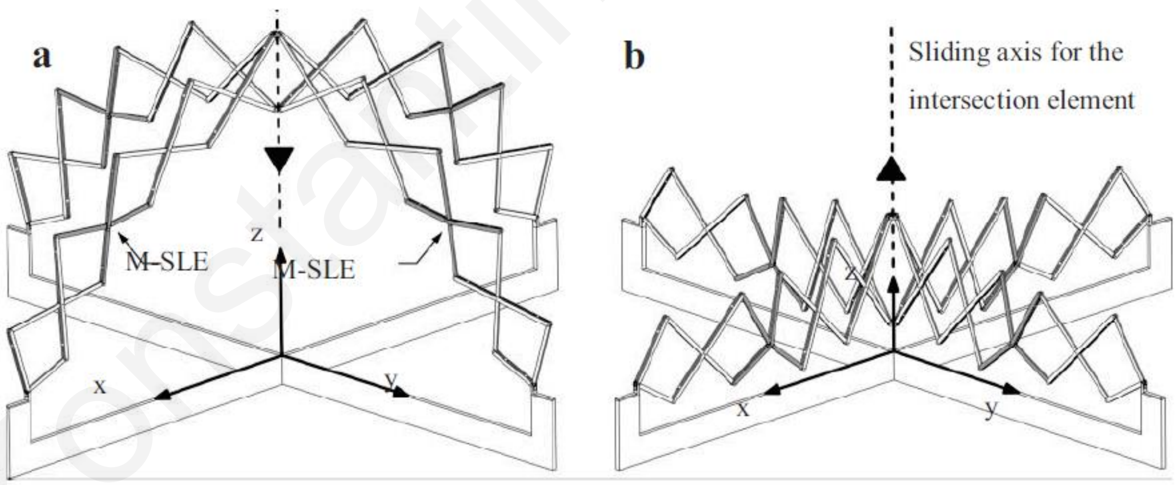

Figure 1.3: Reconfigurable Structures (Korkmaz & Akgun 2011)

1.2 Adaptive Structures

Adaptive structures respond to an external stimuli by adjusting their shape accordingly. These building structures have a potential of superior performance and flexibility compared to traditional fixed–shape ones. In fact, the shape–controlled buildings idea is seen as a promising new application field for robotics. The reconfigurable building

Konstantinos Petrou

structures have the ability to perform shape adjustments. So, superior performance is expected from buildings whose shape can be adjusted in order to accommodate changing needs of human activity, as well as in response to varying environmental or structural loading conditions (Muller, Christoforou & Phocas 2012).

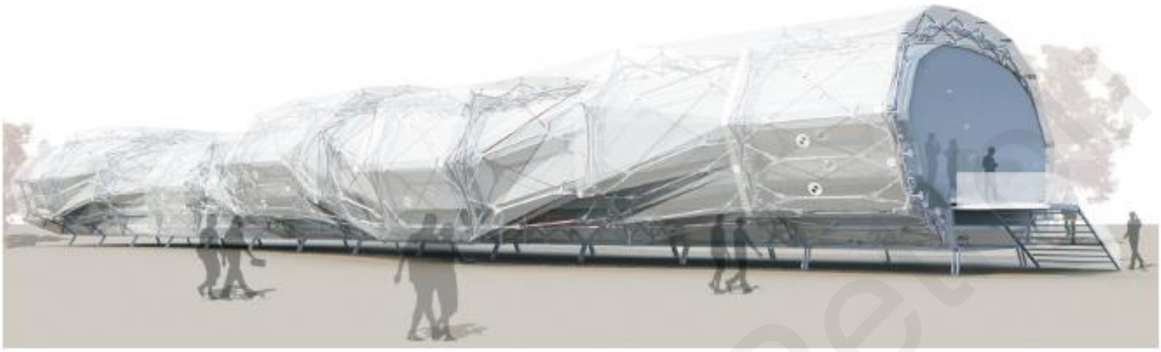

Figure 1.4 An adaptive building, variable geometry structure (Muller, Christoforou & Phocas 2012)

Building shape adjustments may be driven by the sun motion for the maximization of sun protection, optimization of lighting conditions and heating performance, or improve the energy efficiency of a photovoltaic roof (maximization of production energy from sun). Among the environmental factors that could be accounted for is also the wind condition. By varying the form of roof the pressure distribution around the building can be adjusted resulting to improved natural ventilation of spaces or relaxing the aerodynamic loading of the structure.

The adaptive structures may play a role in space applications. Also, such building structures may cover humanitarian, military and commercial needs: temporary or emergency shelters, seasonal storage spaces, helicopter and aircraft hangars, temporary exhibition/exposition venues, etc (Matheou et al. 2013).

1.3 Structure Usage

Earthquakes, pandemics, conflicts, and environmental disasters have challenged architects, planners, designers, and engineers. The goal is to find ways of creating temporary structures adapted to the type of disaster (refugee migration, earthquakes, pandemics, etc.) quickly, easily, efficiently, suiting both the circumstances and the location in which they will be implemented. The crisis of epidemics is an increasing risk.

Konstantinos Petrou

The proposed structure has been designed for emergency situations, like the COVID - 19 pandemic. The main usage of the structure would be to create a space for doctors and community during the performance of Covid tests, vaccinations and to inform the citizens about related measures taken during the pandemic. The size of the structure is appropriate to follow all sanitary protocols, and encourage people to keep social distancing measures. A clear threshold of sanitary protocols for both people and goods will additionally reinforce the inside of the building as a clean zone. As COVID-19 can be transmitted through airborne particles, proper quantities of fresh air in the interior space must be ensured for the users. Thus, the operable openings of the structure can supplement air dilution.

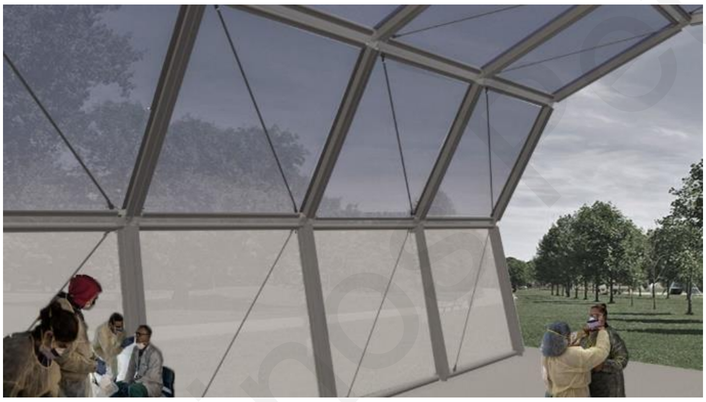

Figure 1.5: Proposed use of the structure for medical purposes

1.4 Design for X

While designing a reconfigurable system there are many issues to be considered. In summarizing them the design for X concept becomes relevant. Redefining design efforts to focus stakeholder requirements, and strive for innovative designs through concurrent efforts, it is inevitable that some overlaps and gaps in total design quality will occur. Without strict design standards there is a need for thought for the solutions chosen and test them through a set of commonsense filters. Design for X can help to provide these logical filters.

Design for X is a family of approaches generally denoted as Design for X (DFX). The letter "X" in DFX is made up of life cycle processes. DFX techniques are part of the Design for Six Sigma (DFSS) road map (see Fig. 1.6) and are ideal approaches to improve life cycle cost, quality, design flexibility, efficiency, and productivity using concurrent design concepts (Maskell, 1991). Benefits usually include improved decision making with competitiveness measures and enhanced operational efficiency (El-Haik & Roy 2005).

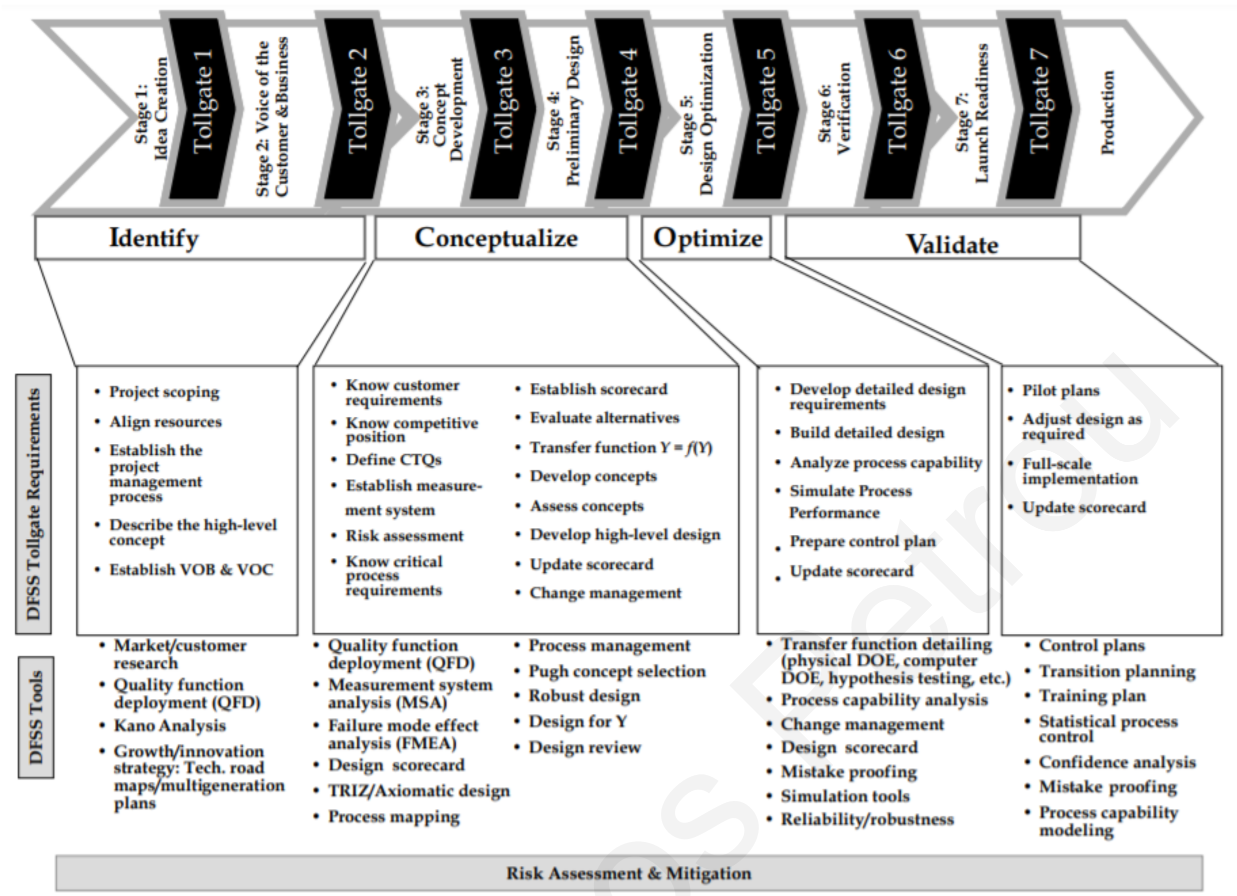

Figure 1.6: Design for Six Sigma road map (El-Haik & Roy 2005)

In many fields X may represent several traits or features including: manufacturability, power, variability, cost, yield, or reliability. This gives rise to the terms design for manufacturability, design for inspection, design for variability and design for cost. Under the design for X, a wide set of specific design guidelines are summarized. Each design guideline addresses a given issue that is caused by, or affects the traits of, a product. The design guidelines usually propose an approach and corresponding methods that may help to generate and apply technical knowledge to control and improve of a product (Wikipedia 2009).

User requirements eventually translate into corresponding design requirements. Informed design will constitute solutions more usable and effective. Towards that direction, the “design for X” (design for excellence) concept becomes relevant and it allows here to effectively summarize key requirements the X variable is associated to it relates to different attributes of the system (e.g., safety) (Pahl and Beitz, 1996), (Bralla, 1996). The identified design parameters are collected in Table 1.1. This design framework spans the whole life-cycle of relevant to the present design problem buildings.

Konstantinos Petrou

Table 1.1: Design for X parameters

Life-Cycle Phase	X Design Parameter		
Development	• Simplicity • Safety • Reliability • Quality	• Modularity • Reprogrammability • Interchangeability • Expandability	• Upgradability • Integrability • Standards • Regulations • Price
Production/ Manufacturing	• Manufacturability • Assembly	• Testing • Integration	• Cost • Materials
Use	• Usability • Human Factors • Ergonomics • Error-Resistance • Aesthetics • User-Friendliness • Customizability	• Multi-Use • Maneuverability • Stability • Energy-Efficiency • Cost Effectiveness	• Maintainability • Serviceability • Physical Safety • Logistics • Cyber-Security • User Privacy • Ethics
Disposal	• Recyclability	• Reusability	• Sustainability

1.5 Structure of the thesis

The second Chapter, focuses on a proposed analysis of the mechanism and its degrees of freedom (DOF), namely a dual crank-slider mechanism for horizontal and vertical motion. Moreover, it refers to the effective links and brakes operation that simplify the system to a 1-DOF (one actuator is required for the movement). Also, it is presented a general equation for these type mechanisms to calculate the DOF, special cases of locked joints, kinematic analysis and all cases of singularities that may occur during shape change of the structure.

In Chapter 3 the focus is on the control sequences for implementing the required shape adjustments of a reconfigurable structure (symmetrical and non-symmetrical) and the investigation of its morphological and kinetic behavior. The steps required in order to adjust each joint angle of the planar system from an initial to a target position are defined. Among different feasible sequences, the ones with less required steps are selected and future investigated.

Konstantinos Petrou

As part of Chapter 4, construction design and assembly of the structures are presented, which they are based on the software Solidworks. Furthermore, it is referred to the system supports, the members and their joint connections, as well as the actuation components that enable horizontal or vertical reconfigurations.

Chapter 5 focuses on the proposed kinematic approach. The motion analysis studies use the software Solidworks (motion analysis). Also, the simulations include the brake torques analysis, based on the self-weight and the material stresses.

In Chapter 6, is proposed an actuation method based on wind forces. It refers to an aerodynamic system where it assists the horizontal structure in moving the slider sideways in a natural way. Also, results are presented for lift and drag forces based on the shape of the fins and the mechanism developed using the software Solidworks is presented.

Chapter 7, refers to a solar gain and lighting simulation analysis using the software Design Builder. The simulation analysis includes in all reconfiguration steps of the system from the initial to the target position. The case study refers to Larnaca, Cyprus and the solstices that occur annually.

Finally Chapter 8 presents the conclusions of the thesis and the proposed future work.

Konstantinos Petrou

Chapter 2

2 STRUCTURAL AND RECONFIGURATION CONCEPT

A basic structural element of a shape-controlled structure to be considered here is comprised of a dual crank slider mechanism (horizontal and vertical) of planar serially-connected links. The ground of the building provides one link to the linkage, and the remaining kinematic chain comprising of members is pivoted to the ground on either side. Using an array of such interconnected closed–chain linkages formulates the skeleton of the structure. Synchronized motion of the individual linkages will adjust the overall shape of the building accordingly. One linear actuator is associated to the motion of the slider and brakes are installed on the rotational joints.

The control system manages the operation of the motion actuator and the brakes while implementing appropriately planned sequences in order to realize the required shape adjustments. Before the proposed control approach is presented it is important to refer the degrees of freedom for the proposed structure.

2.1 Mechanisms and Degrees of Freedom

Each independent motion variable will need some type of actuator to determine its position. The multiple input (variables) will have to have their actions coordinated by a controller such as a computer but can also be mechanically programmed into the mechanism design. There is no requirement that every mechanism has only one Degree of Freedom (DOF) but that is often desirable for simplicity and simplifying actuation (Robert L. Norton 2008).

Mechanisms chains may be either open or closed:

- An open chain mechanism of more than one link will always have more than one degree of freedom, thus requiring as many actuators (motors) as it has DOF (see for example Fig 2.1a).
- A closed chain mechanism will have no open attachment points or nodes and may have one or more degrees of freedom (see for example Fig 2.1b).

Konstantinos Petrou

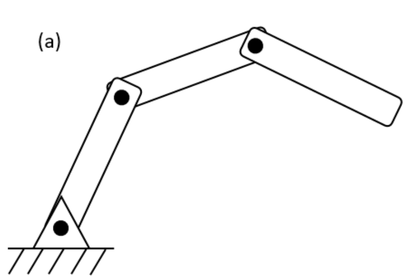

Figure 2.1: (a) Example of Open mechanism chain (3-link planar manipulator), (b) Example of Closed mechanism chain (4-bar mechanism)

To determine the overall DOF of any mechanism, we must account for the number of links and joints, and for the interactions among them. The Degrees of Freedom of any assembly of links can be predicted from the equation of Gruebler. Therefore, a system of L not assembled links in the same plane will have 3L DOF, so the two unconnected links, as shown in Fig. 2.2 have a total of six DOF: $\Delta\theta_1$, Δy_1, Δx_1, $\Delta\theta_2$, Δy_2 and Δx_2 (shown in Fig. 2.2 [a]) (Robert L. Norton 2008). When these links are connected between them by a full joint, this removes two DOF. The Δy_1 and Δy_2 are done Δy and Δx_1 and Δx_2 are done Δx ending up four with DOF as shown in the figure: Δy, Δx, $\Delta\theta_1$ and $\Delta\theta_2$ (shown in Fig. 2.2 [b]). The half joint removes only one DOF from the system, leaving the system of two links connected by a half joint with a total of five DOF: Δy, Δx_1, Δx_2, $\Delta\theta_1$ and $\Delta\theta_2$ (shown in Fig. 2.2 [c]).

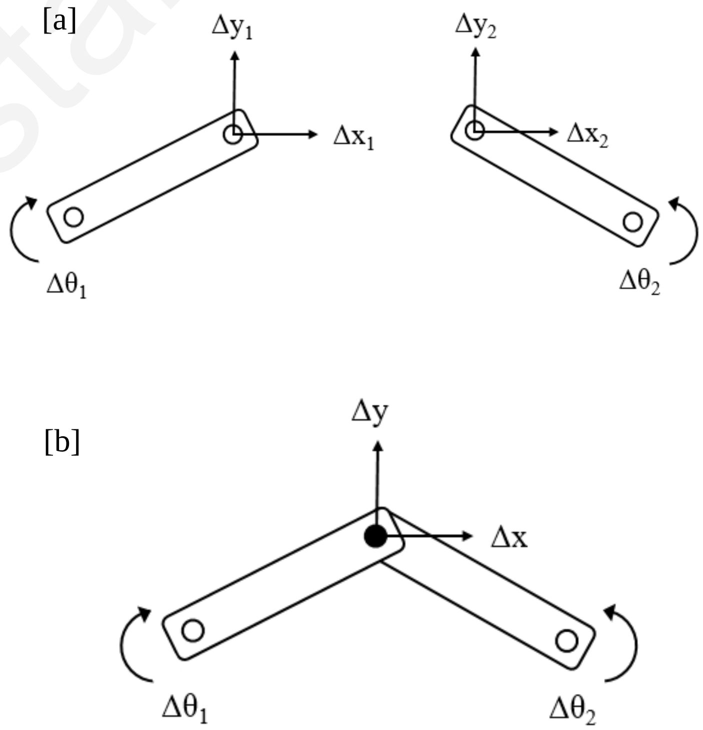

Konstantinos Petrou

[c]

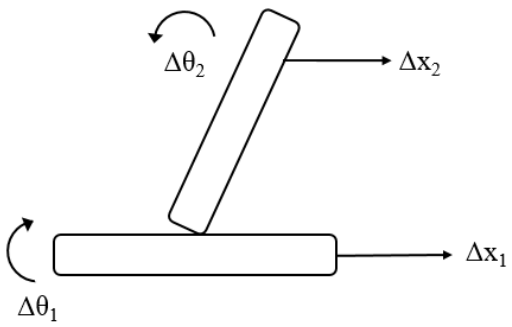

Figure 2.2: [a] Two unconnected links DOF = 6, [b] Connected by a full joint DOF = 4, [c] Connected by a roll-slide (half) joint DOF = 5

Moreover, when any link is grounded all three of its DOF will be removed. This reasoning leads to Gruebler's equation that is:

$$M = 3L-2J -3G$$

Where: M = degree of freedom or mobility

L = number of links

J = number of joints

G = number of grounded links

Note that in any real mechanism, even if more than one link of the kinematic chain is grounded, the effect will be that there is only one ground plane (Robert L. Norton 2008). Thus G is always 1, and Gruebler's equation becomes:

$$M = 3(L-1)-2J$$

The value of J in equations represents the value of all joints in the mechanism that are half joints and full joints. This way the equation Gruebler's can be adjusted as:

$$M = 3(L-1)-2J_1-J_2$$

Where: M = degree of freedom or mobility

L = number of links

J_1 = number of 1 DOF (full) joints

J_2 = number of 2 DOF (half) joints

Konstantinos Petrou

2.1.1 Mechanism and Structures

The degree of freedom of an assembly of links completely predicts its character (Robert L. Norton 2008). There are three possibilities:

- If the DOF is positive, it will be a mechanism and the links will have relative motion.
- If the DOF is exactly zero, then it will be a structure and no motion is possible.
- If the DOF is negative, then it is a preloaded structure, which again means that no motion is possible.

Example of each case are given in Fig. 7.3. In our case we deal with mechanisms.

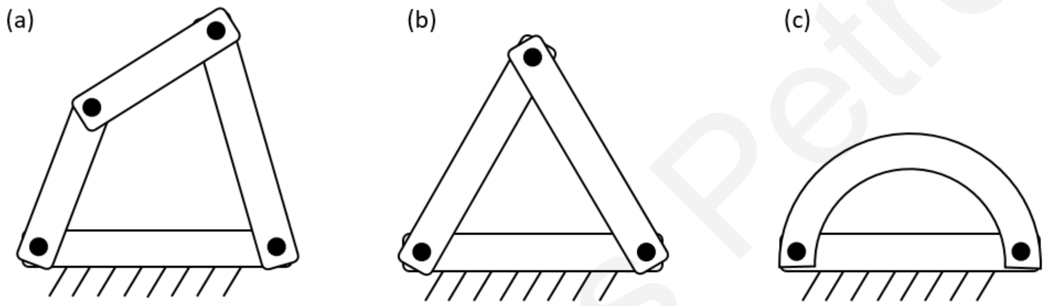

Figure 2.3: (a) Mechanism DOF = +1, (b) Structure DOF = 0,
(c) Preloaded structure DOF = -1

2.2 The basic kinematic configuration and motion analysis

The mechanism chain below is the basic system used and it comprises four links and one slider with horizontal movement. The links assembly includes joints between the links and there are two joints pivoted to the ground, one on each side, as shown in Fig. 2.4.

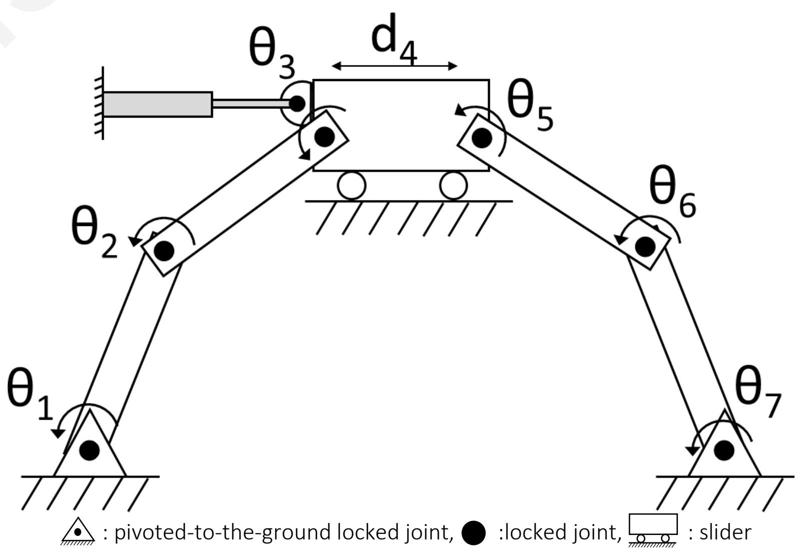

Figure 2.4: Basic Dual Crank-Slider (Horizontal) Mechanism

Konstantinos Petrou

The DOF of this mechanism is calculated from Gruebler's equation with

L = 6, J1 = 7, J2 = 0:

M = 3(L-1)-2J1-J2 = 3(5)-2(7) = 15-14 = 1 DOF

So one actuator is sufficient to control the system.

Then, a similar mechanism chain with four links is presented. It has one slider with vertical movement and the rest of the chain is assembled as in the previous one, as shown in Fig. 2.5.

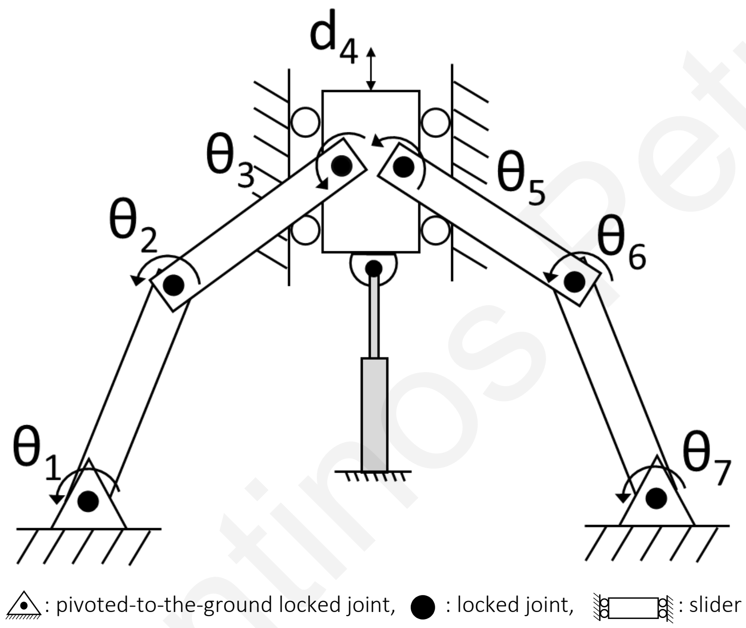

Figure 2.5: Basic Dual Crank-Slider (Vertical) Mechanism

The DOF of this mechanism is calculated from Gruebler's equation with

L = 6, J_1 = 7, J_2 = 0:

M = 3(L-1)-2J_1-J_2 = 3(5)-2(7) = 15-14 = 1 DOF

So one actuator is sufficient to control the system.

2.3 The multi-DOF system

If the mechanism chain has more than four links then, it has more than 1 DOF. Therefore more actuators are required to control the system. For example, if the mechanism chain has 3 DOF then are needed 3 actuators and control becomes more complicated. With the help of the brakes the mechanism can be reduced to a 1-DOF

Konstantinos Petrou

system. This is the basis of the approach which will be explained below through an example.

The mechanism consists of ten links, five links on each side, one slider and one actuator with horizontal movement. Each link assembly includes rotational joints between the links and there are two joints pivoted to the ground, one on each side, as shown in Fig. 2.6.

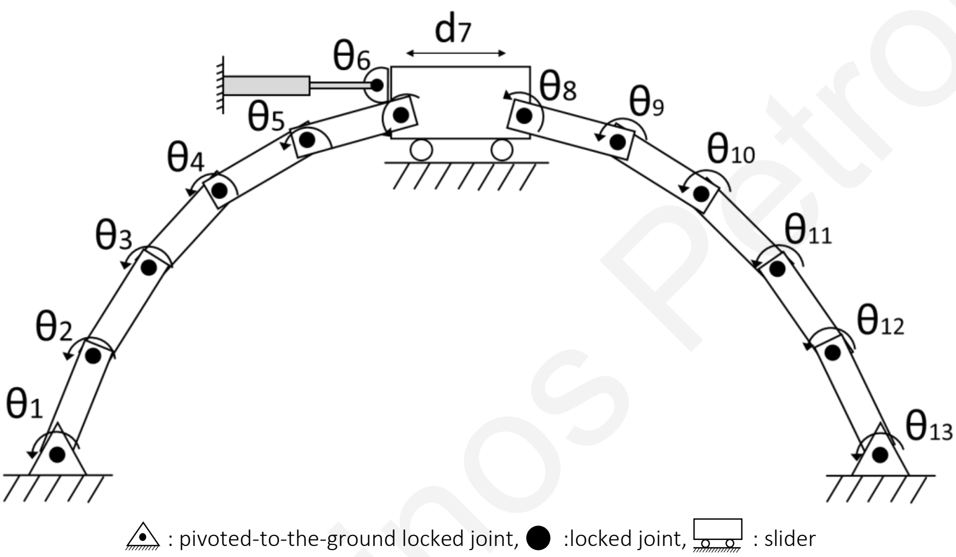

Figure 2.6: Basic Dual Crank-Slider (Horizontal) Mechanism with many links

The DOF of this mechanism is calculated from Gruebler's equation with

$L=12$, $J_1 = 13$, $J_2=0$:

$M = 3(L-1) - 2J_1 - J_2 = 3(11) - 2(13) = 33 - 26 = 7$ DOF

This mean that 7 actuators are necessary to control the system. By appropriated applying the brakes, the system can be reduced to a system analogous to the mechanism in Fig. 2.4, which has 1 DOF. This is achieved by activating six brakes, three on each side of the slider since two or more links will function as one link (“effective link”). We refer to this, as an “effective” dual crank-slider.

In the particular example there are activated brakes on the joints θ_2, θ_4, θ_5, θ_9, θ_{11} and θ_{12}. In this way, the system is modified to a 1 DOF system and one motion actuator is enough to control its position. The effective links in Fig. 2.7 show which links operate as one (effective links) with the activation of specific brakes.

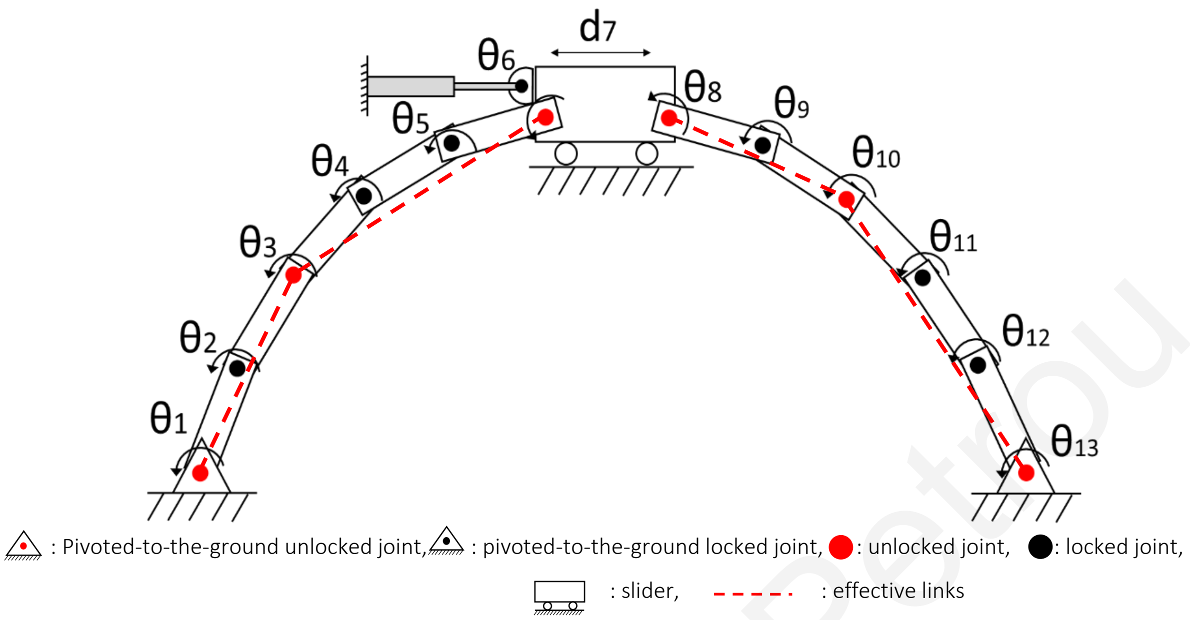

Figure 2.7: Effective Dual Crank-Slider (Horizontal) Mechanism with many links and brakes

Similarly, a mechanism chain with ten links is presented with one slider but with vertical movement which is assembled as in the previous one, as shown in Fig. 2.8.

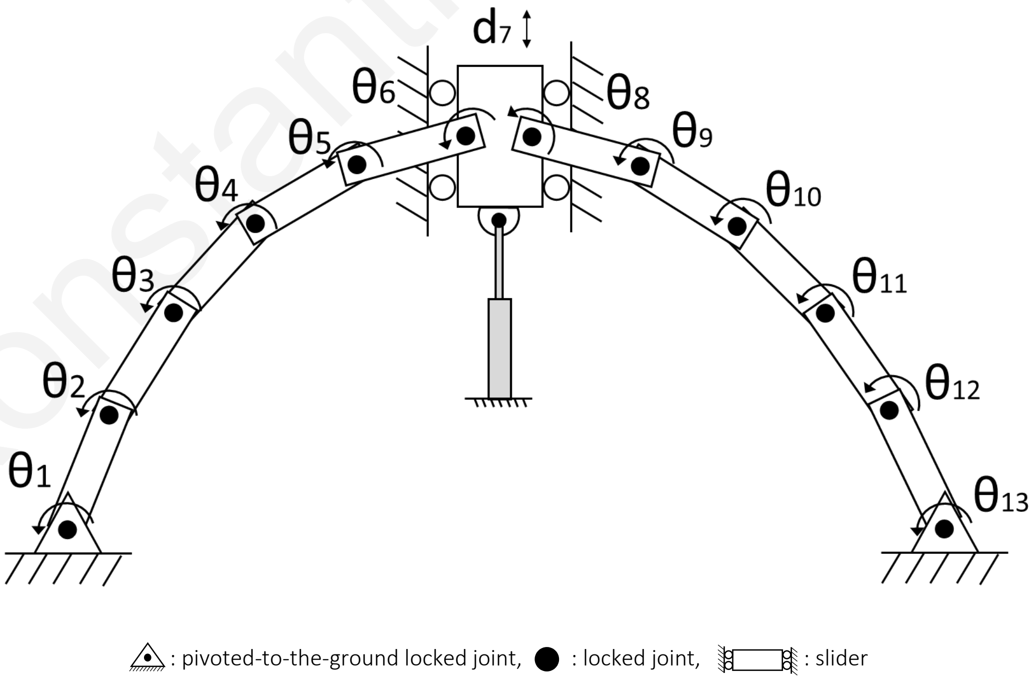

Figure 2.8: Basic Dual Crank-Slider (Vertical) Mechanism with many links

Konstantinos Petrou

The DOF of this mechanism is calculated from Gruebler's equation with
$L = 12$, $J_1 = 13$, $J_2 = 0$:

$$M = 3(L-1) - 2J_1 - J_2 = 3(11) - 2(13) = 33 - 26 = 7 \text{ DOF}$$

This mean that 7 actuators are necessary to control the system. The mechanism chain has 7 DOF. By appropriately applying the brakes, the system is reduced to a basic 1 DOF system. This is achieved by activating six brakes, three on each side since two or more links will be function as one link.

In particular there are activated brakes on the joints θ_2, θ_3, θ_5, θ_9, θ_{10} and θ_{12}. In this way, this system is modified to a 1 DOF and one actuator is enough to control it. The effective links in figure 2.9 show which links operate as one with the activation of specific brakes (effective links).

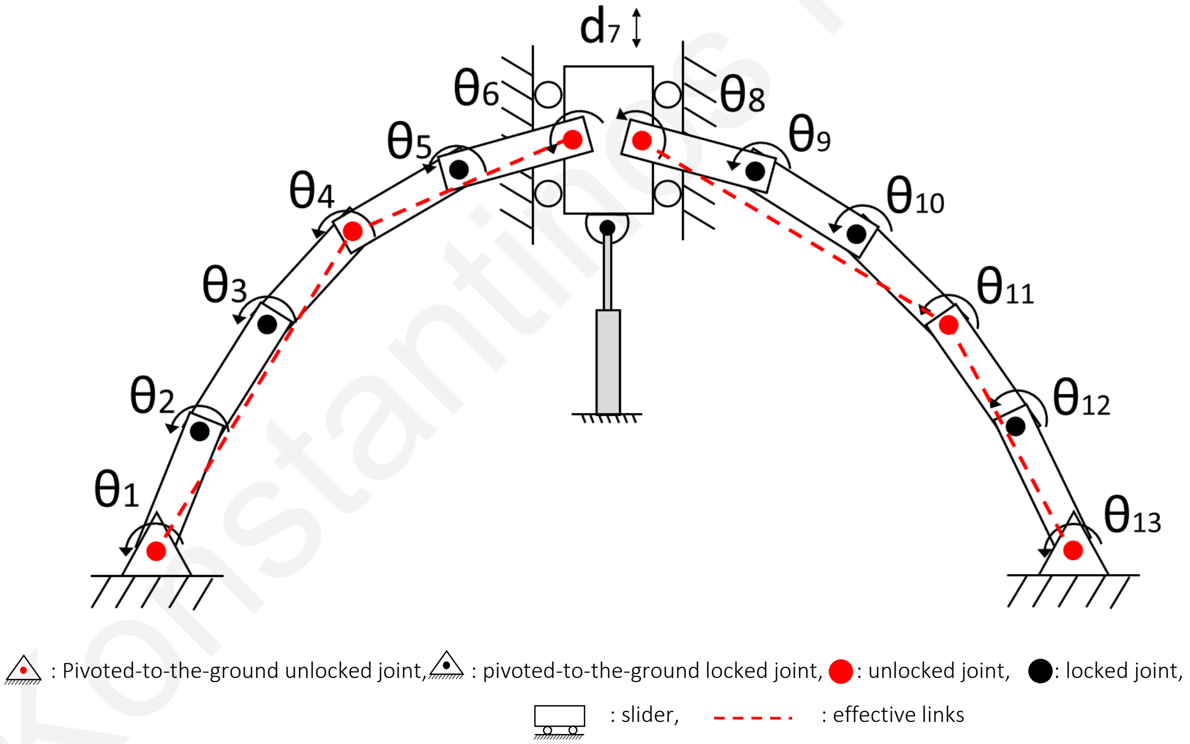

Figure 2.9: Basic Dual Crank-Slider (Vertical) Mechanism with many links and brakes

In this way, the mechanism chain can be converted to 1 DOF using the brakes and the use of many actuators can be avoided, that is an actuator is sufficient to control the system. This makes the mechanisms chain simple and reduces cost. Locking the brakes can be made differently depending on which effective crank-slider is required to define.

2.3.1 General Equation for DOF of the multi-link structure

According to the above examples and based on the equation of Gruebler's can be derived a general formula for such type of mechanism chains.
If there are n links

L = n (including ground)

Always in this type of systems the number of full joints are one more than the number of links and there are not half joints. Therefore, $J_1 = n+1$ and $J_2 = 0$
$M = 3(L-1) - 2J_1 - J_2 = 3(n-1) – 2(n+1) – 0 = 3n-3-2n-2 = n – 5$

The general equation for the DOF of this type mechanism chains is:

M = n-5 (n includes the ground and slider block)

2.4 The Control Concept

By appropriately applying different brakes in the joints an effective 1 DOF system is defined. This process must be done with a certain logic and not in a random way. Initially, all joints are locked except those of the slider. The two joints unlocks one on each side and the slider moves (right/left or top/down) until an angle is adjusted. This angle stays locked for the subsequent steps. The procedure is repeated until the structure reaches the target position.

2.4.1 Limitations on the distribution of locked joints

In the following chain mechanism (Fig. 2.10) is observed a model with many links, which has 7 DOF.

Konstantinos Petrou

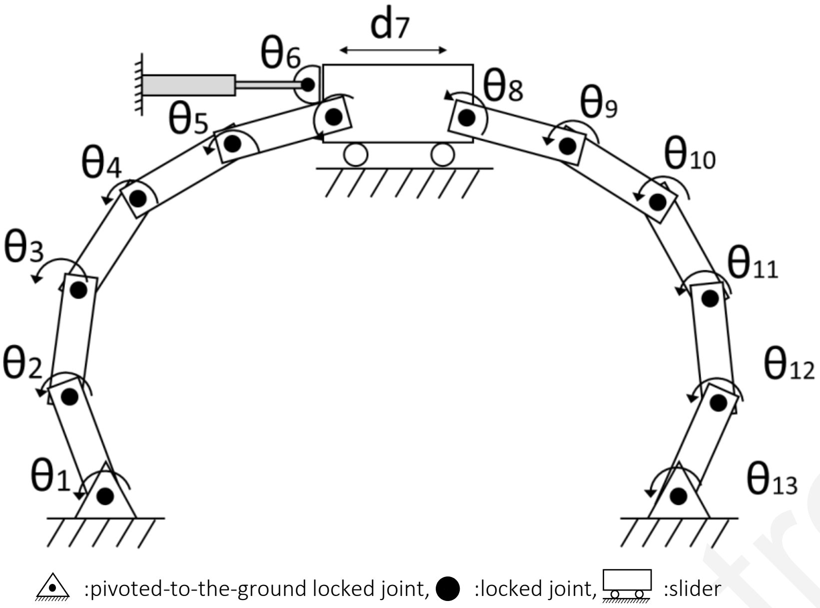

Figure 2.10: Basic Dual Crank-Slider (Horizontal) Mechanism with many links and brakes

The mechanism chain is shown in Fig. 2.11 with some brakes activated.

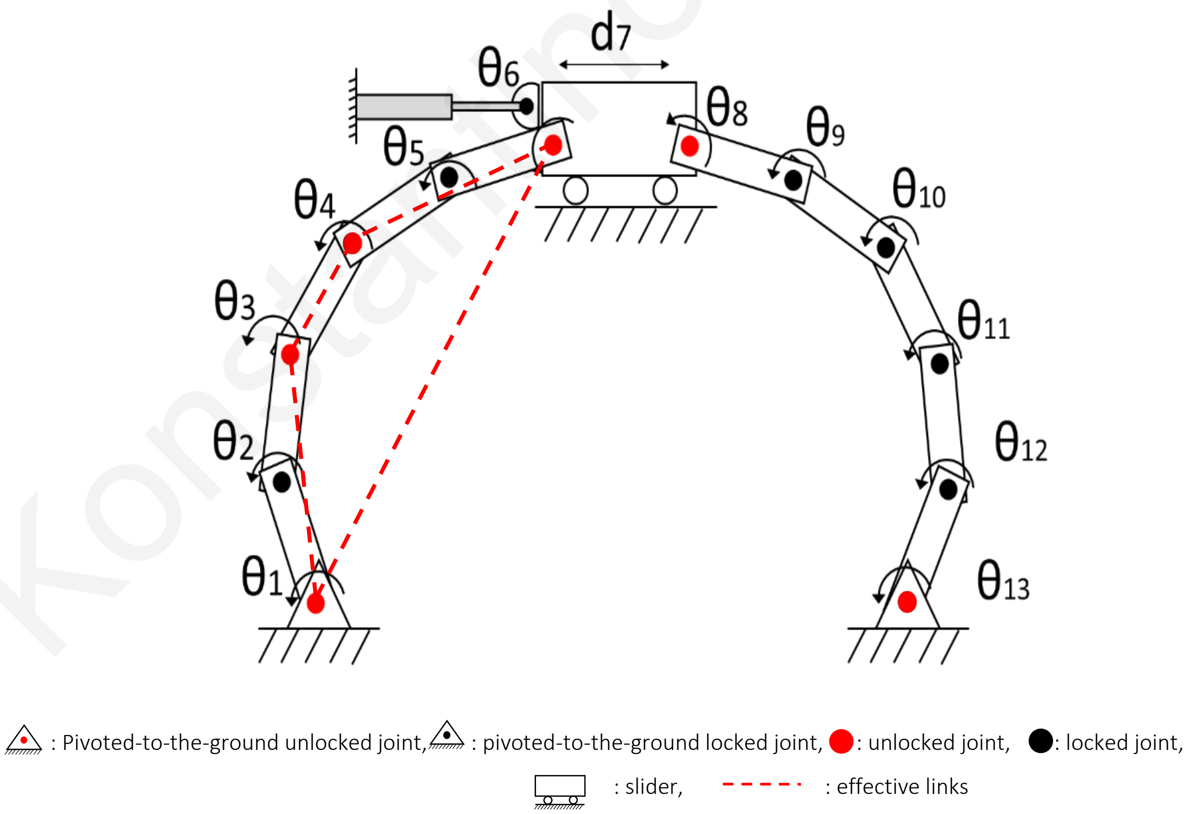

Figure 2.11: Basic Dual Crank-Slider (Horizontal) Mechanism with many links and more brakes

Konstantinos Petrou

In this way the modified system has in 1 DOF but the activated brakes were placed in one basic crank-slider only. Now with this modification, the left side is uncontrollable and the right side is a structure. When one side becomes structure then the interconnecting element (slider) also loses its mobility. Therefore, for a chain mechanism of this type to have controlled movement with one actuator it is not enough to have 1 DOF but also the brakes must be placed in the correct position. It is required to have applied brakes distributed on both basic crank-sliders as with the examples before.

The same requirement applies to the vertical motion slider version of the mechanism as shown in Fig. 2.12.

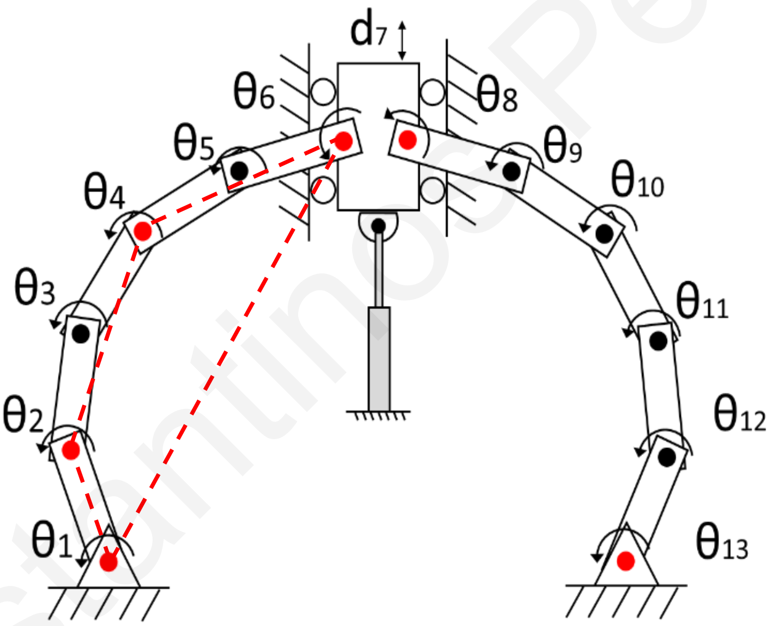

: Pivoted-to-the-ground unlocked joint, : pivoted-to-the-ground locked joint, : unlocked joint, : locked joint,
: slider, : effective links

Figure 2.12: Basic Dual Crank-Slider (Vertical) Mechanism with many links and brakes

In conclusion, the distribution of locked joints is important. So, the locked joints must be equal on both sides of the system, to control the movement with one actuator and the system not to become uncontrollable.

2.5 Singularity Analysis of a basic Crank-Slider

Singularities are positions for the mechanism where the system may not move any further or there is ambiguity recording the direction of the motion. Therefore, it is important to know the singular positions of a mechanism and consider this information

Konstantinos Petrou

as part of motion planning. The basic crank-slider mechanism encounters a singularity in the following situations:

a) When actuator is acting on slider, singularities are in the fully-stretch and fully-folded configurations.
b) When actuator is acting on ground joint, singularity occurs when the coupler link becomes perpendicular to the slider's motion direction.

These situations are explained below and also for the case of a dual crank-slider mechanism. Fig. 2.13 shown a crank-slider with actuation only on the slider.

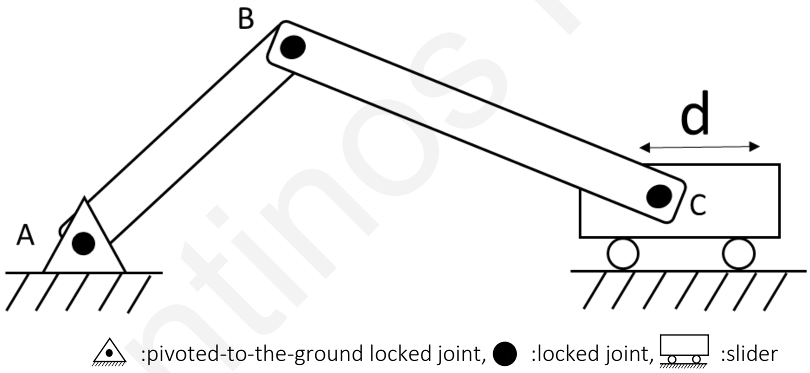

Figure 2.13: Crank Slider

The first case of a singularity positions are determined by two collinear extended moving links. That is, linkages AB and BC are in the same line, then with the movement of the slider the links will not be able to move except with an external intervention. If the actuator is at joint A there is no singularity and the links would move normally. This singularity is shown in Fig. 2.14.

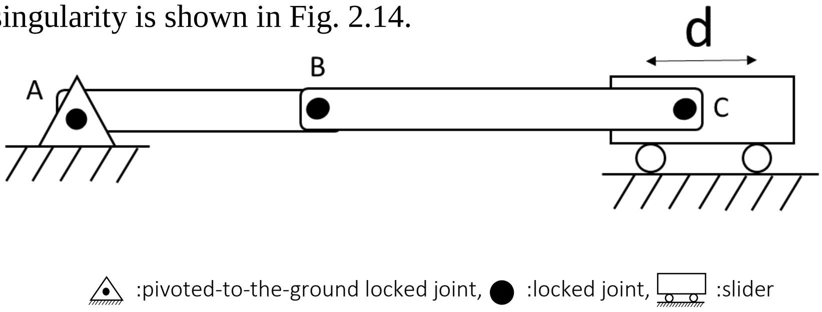

Figure 2.14: Crank Slider (Singularity collinear extended)

Konstantinos Petrou

The second case of a singularity is when toggle positions are determined by the overlapping collinear moving links. That is, linkages AB and BC are in the same line but the linkages are on top of each other. With the movement of the slider the links will not be able to move except with external intervention. If the actuator is at joint A there is no singularity and the links would move normally. This singularity is shown in Fig. 2.15.

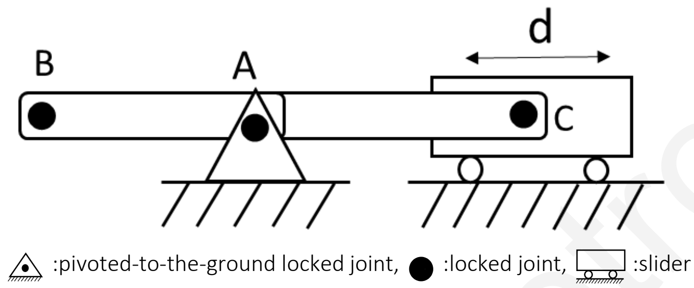

Figure 2.15: Crank Slider (Singularity overlapping collinear)

The third case is when the actuator is at the joint A. Then a “toggle position” is determined by the linkage BC that is perpendicular with the slider. Then with the movement of the actuator the links will not be able to move except with external intervention. If the actuator is acting on the slider it is not caused any singularity and the links would move normally. This singularity is in below Fig. 2.16.

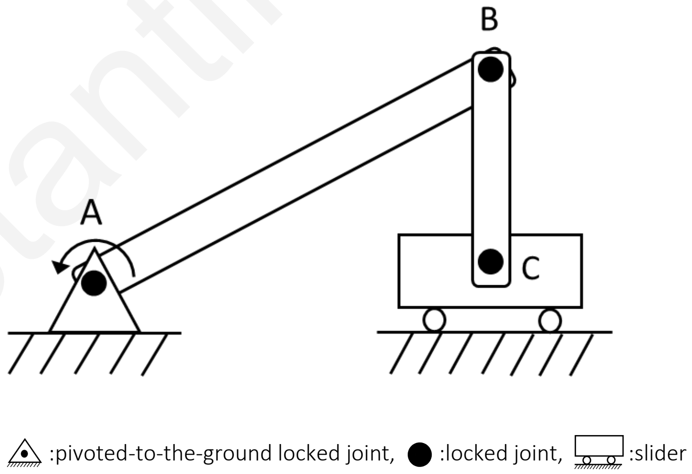

Figure 2.16: Crank Slider Singularity

2.6 Singularities of the Dual Crank-Slider Mechanism

As an extension to the abovementioned discussion, the Dual Crank-Slider Mechanism will encounter a singularity when the sub-mechanism on the Left-Hand-Side (LHS) and/or (for this application to have singularity both side is less unlikely) the sub-mechanism on the Right-Hand-Side (RHS) reaches a singularity. These situations are explained below and illustrated with examples.

Konstantinos Petrou

The actuator is considered on the slider block that can move up, down or right, left. In the figures below are shown the cases where there is singularity on one side and involves collinear extended or overlapping collinear links (Fig. 2.17 – 2.18).

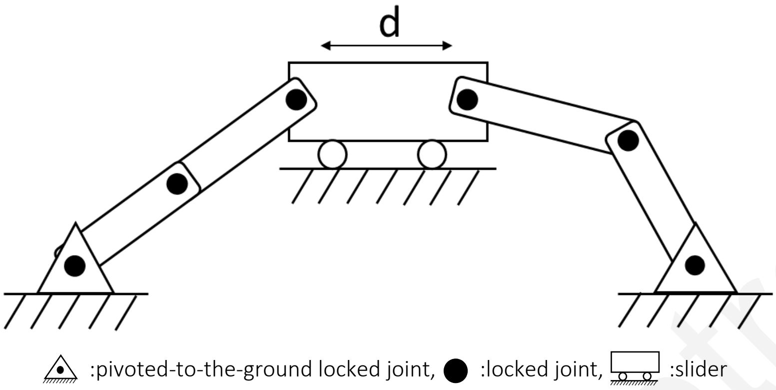

Figure 2.17: Dual Crank-Slider Mechanism (Singularity collinear extended)

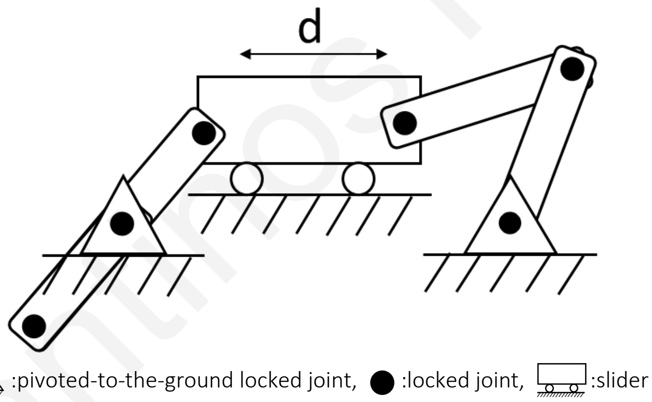

Figure 2.18: Dual Crank-Slider Mechanism (Singularity overlapping collinear)

Below are shown the cases where there is a singularity at both sides either collinear extended or overlapping collinear (Fig. 2.19 – 2.20).

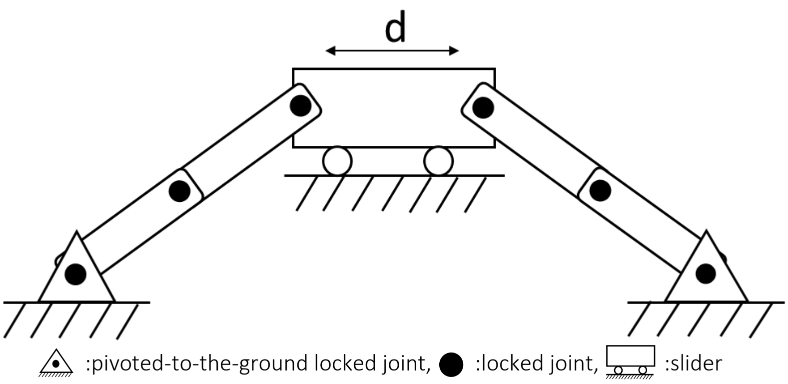

Figure 2.19: Dual Crank-Slider Mechanism (Singularity collinearity extended)

Konstantinos Petrou

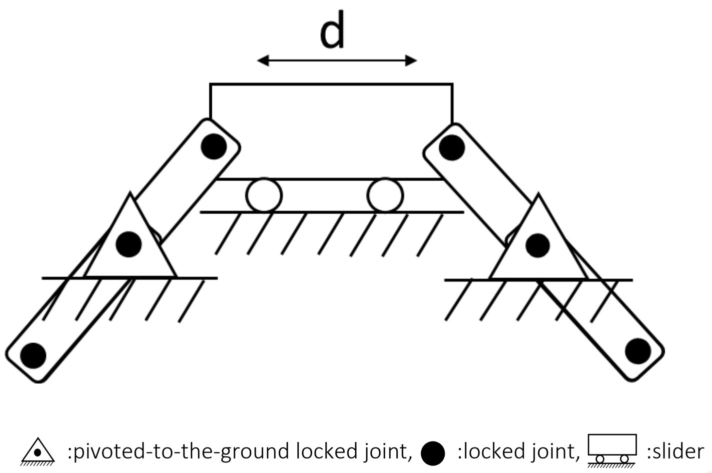

Figure 2.20: Dual Crank-Slider Mechanism

When there are more links and application of the brakes reduces the system to a dual effective crank-slider, then singularities appear when two effective links are collinear extended or overlapping. In this case, the same applies as above for the case where the actuator is acting only on the slider. In the example shown in Fig. 2.21, one of its singularities occurs when two effective links are collinear extended.

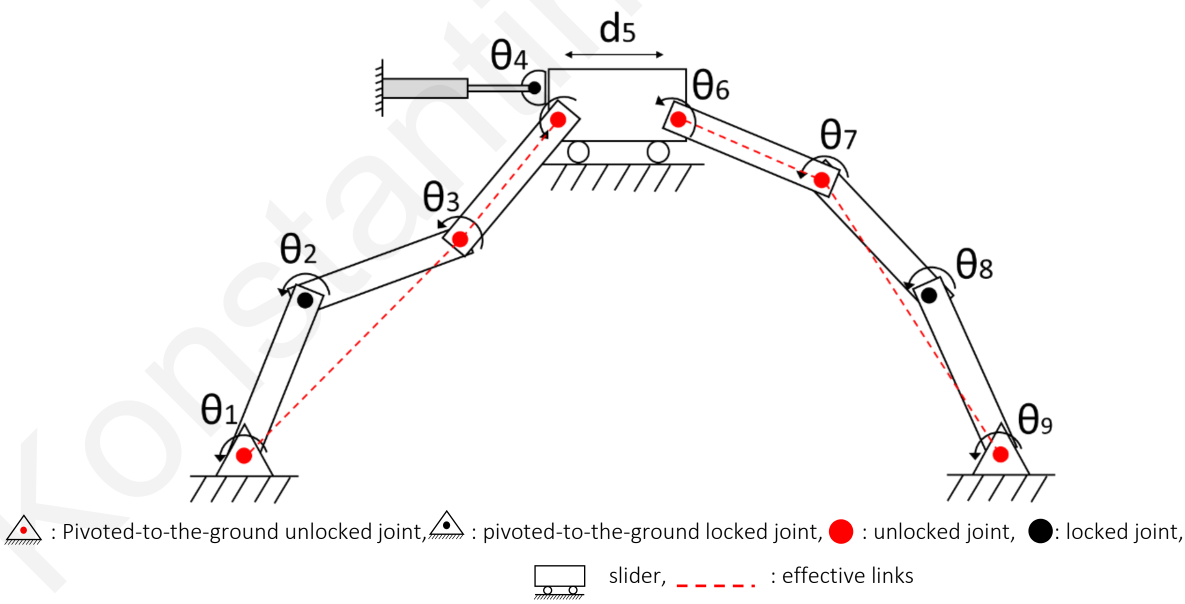

Figure 2.21: Effective Dual Crank-Slider (Horizontal) Mechanism
with six links and two brakes (singularity collinear extended)

Konstantinos Petrou

Chapter 3

3 MOTION PLANNING

The current research focuses on the design and analysis of a reconfigurable structure and the investigation of its morphological and kinetic behavior. It refers to the Effective Crank–Slider reconfiguration approach, namely a kinematics approach that reduces a planar system to an externally actuated 1-DOF system, in order to adjust each joint angle of the planar system from an initial to a target position. Through movement of the slider in each step, the selected joint angles adjustment may provide symmetrical or non-symmetrical configurations of the system. Two control system configurations are proposed, following horizontal and vertical actuation of the structure, respectively.

Firstly, in the initial position of the system, the linkages and the joints of the structure are locked. During the control of the sequences for implementing the required shape adjustment, there are locked and unlocked brakes in joints. Also, the movement of the slider, in each step achieves symmetrical and non-symmetrical forms. The adjustment of two angles allow the symmetrical forms and the adjustment of one angle allow non-symmetrical forms. At the same time, during each step, the angles are adjusted to complete the target position. The first and the last joints of the structure are pivoted to the ground. The left and the right joints of the slider are the only joints of the system without brakes. The brakes are used for the activation and the deactivation of the joints.

There are many sequences that can accomplish the target position. After a joint is adjusted, in the other steps will remain locked. In this case, singularities are possible to appear and the target position is not able to achieve (they are not feasible). In the tables below, all the sequences presented, whether they are achieved or not.

3.1 Motion Planning Procedure

The motion planning procedure includes the following steps:

1. Generation of alternating sequences. Production of scheduling tables.

2. Singularities checks should be done for all steps both for the initial and final can figuring as for the intermediate steps. So when a peculiarity occurs in a step, the specific sequence will be rejected as non-feasible.

Konstantinos Petrou

3. Checks for conflicts on the ground or neighboring structures (collisions). In sequences where this happens, the specific sequence must be rejected, the order of the steps modified, or if possible the construction modified.

4. Select the optimal sequence using criteria including the energy consumption, less energy, less movements.

5. Perform simulation for verification.

3.2 Control sequences for implementing the required shape adjustment

The can to sequences that will be using in our café studied are defined and the related scheduling tables are produced. The **Sequence 1** is a symmetrical form and the movement of the slider is vertical. During the slider's movement, there are two locked joints and two adjusted angles, in each step. The target position is completed, after two steps.

3.2.1 Sequence 1a (S1a):

All the joints in the Initial position (STEP 0) are locked and the height of the structure is 4.50m. The first and the last joints are locked. In the first step the slider moves the structure by 0.5164m downwards, so the Joint 3 and 7 are currently adjusted. In the last step, the Joints 1 and 9 are unlocked and the Joints 3 and 7 are locked. The slider moves the structure by 0.7864m upwards, so we achieve the target position (STEP 2) (shown in Fig. 3.1 and Table 3.1).

STEP 0 $[\theta_1, \theta_2, \theta_3, \theta_4, H_5, \theta_6, \theta_7, \theta_8, \theta_9]$ = [98°, 143.6°, 143.42°, 155°, 0m, 155°, 143.42°, 143.6°, 98°]

STEP 1 $[\theta_1, \theta_2, \theta_3, \theta_4, H_5, \theta_6, \theta_7, \theta_8, \theta_9]$ = [98°, 149.08°, 120°, 172.92°, -0.5164m, 172.92°, 120°, 149.08°, 98°]

STEP 2 $[\theta_1, \theta_2, \theta_3, \theta_4, H_5, \theta_6, \theta_7, \theta_8, \theta_9]$ = [67.32°, 203.02°, 120°, 149.66°, +0.7864m, 149.66°, 120°, 203.02°, 67.32°]

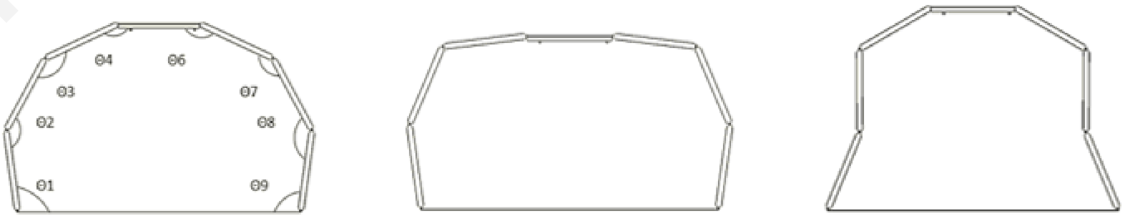

Initial Position – STEP 0 STEP 1 Target Position – STEP 2

Figure 3.1: Structure reconfigurations for sequence 1a

Konstantinos Petrou

Table 3.1: Scheduling tables for sequence 1a

	J_1	J_2	J_3	J_4	J_5	J_6	J_7	J_8	J_9
Step 1	⊗△	⊙	⊙	⊙	↕	⊙	⊙	⊙	⊗△
Step 2	△	⊙	⊗	⊙	↕	⊙	⊗	⊙	△

△: pivoted-to-the-ground unlocked joint, ⊗△: pivoted-to-the-ground locked joint, ⊙: unlocked joint, ⊗: locked joint,

- - - : effective link, : slider, ⊙ : currently adjustment

In Step 1 where the Joints 1 and 9 are locked, the ground level is shifted between Joints 2 and 8. Also, in the Step 2, Joints 3 and 7 are unlocked, so the two linkages between Joints 2 and 4 are move as one. The same happens with the Joints 6 and 8.

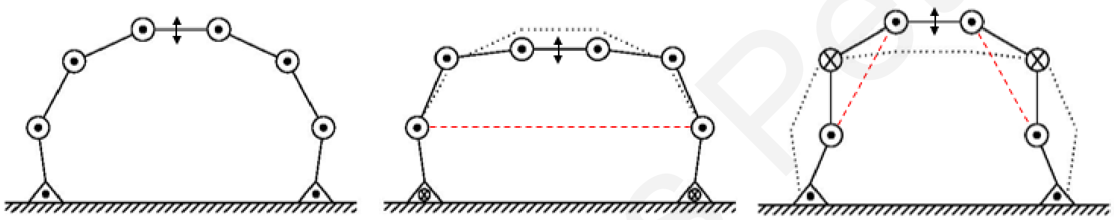

Initial Position – STEP 0 STEP 1 Target Position – STEP 2

Figure 3.2: Selected feasible motion sequences to the system

3.2.2 Sequence 1b (S1b):

All the joints in the Initial position (STEP 0) are locked and the height of the structure is 4.50m. The Joints 2 and 8 are locked. In the first step the slider moves the structure 0.665m to the ground, so the Joints 3 and 7 are currently adjusted. In the last step, the Joints 2 and 8 are unlocked and the Joints 3 and 7 are locked. The slider moves the structure by 0.935m upwards, so we achieve the target position (STEP 2).

STEP 0 $[\theta_1, \theta_2, \theta_3, \theta_4, H_5, \theta_6, \theta_7, \theta_8, \theta_9]$ = [98°, 143.6°, 143.42°, 155°, 0m, 155°, 143.42°, 143.6°, 98°]

STEP 1 $[\theta_1, \theta_2, \theta_3, \theta_4, H_5, \theta_6, \theta_7, \theta_8, \theta_9]$ = [100.77°, 143.6°, 120°, 175.63°, -0.665m, 175.63°, 120°, 143.6°, 100.77°]

STEP 2 $[\theta_1, \theta_2, \theta_3, \theta_4, H_5, \theta_6, \theta_7, \theta_8, \theta_9]$ = [67.32°, 203.02°, 120°, 149.66°, +0.935m, 149.66°, 120°, 203.02°, 67.32°]

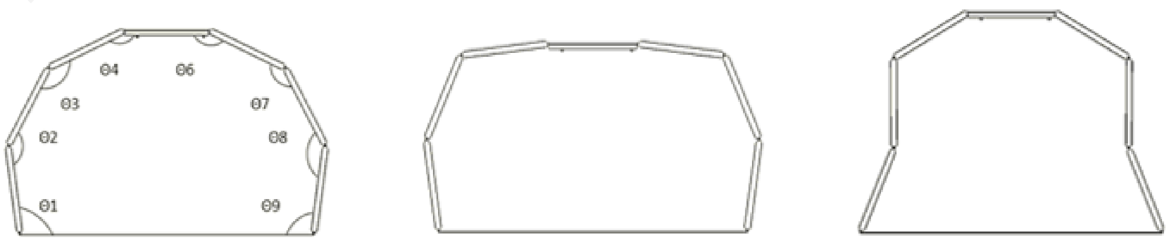

Initial Position – STEP 0 STEP 1 Target Position – STEP 2

Figure 3.3: Structure reconfigurations for sequence 1b

Konstantinos Petrou

Table 3.2: Scheduling tables for sequence 1b

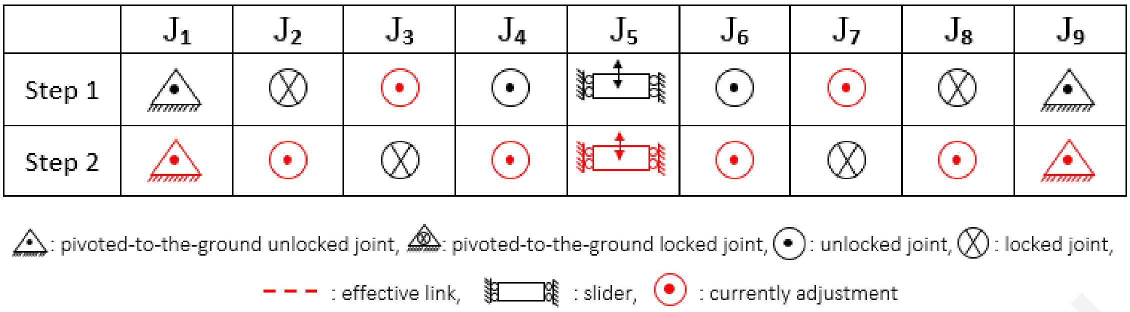

In the Step 1, Joints 2 and 8 are locked, so the two linkages between Joints 1 and 3 move as one. The same happens with the Joints 7 and 9. In the final step, Joints 3 and 7 are locked, so the links between them move as one. The form is symmetrical, so the same happens the other side of structure. The Joints 3 and 7 are locked, so the links between them are move as one.

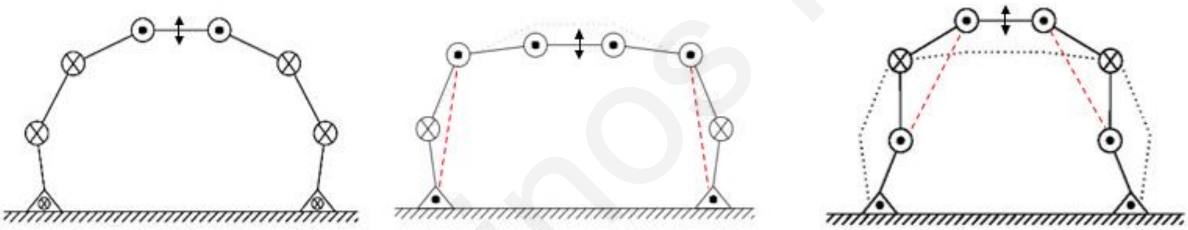

Figure 3.4: Selected feasible motion sequences to the system

3.2.3 Sequence 1c (S1c):

All the joints in the Initial position (STEP 0) are locked and the height of the structure is 4.50m. In the first step, Joints 3 and 7 are locked and the slider moves the structure by 0.649m upwards, so the first and the last joints are currently adjustment. In the second step, the Joints 1 and 9 are locked and all others are unlocked. The slider moves the structure by 0.935m downwards, so we achieve the target position (STEP 2).

STEP 0 $[\theta_1, \theta_2, \theta_3, \theta_4, H_5, \theta_6, \theta_7, \theta_8, \theta_9]$ = [98°, 143.6°, 143.42°, 155°, 0m, 155°, 143.42°, 143.6°, 98°]

STEP 1 $[\theta_1, \theta_2, \theta_3, \theta_4, H_5, \theta_6, \theta_7, \theta_8, \theta_9]$ = [67.32°, 194.14°, 143.42°, 135.12°, +0.6487m, 135.12°, 143.42°, 194.14°, 67.32°]

STEP 2 $[\theta_1, \theta_2, \theta_3, \theta_4, H_5, \theta_6, \theta_7, \theta_8, \theta_9]$ = [67.32°, 203.02°, 120°, 149.66°, -0.3787m, 149.66°, 120°, 203.02°, 67.32°]

Konstantinos Petrou

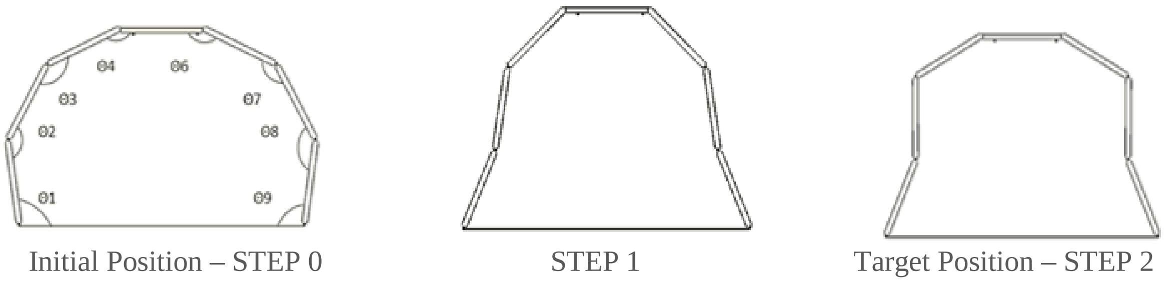

Figure 3.5: Structure reconfigurations for sequence 1c

Table 3.3: Scheduling tables for sequence 1c

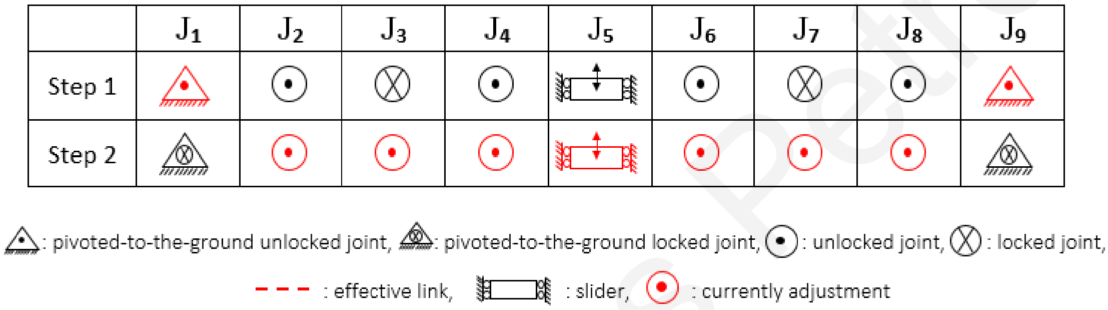

In the Step 1, Joints 3 and 7 are locked, so the two linkages between Joints 2 and 4 move as one. The same happens with the Joints 7 and 9. In the third step, where the Joints 1 and 9 are locked, the ground level is defined between to the Joints 2 and 8.

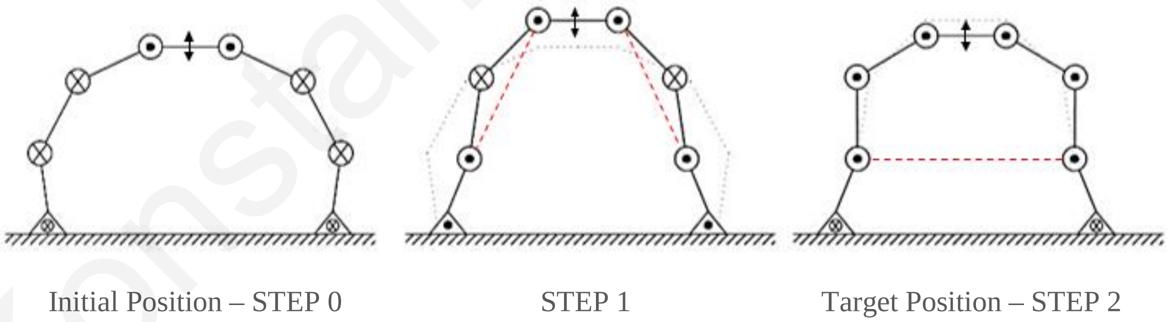

Figure 3.6: Selected feasible motion sequences to the system

3.2.4 Sequence 1d (S1d):

All the joints in the Initial position (STEP 0) are locked and the height of the structure is 4.50m. In the first step, the Joint 2 and 8 are currently adjustment and Joint 1 and 9 are locked. In the second step, the Joints 2 and 8 are locked and all others are unlocked. It is not possible to complete the configuration because of the singularity.

Table 3.4: Scheduling tables for sequence 1d

	J_1	J_2	J_3	J_4	J_5	J_6	J_7	J_8	J_9
Step 1	△⊗	◉	⊙	⊙	▭	⊙	⊙	◉	△⊗
Step 2	▲	⊗	◉	◉	▬	◉	◉	⊗	▲

△: pivoted-to-the-ground unlocked joint, △⊗: pivoted-to-the-ground locked joint, ⊙: unlocked joint, ⊗: locked joint,
- - - : effective link, ▭ : slider, ◉ : currently adjustment

3.2.5 Sequence 1e (S1e):

In this case, there two locked and two adjusted joints in each step, but it is not possible to complete the configuration because of the singularity. If there are more steps, the target position will be completed.

Table 3.5: Scheduling tables for sequence 1e

	J_1	J_2	J_3	J_4	J_5	J_6	J_7	J_8	J_9
Step 1	▲	⊗	⊙	⊙	▭	⊙	⊙	⊗	▲
Step 2	△⊗	◉	◉	◉	▬	◉	◉	◉	△⊗

△: pivoted-to-the-ground unlocked joint, △⊗: pivoted-to-the-ground locked joint, ⊙: unlocked joint, ⊗: locked joint,
- - - : effective link, ▭ : slider, ◉ : currently adjustment

3.2.6 Sequence 1f (S1f):

All the joints in the Initial position (STEP 0) are locked and the height of the structure is 4.50m. In the first step, Joints 2 and 8 are currently adjustment and Joints 3 and 7 are locked. In the second step, Joints 2 and 8 are locked and all others are simultaneously adjusted. It is not possible to complete the configuration because of a singularity.

Table 3.6: Scheduling tables for sequence 1f

	J_1	J_2	J_3	J_4	J_5	J_6	J_7	J_8	J_9
Step 1	△	◉	⊗	⊙	▭	⊙	⊗	◉	△
Step 2	▲	⊗	◉	◉	▬	◉	◉	⊗	▲

△: pivoted-to-the-ground unlocked joint, △⊗: pivoted-to-the-ground locked joint, ⊙: unlocked joint, ⊗: locked joint,
- - - : effective link, ▭ : slider, ◉ : currently adjustment

Konstantinos Petrou

The **Sequence 2** is a non-symmetrical form where the slider's movement is horizontal. In every step, there are two locked joints and one adjusted joint. They needed three steps to complete the target position.

3.2.7 Sequence 2a (S2a):

All the joints in the Initial position (STEP 0) are locked and the height of the structure is 4.50m. In the first step Joints 3 and 8 are locked and Joint 7 is adjusted. The slider moves towards the right, for 0.4786m. In the second step, the Joints 3 and 8 are unlocked and the Joints 1 and 7 are locked. The Joint 3 is adjusted and the slider moves to the left, by 0.9712m. In the last step, all the joints are adjusted and the joints 3 and 7 are locked. The target position is achieved.

STEP 0 $[\theta_1, \theta_2, \theta_3, \theta_4, H_5, \theta_6, \theta_7, \theta_8, \theta_9]$ = [98°, 143.6°, 143.42°, 155°, 0m, 155°, 143.42°, 143.6°, 98°]

STEP 1 $[\theta_1, \theta_2, \theta_3, \theta_4, H_5, \theta_6, \theta_7, \theta_8, \theta_9]$ = [84.53°, 156.85°, 143.42°, 155.2°, +0.4786m, 156.75°, 134°, 143.6°, 105.65°]

STEP 2 $[\theta_1, \theta_2, \theta_3, \theta_4, H_5, \theta_6, \theta_7, \theta_8, \theta_9]$ = [84.53°, 172.18°, 105°, 162.65°, -0.9712m, 157.66°, 134°, 168.86°, 79.48°]

STEP 3 $[\theta_1, \theta_2, \theta_3, \theta_4, H_5, \theta_6, \theta_7, \theta_8, \theta_9]$ = [62°, 218.19°, 105°, 154.81°, +0.377m, 158.38°, 134°, 156.32°, 91.3°]

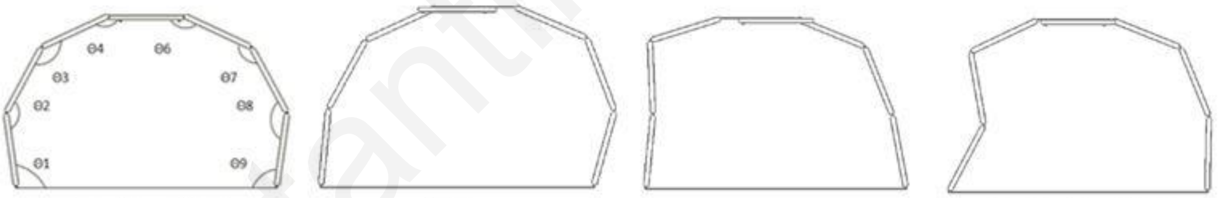

Initial Position – STEP 0 | STEP 1 | STEP 2 | Target Position – STEP 3

Figure 3.7: Structure reconfigurations for sequence 2a

Table 3.7: Scheduling tables for sequence 2a

	J_1	J_2	J_3	J_4	J_5	J_6	J_7	J_8	J_9
Step 1	△	⊙	⊗	⊙	↔▭	⊙	⊙	⊗	△
Step 2	⊗△	⊙	⊙	⊙	↔▭	⊙	⊗	⊙	△
Step 3	△	⊙	⊗	⊙	↔▭	⊙	⊗	⊙	△

△: pivoted-to-the-ground unlocked joint, ⊗△: pivoted-to-the-ground locked joint, ⊙: unlocked joint, ⊗: locked joint,

- - - : effective link, ▭ : slider, ⊙ : currently adjustment

Konstantinos Petrou

In the Step 1, Joints 3 and 8 are locked, so the two linkages between Joints 2 and 4 are move as one. The same happens with the Joints 7 and 9. In the second step, the Joints 1 and 7 are locked, the ground level is replaced to the Joints 2 and 9. Also, the links between Joints 6 and 8 are act as one. In the final Step the Joint 3 and 7 are locked, so the links between Joints 2 and 4 and Joints 6 and 8, are move as one.

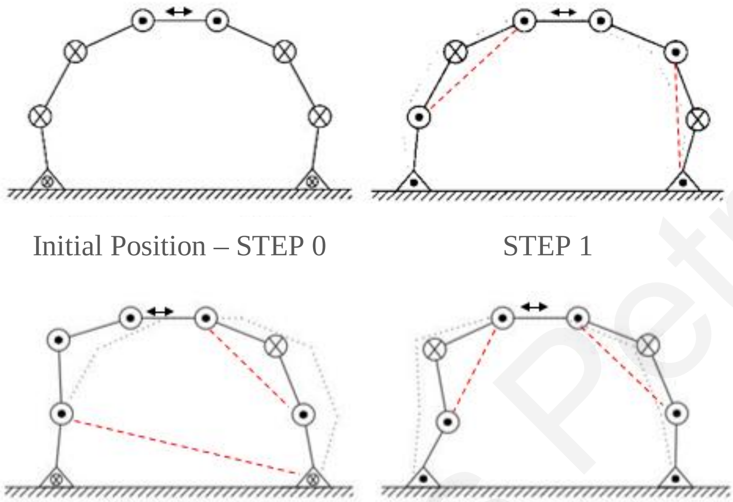

Initial Position – STEP 0 STEP 1

STEP 2 Target Position – STEP 3

Figure 3.8: Selected feasible motion sequences to the system

For each sequence there are many combinations, to reach the target position, but sometimes there are singularities and the target position cannot be achieved. These combinations were calculated manually without software and are presented in the appendix. There are 144 alternative sections that can be checked if they can reach the target position 2 or if any of them have singularities.

The **Sequence 3** is a symmetrical form and the movement of the slider is vertical. During the slider's movement, there are two locked joints and two adjusted joints. So, after one step the final position is completed.

3.2.8 Sequence 3a (S3a):

In the Step 1, all the Joints are currently adjusted expect the Joints 3 and 7 which are locked.

STEP 0 [θ_1, θ_2, θ_3, θ_4, H_5, θ_6, θ_7, θ_8, θ_9] = [98°, 143.6°, 143.42°, 155°, 0m, 155°, 143.42°, 143.6°, 98°]

STEP 1 [θ_1, θ_2, θ_3, θ_4, H_5, θ_6, θ_7, θ_8, θ_9] = [120°, 101.7°, 143.42°, 174.88°, -1.3445m, 174.88°, 143.42°, 101.7°, 120°]

Konstantinos Petrou

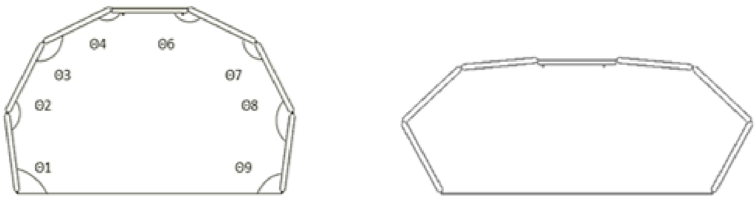

Initial Position – STEP 0 Target Position – STEP 1

Figure 3.9: Structure reconfigurations for sequence 3a

Table 3.8: Scheduling tables for sequence 3a

	J1	J2	J3	J4	J5	J6	J7	J8	J9
Step 1	△	⊙	⊗	⊙	↕	⊙	⊗	⊙	△

△: pivoted-to-the-ground unlocked joint, △: pivoted-to-the-ground locked joint, ⊙: unlocked joint, ⊗: locked joint,

- - - : effective link, : slider, ⊙ : currently adjustment

In Step 1, Joints 3 and 7 are locked, so the two linkages between Joints 2 and 4 move as one. The same happens with the Joints 6 and 8.

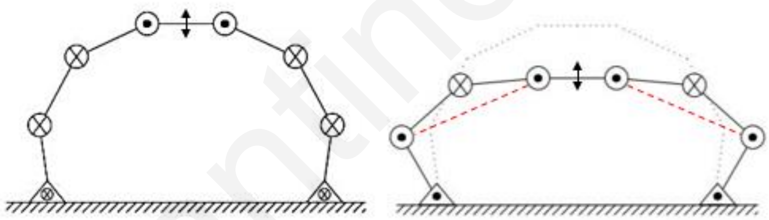

Initial Position – STEP 0 Target Position – STEP 1

Figure 3.10: Selected feasible motion sequences to the system

3.2.9 Sequence 3b (S3b)

In Step 1, all the Joints are simultaneously adjusted expect the Joints 2 and 7 which are locked. It is not possible to complete the configuration because of a singularity

Table 3.9: Scheduling tables for sequence 3b

	J1	J2	J3	J4	J5	J6	J7	J8	J9
Step 1	△	⊗	⊙	⊙	↕	⊙	⊗	⊙	△

△: pivoted-to-the-ground unlocked joint, △: pivoted-to-the-ground locked joint, ⊙: unlocked joint, ⊗: locked joint,

- - - : effective link, : slider, ⊙ : currently adjustment

3.2.10 Sequence 3c (S3c):

In the Step 1, all the Joints are simultaneously adjusted expect the Joints 1 and 9 which are locked. It is not possible to complete the reconfiguration because of a singularity.

Table 3.10: Scheduling tables for sequence 3c

	J_1	J_2	J_3	J_4	J_5	J_6	J_7	J_8	J_9
Step 1	⨂	⊙	⊙	⊙	↕	⊙	⊙	⊙	⨂

△ : pivoted-to-the-ground unlocked joint, ⨂ : pivoted-to-the-ground locked joint, ⊙ : unlocked joint, ⨂ : locked joint,

- - - : effective link, ▭ : slider, ⊙ : currently adjustment

There are many sequences to achieving specific symmetrical and non-symmetrical configurations but it is reasonable to choose the sequences with as few reconfiguration steps as possible. This happens, because of the kinematics approach that is proposed provides flexibility in motion planning and control complexity is avoided.

Konstantinos Petrou

Chapter 4

4 CONSTRUCTION DESIGN

The current chapter refers to the structural and construction design of the planar and spatial linkage structure and it is based on the software Solidworks. Main parameters that influence the design refer to the supports of each linkage, the members and their joint connections, as well as the actuation components that are integrated within the system to enable horizontal or vertical transformations. In this framework, two alternatives have been developed, based on the integration of a horizontal and four vertical linear motion actuators, respectively. In both cases, the primary planar linkage consists of seven hinge connected beams supported on a structural grid that serves as the floor structure. At midspan the structural linkage is further supported on diagonals positioned within the system to form a V-shape or X-shape according to the reconfiguration requirements of the system.

4.1 Modeling in Solidwork Software

The system was modelled using the software Solidworks with precise dimensions, laminates, pins, bolts and nuts and actuators. The two models were made separately, one model with horizontal motion and the other with vertical motion (shown in Fig. 4.1) as will be designed in detail.

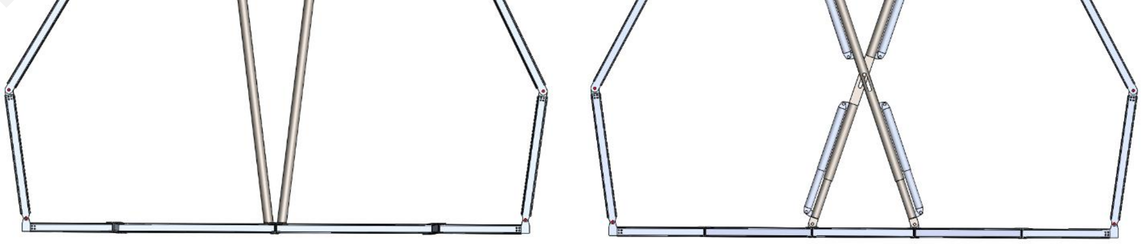

Figure 4.1: Models with horizontal (left) and vertical (right) movement

Konstantinos Petrou

The beams in both cases were assembled in the same way. The models consist of six beams, three on each side, with length of two meters from joint to joint. Moreover, the beams of the linkage are interconnected through a steel plate inserted between the UPN 140/60 sections of the beam and two steel plates. They have at one end a single plate and in the other, double plates for easy assembly between them (shown in Fig. 4.2).

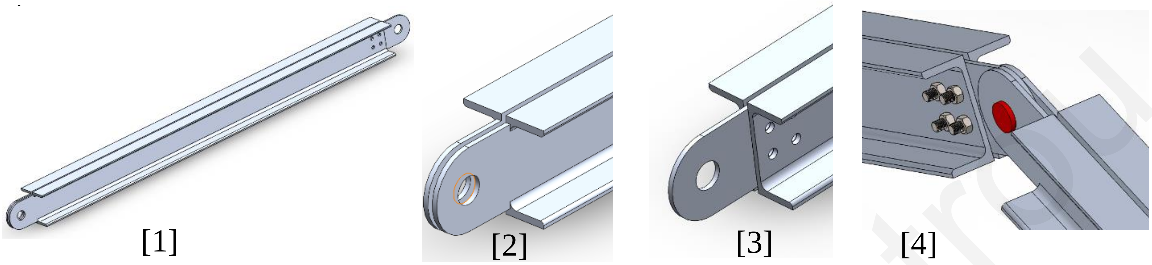

Figure 4.2: [1] Complete beams with plates, [2] Double plates at one end of the link, [3] Single plate at other end of the link, [4] Assembly between the beams with bolts/nuts and pins

In the software Solidworks is used the subprogram "assembly", for the realization and assembly of the models. In the subprogram assembly, the parts are entered using the command "insert components" and the assembly of the parts are done by selecting the appropriate "mates". The connection of the plates on the beams is done with bolts and nuts. The assembly is realized using the commands standard mates ("coincident" and "concentric") and mechanical mates ("screw").

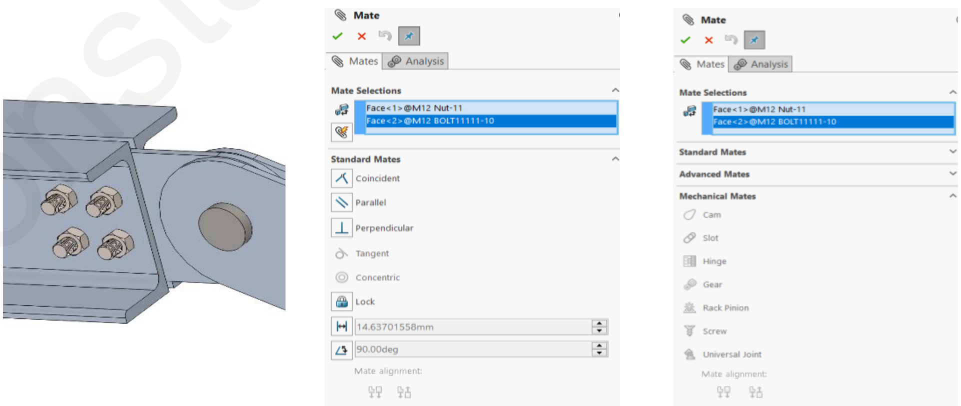

Figure 4.3: Assembling bolts and nuts to the beams with commands from standard and mechanical mates

Konstantinos Petrou

The beams connection between them is done using pins. The beams of each linkage are hinge connected to the structural grid through a steel plate. Thus, the supports of the linkages allow rotations of the members in span direction. For the placement of the pins the command mechanical mates ("hinge") is used. The pins connecting the links are made of material cast carbon steel, where it was set separately at custom material with increased density to represent the weight of the brakes, which were not included on the assebled system.

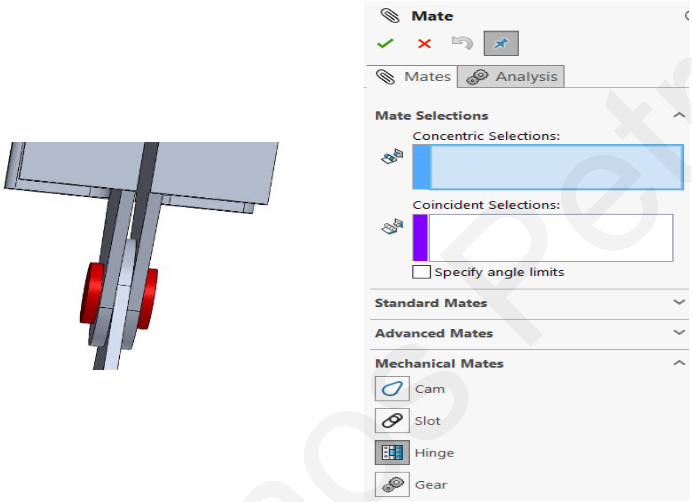

Figure 4.4: Assembling pins to the beams with commands from mechanical mates

At the top of the models there is a horizontal beam aluminum of 2.5 meters length, where it is assembled in the same way as the rest with the difference that the weight of the brakes is not included in the certain material of the pins since in the specific joints there are not any brakes.

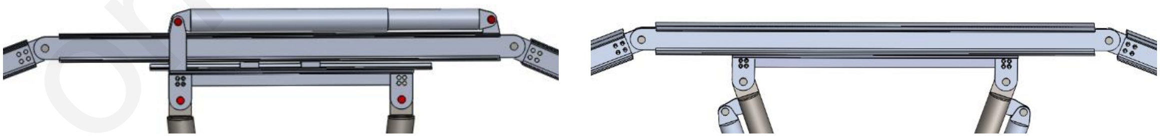

Figure 4.5: Assembly of a horizontal beam in the horizontal and vertical model

At the bottom of the models are placed UPN beams, where they form at specific distances cross shapes (+). The UPNs are assembled together with the command standard mates ("coincident") with a gap between them, because the plates are placed there. The plates at the intermediate points are " + " shaped while at both ends have angle shape. These are assembled with the command from the standard mates

Konstantinos Petrou

("coincident" and "distance") for the correct placement and the exact distance from the beams.

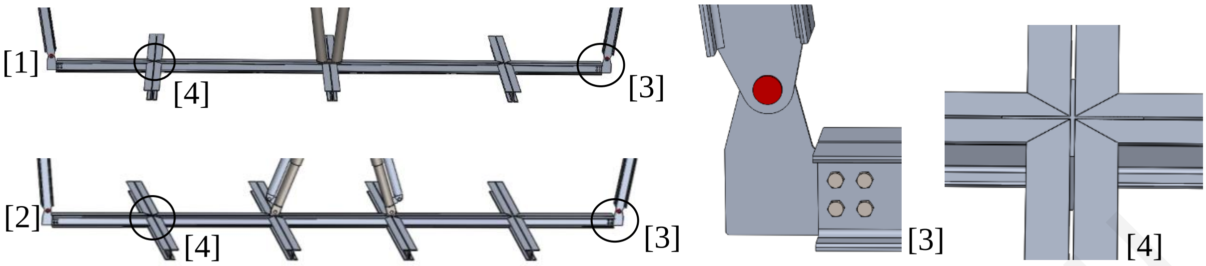

Figure 4.6: [1] Bottom central base of horizontal model, [2] Bottom central base of vertical model, [3] Plate of base with angle shape, [4] Plate of base with cruciform "+" shape

4.2 Horizontal Motion Model

The horizontal model has centrally placed cylindrical pipes of shape "V" so that the model has the desired height, namely 4.5 meters. The connection of the V-diagonals at midspan of the system in the alternative with horizontal actuation takes place over two horizontal steel plates, whereas the lower one is connected to the structural grid joint in the central plate " + " and the upper one, welded to the diagonals. The way of assembly in the software is done with the command standard mates ("coincident") for the correct placement of the plates but also of the pins and bolts/nuts. Furthermore, for pins and bolts/nuts are used the commands mechanical mates ("hinge" and "screw") (shown in Fig. 4.7).

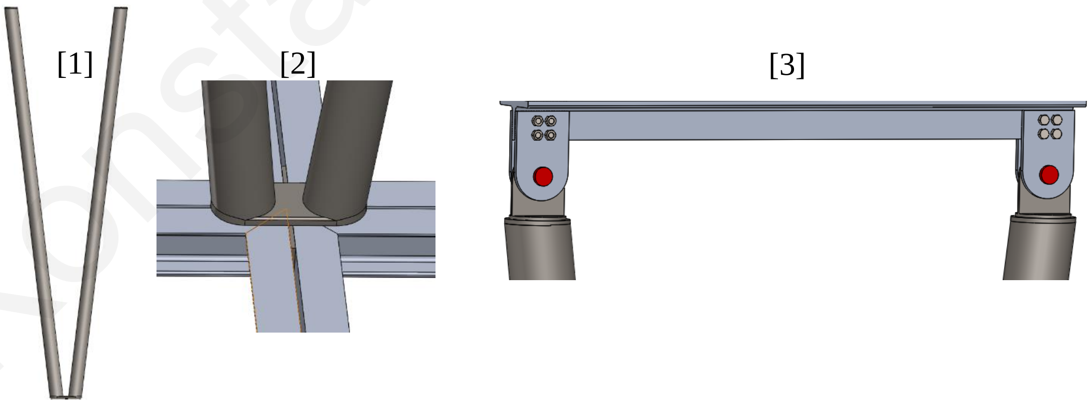

Figure 4.7: [1] Centrally cylindrical pipes of shape "V", [2] Connecting V pipes to the bottom base, [3] Connecting V pipes to the top base of the slider

The base of the slider is "T" shape and are placed at the bottom the plates of the pipes "V" and at the top is the rail where the slider moves. The actuator's ends are connected to the horizontal structural members through steel plates. The linkage beam may roll on the interconnecting member with a section of T 140/140 mm over specially formed

Konstantinos Petrou

sliding elements. A linear motion actuator is positioned above the linkage beam using standard mates and connected on one side with the latter and so that operation of the actuator provides relative displacements of the linkage to its support elements.

The actuator is linear and is pin connected on either side. The pins are made of cast carbon steel and the rest are made of aluminum. The assembly is done with standard mates ("concentric") and advanced mates ("distance") (see in Fig. 4.8).

The way the assembly is done in the horizontal model (shown in Fig. 4.9) can go through the distances set so that the model can reach its final position through a number of steps.

Figure 4.8: Assembly of slider and actuator on the horizontal bar

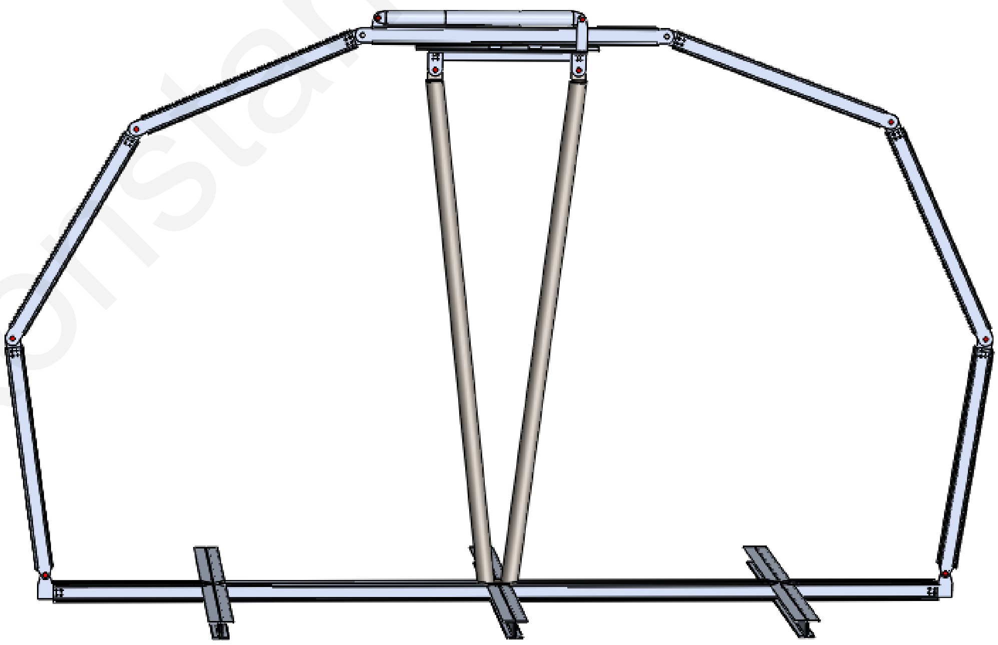

Figure 4.9: Complete model with horizontal movement

Konstantinos Petrou

4.3 Vertical Motion Model

For the second model with the vertical motion were centrally placed two cylindrical telescopic X-shaped actuators to raise and lower the system so that reconfigurations can be implemented. The telescopic system consists of two small cylindrical pipes each and a central pipe of larger diameter. The way the movement is done in the telescopic is with the use of actuators as in the model with the horizontal movement, that is, there is an actuator in each small diameter tube of the telescopic that connects it to the central tube of larger diameter. So there are a total of four actuators in the X-shaped telescopic mechanism. It is assembled in the software Solidworks using the commands standard mates ("concentric") so that the telescopic tubes and the actuators can be placed one inside the other. In addition, the command from the advance mates ("distance") is used to adjust the maximum and minimum length that the tubes can travel through each other in both the telescopic and actuators (shown in Fig. 4.10).

Figure 4.10: Centrally cylindrical telescopic X-shape with four actuators and telescopic pipes small and large diameter

Generally, the length of the actuators and telescopic pipes is such that they can have the desired travel length at each step. At the center of the X-shaped telescopic is a slotted pin joint, so that the telescopic can operate without changing the mounting positions at the top and bottom joints. The adjustment of the pin movement in the hole is done using the command mechanical mates ("hinge") (shown in Fig 4.11).

Konstantinos Petrou

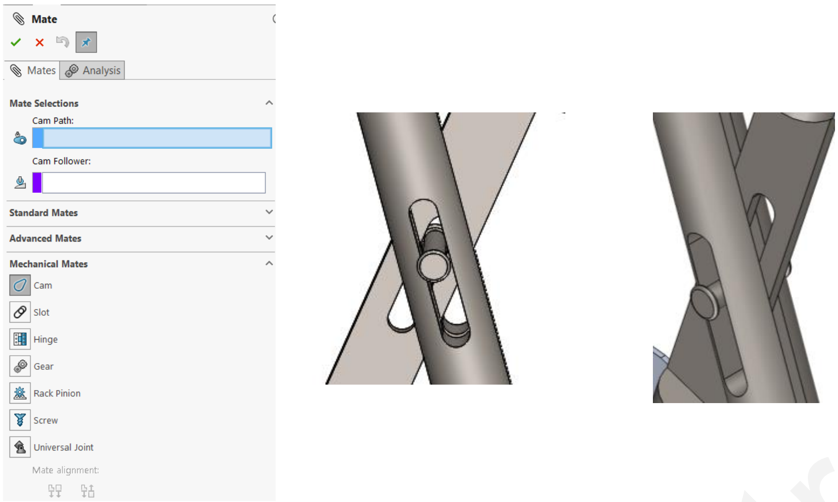

Figure 4.11: Central hole in X-shaped telescopes and adjusting to the solidworks in mechanical mates

The X-shaped telescopic is connected to the base with the plates " + " and at the top with plates at the base " T " of the horizontal bar with pin, bolts and nuts, similar to the horizontal model. The assembly of these parts in the software Solidworks are done with the commands standard mates (" coincident " and " concentric"). Furthermore, the pins, bolts and nuts use the commands advanced and mechanical mates (" width " and " screw "), respectively. Thus, in the base "T" are placed at the bottom the plates of the telescopic and at the top the horizontal beam of the model with the help of the command standard mates ("coincident") to join the beam with the base "T" (shown in Fig. 4.12).

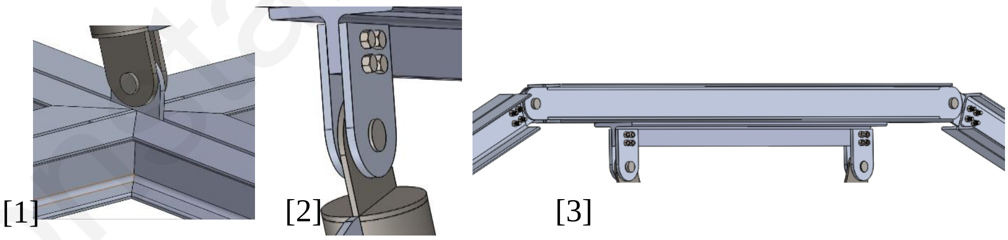

Figure 4.12: Connecting [1] telescope pipes to the bottom base, [2] telescope pipes to the top base of the horizontal bar, [3] horizontal bar

The vertical motion model (shown in Fig. 4.13) is assembled as described above and in this way reconfiguration steps can be implemented and studied.

Konstantinos Petrou

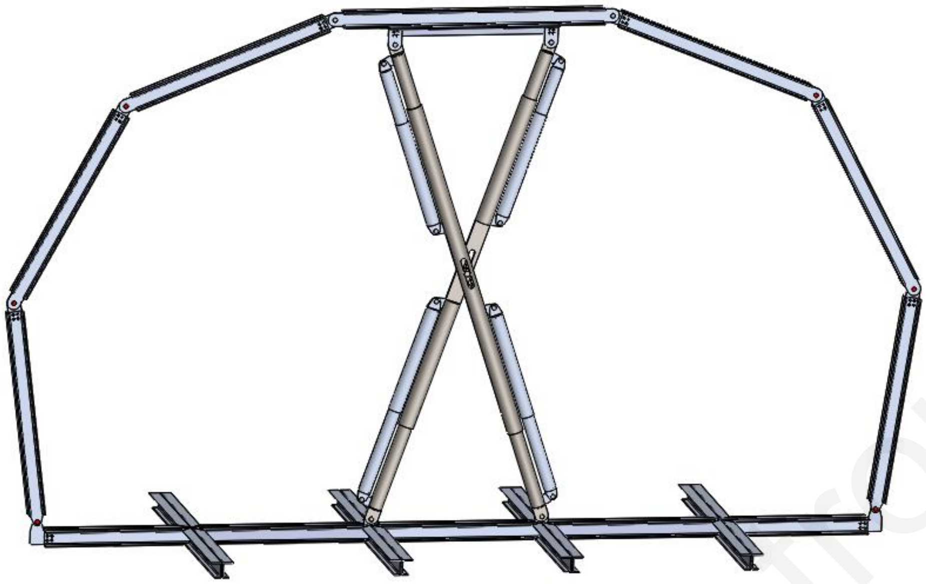

Figure 4.13: Complete model with vertical movement

4.4 Spatial Models

After the models final dimensioning was done and their assembly, was completed the above models are connected lay ether to create a spatial model structurein the form of a building. The structure has active linkages (with an actuator) only at the two ends. The intermediate planar linkages are passive.

Therefore, since actuators exist only at the ends, the intermediate bar linkages should be connected in such a way that the slider activates, all the bars movement and they get the desired shape throughout the spatial model. On the plates at the ends of the beams are connected two cylindrical pipes in each beam and all the bars move together in parallel with the ones at the two ends.

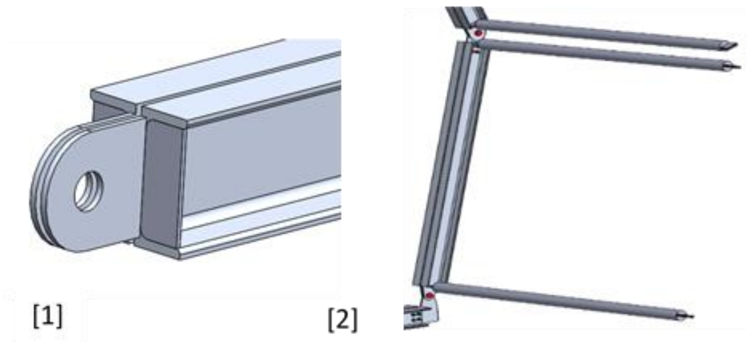

Figure 4.14: [1] laminates to the ends of the bars, [2] two cylindrical pipes connected in laminates of the bar

Konstantinos Petrou

The Rodans were used in the structures to reduce the stresses. These were assembled diagonal to the cylindrical pipes with the help of plates. The materials of the cylindrical pipes, laminates and Rodans are Aluminum 1060. Also, Rodan dimensions are from standard tables (Dorma 2002), so for these models a choice were made of Rodan RDA12 and the dimensions of the RDA12 are shown below in Table 4.1. The Rodans are placed diagonally and alternately upwards and inwards, to function as a grid and offer more stiffness to the model. This can be better understood with the help of the Fig. 4.15.

[1]

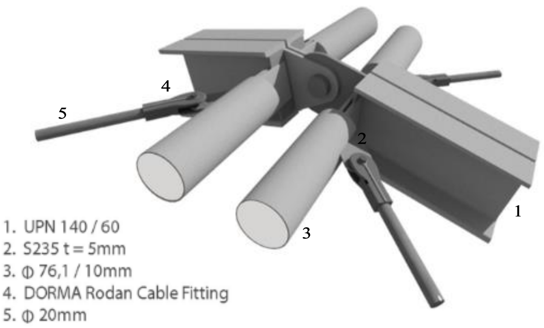

[2]

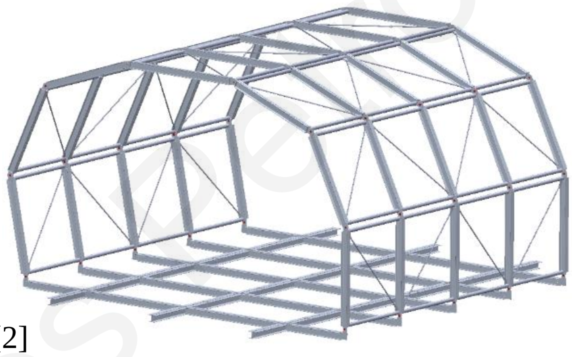

Figure 4.15: [1] assembly of laminates and Rodans in the cylindrical pipes,
[2] rodan configuration on the model

Table 4.1: Standard dimensions of Rodan (Dorma 2002)

	RDA5	RDA6	RDA8	RDA10	RDA12	RDA16	RDA20	RDA24	RDA27	RDA30	RDA36	RDA42	RDA48	RDA52	RDA56	RDA60
r	8	9	12	15	18	24	29	35	39	43	51	60	69	75	81	88
$b^{+0.5}_{-0}$	4.5	5	7	8	10	15	18	20	22	25	30	35	40	45	50	55
q_{355}	14	16.7	21.3	25.5	30	40	49	58	64.5	71.5	84.5	100	116	124	134.5	146
q_{235}	14	18	21	28	33	42	54	66	76	82	97	108	127	141	152	158
øj	5.5	6.5	7.5	9.5	11.5	14.5	18.5	21.5	24.5	26.5	30.5	35.5	42.5	45.5	50.5	52.5

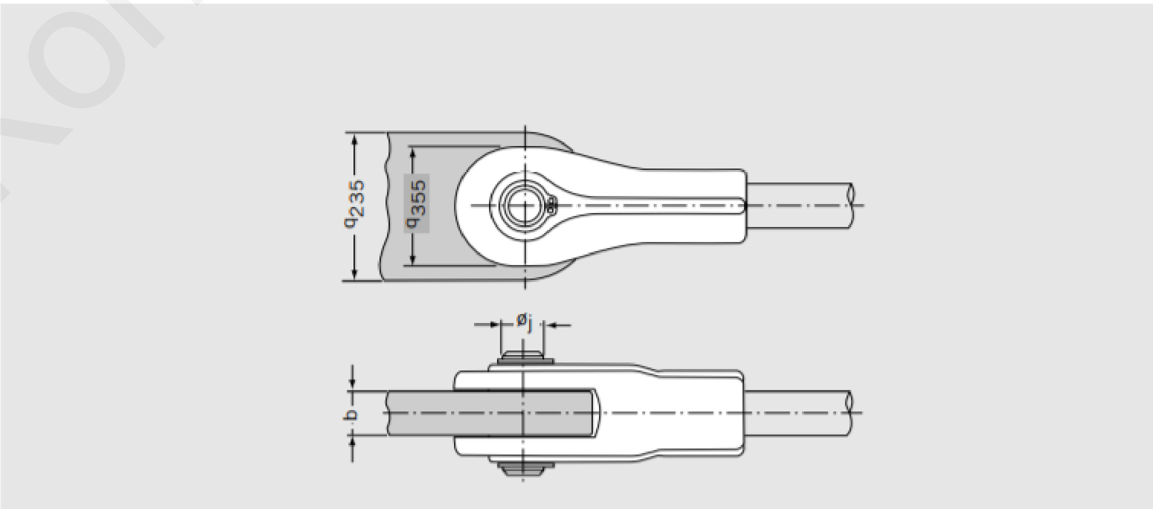

Konstantinos Petrou

These components were assembled in Solidworks with the help of command mates from the standard mates ("coincident", "concentric", "parallel"). The distance between the beams in the spatial model is 2 m, as well as the cylindrical pipes that connect them. Moreover, the spatial models in both cases consist of 10 planar linkages (see Fig. 4.16 and 4.17).

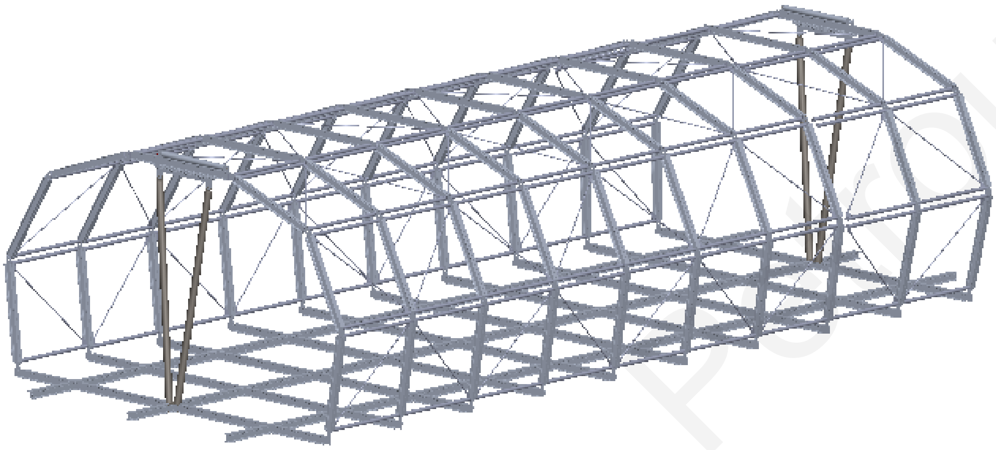

Figure 4.16: spatial model with V-shapes pipes in the center

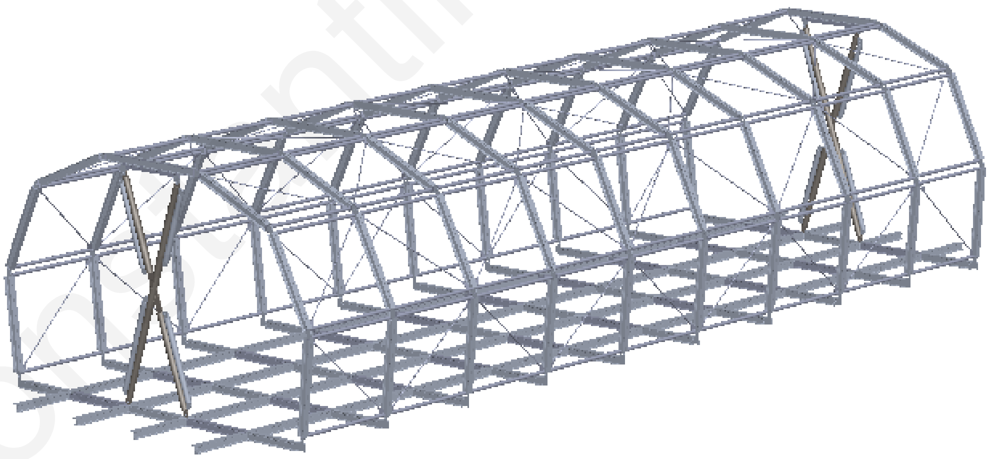

Figure 4.17: spatial model with X-shapes

After the spatial models have been assembled, they can be reconfigured using by the sequences and the final positions as defined before in the previous chapter. The implantation of the sequences along with the steps from the initial to the final positions appear below in spatial form.

Konstantinos Petrou

4.4.1 Sequence 1

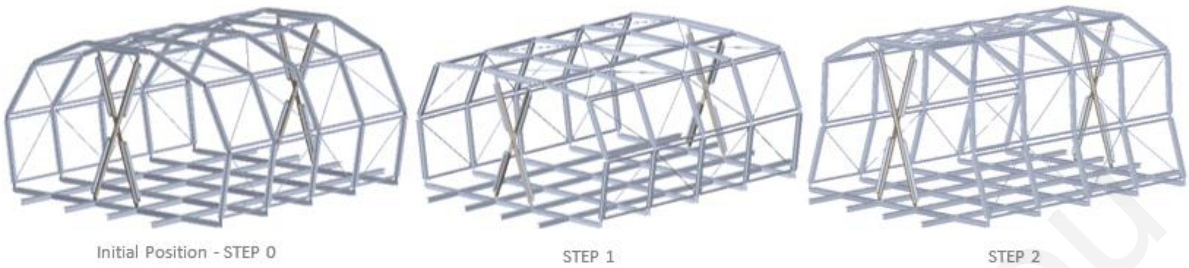

Figure 4.18: Spatial models with all steps of sequence 1

4.4.2 Sequence 2

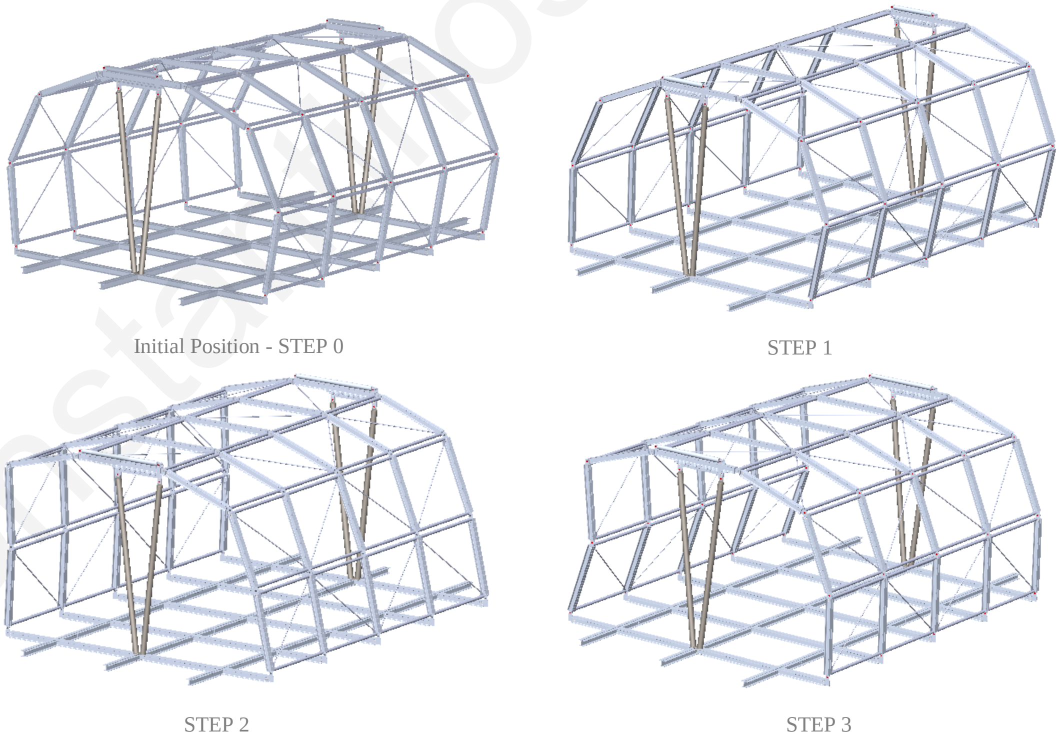

Figure 4.19: Spatial models with all steps of sequence 2

Konstantinos Petrou

4.4.3 Sequence 3

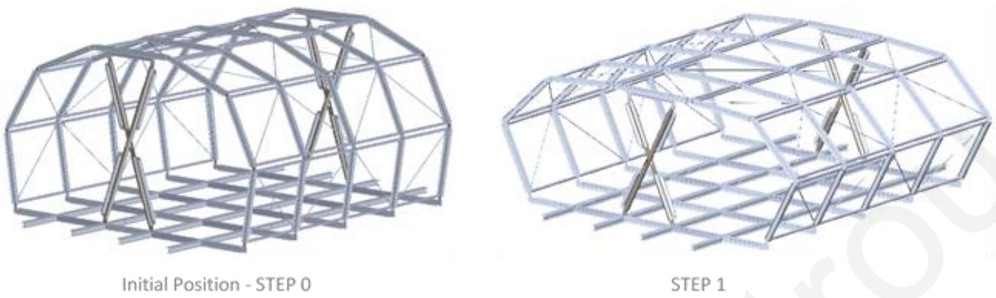

Figure 4.20: Spatial models with all steps of sequence 3

Konstantinos Petrou

Chapter 5

5 NUMERICAL SIMULATIONS

The numerical analysis of the structure was based on its kinematics and the implantation of the effective crank-slider reconfiguration approach. In the current stage, the analysis focuses on the motion analysis of the structure using Solidworks. Following the preliminary stage of determining the control sequences for implementing the required shape adjustment and the construction design, a new model has been created, based on the same geometric characteristics and dimensions of the basic system. New model because it requires minimal "mates" the software to calculate brakes torques. In addition, were entered the members and the materials of the structure. The model was created twice, a model for the case of the horizontal and vertical actuation motion, respectively.

The model was designed in the 3D drawing interface of the software and then all the data needed for the simulation were entered into the database (input data). First of all, was designed in the drawing interface the members of the structure and then with the assembly method, the initial position was developed. The linkages were connected with pins and the linkages and the steel plates, with nuts and bolts, according to the software library.

Also, the linkage for the actuator's position was created and with the assembly method and motor type the actuator was selected, for the structure's movement. The same procedure was followed for the modelling of the horizontal and vertical actuation system.

5.1 Configurations Analysis

Following the modelling of the horizontal and vertical motion system, the joint angles have been determined as below for the initial, intermediate and target positions of the systems, according to the respective control sequences for implementing the required shape adjustments. After the step of redefining the angles, the spatial models of the structure were created within the software interface, and a motion analysis was conducted.

Konstantinos Petrou

Sequence 1a (S1a)

STEP 0 [θ_1, θ_2, θ_3, θ_4, H_5, θ_6, θ_7, θ_8, θ_9] = [98°, 144.6°, 139°, 158.4°, 0m, 158.4°, 139°, 144.6°, 98°]

STEP 1 [θ_1, θ_2, θ_3, θ_4, H_5, θ_6, θ_7, θ_8, θ_9] = [98°, 148.25°, 118.5°, 175.3°, -0.5164m, 175.3°, 118.5°, 148.25°, 98°]

STEP 2 [θ_1, θ_2, θ_3, θ_4, H_5, θ_6, θ_7, θ_8, θ_9] = [72.3°, 194.65°, 118.5°, 154.5°, +0.7864m, 154.5°, 118.5°, 194.65°, 72.3°]

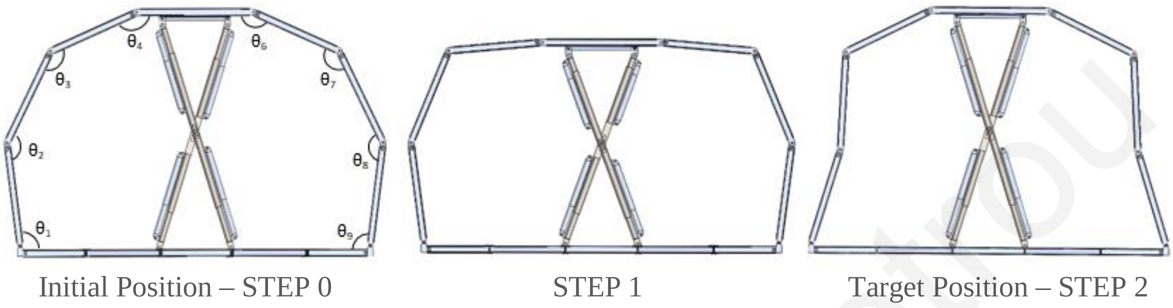

Figure 5.1: Structure Configurations for sequence 1a

Sequence 2a (S2a)

STEP 0 [θ_1, θ_2, θ_3, θ_4, H_5, θ_6, θ_7, θ_8, θ_9] = [98°, 144.6°, 139°, 158.4°, 0m, 158.4°, 139°, 144.6°, 98°]

STEP 1 [θ_1, θ_2, θ_3, θ_4, H_5, θ_6, θ_7, θ_8, θ_9] = [86.8°, 155.48°, 139°, 158.7°, +0.4786m, 159.85°, 131.13°, 144.6°, 104.4°]

STEP 2 [θ_1, θ_2, θ_3, θ_4, H_5, θ_6, θ_7, θ_8, θ_9] = [86.8°, 185.6°, 102°, 165.57°, -0.9407m, 160.2°, 131.13°, 171°, 77.7°]

STEP 3 [θ_1, θ_2, θ_3, θ_4, H_5, θ_6, θ_7, θ_8, θ_9] = [71.65°, 203.94°, 102°, 162.4°, +0.377m, 161.2°, 131.13°, 157.8°, 89.85°]

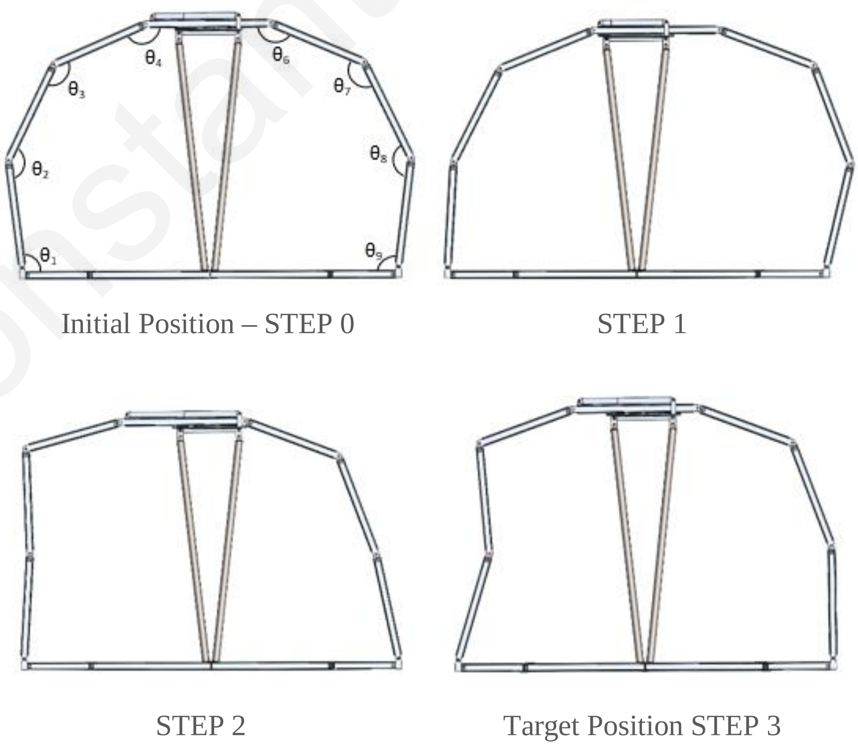

Figure 5.2: Structure Configurations for sequence 2a

Konstantinos Petrou

Sequence 3a ($S3_a$)

STEP 0 [θ_1, θ_2, θ_3, θ_4, H_5, θ_6, θ_7, θ_8, θ_9] = [98°, 144.6°, 139°, 158.4°, 0m, 158.4°, 139°, 144.6°, 98°]

STEP 1 [θ_1, θ_2, θ_3, θ_4, H_5, θ_6, θ_7, θ_8, θ_9] = [116.8°, 107.6°, 140.15°, 175.5°, -1.15m, 175.5°, 140.15°, 107.6°, 116.8°]

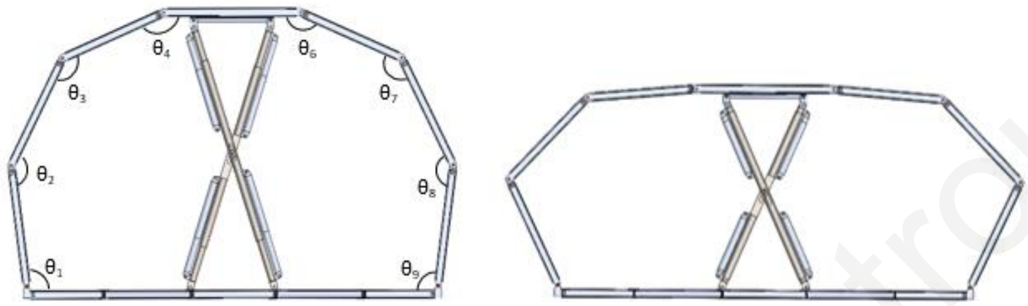

Initial Position – STEP 0 Target Position - STEP 1

Figure 5.3: Structure Configurations for sequence 3a

5.2 Motion Analysis

The torques determination in the joints throughout the transformation process, is crucial for the reconfiguration of the structure. This stage is divided into three sub-stages. First, the calculation process includes the definition of the angles of the joints for the initial and target positions, then the positions of the linkages that need to be locked by the mates list.

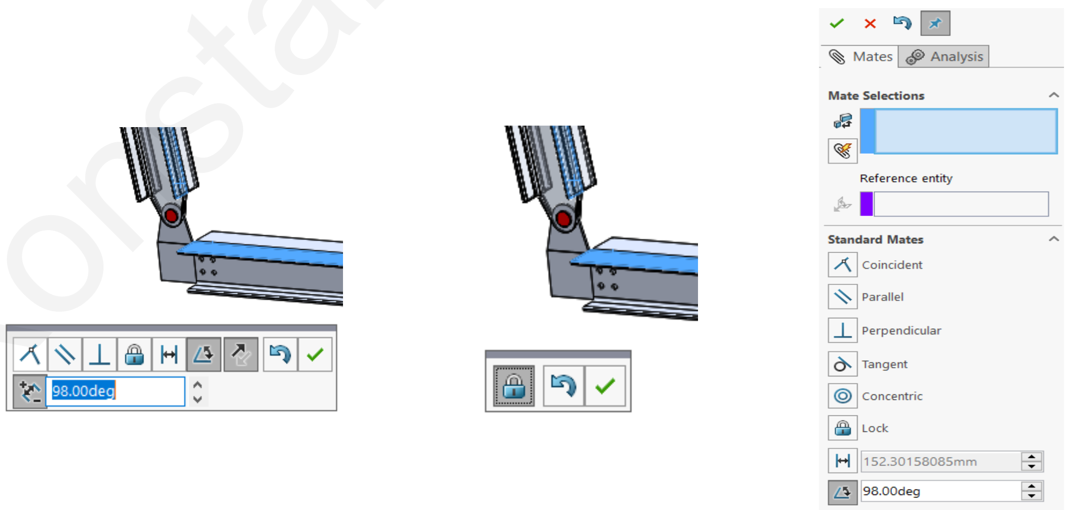

Figure 5.4: commands “Angle” and “Lock” from standard mates list

Konstantinos Petrou

The second stage is to select the type (servo motor) of the linear actuator from the library and the direction of the model (e.g., gravity). The direction of weight is defined based on the x, y, z axes, where as in this model the direction is downwards, corresponding to the y-axis.

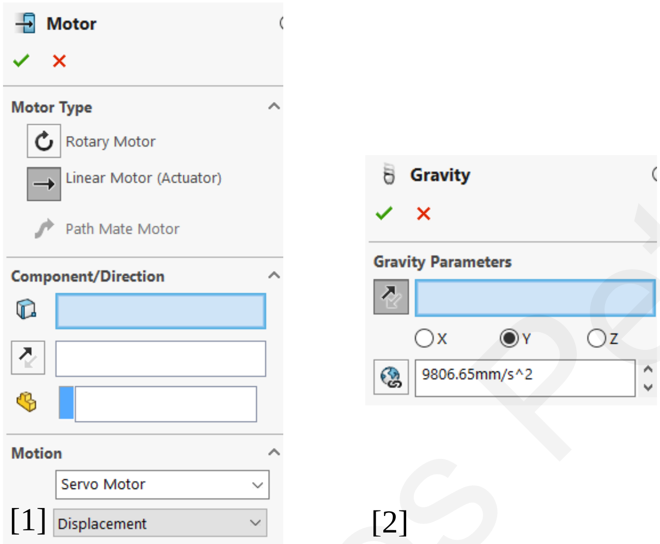

Figure 5.5: [1] definition of motor, [2] definition of gravity

The last step is about the actuator's displacement. According to the timeline data, the actuator is activated, and the steps of the displacement and the respective time are defined.

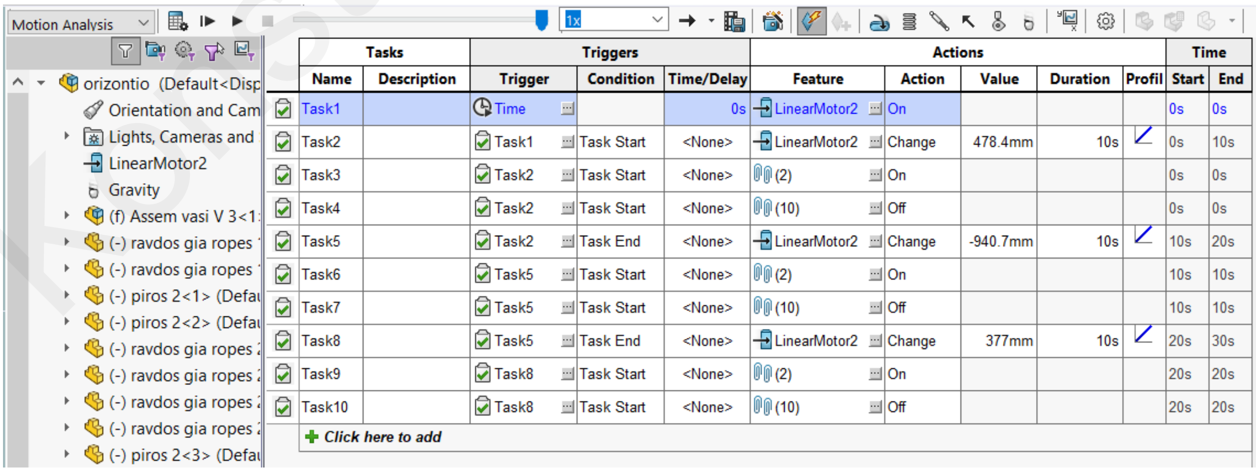

Tasks		Triggers			Actions					Time	
Name	Description	Trigger	Condition	Time/Delay	Feature	Action	Value	Duration	Profil	Start	End
Task1		Time		0s	LinearMotor2	On				0s	0s
Task2		Task1	Task Start	<None>	LinearMotor2	Change	478.4mm	10s		0s	10s
Task3		Task2	Task Start	<None>	(2)	On				0s	0s
Task4		Task2	Task Start	<None>	(10)	Off				0s	0s
Task5		Task2	Task End	<None>	LinearMotor2	Change	-940.7mm	10s		10s	20s
Task6		Task5	Task Start	<None>	(2)	On				10s	10s
Task7		Task5	Task Start	<None>	(10)	Off				10s	10s
Task8		Task5	Task End	<None>	LinearMotor2	Change	377mm	10s		20s	30s
Task9		Task8	Task Start	<None>	(2)	On				20s	20s
Task10		Task8	Task Start	<None>	(10)	Off				20s	20s

Figure 5.6: Specifying the model steps in the timeline view

Konstantinos Petrou

The actuator's movement to the top or to the right of the structure is signed with the symbol "+", in contrast of the movement to the bottom or the left side of the structure that is signed with the symbol "-". The velocity of the actuator movement is defined as the ratio of displacement over time (Dx/Dt). In addition, all the steps of the structure have been defined, so that all the torques on the joints are calculated and presented in the Results interface of the software in graphs.

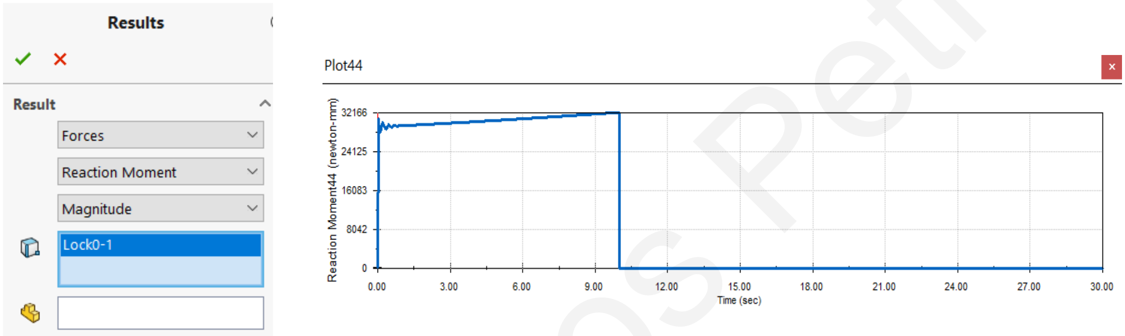

Figure 5.7: One example for calculation of torque graph using the "result" command

5.3 Numerical Results

The system configurations, as well as the brake torques and the displacements of the actuator have been determined, for both on the horizontal and the vertical actuation systems. Among different feasible sequences, the ones with less required steps are selected and investigated with regard to the highest maximum brake torques and slider displacements. Figs 5.1-5.3 illustrate the reaction moments on the joints, in each sequence. The reconfiguration steps have a duration of 10 seconds.

Sequence 1

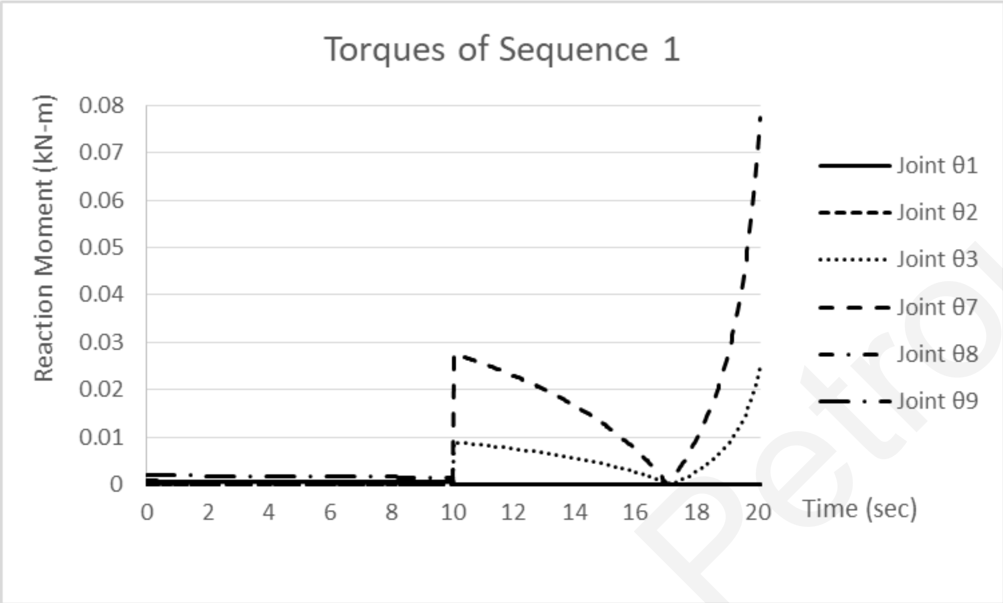

Graph 5.1: Brake torques of all Joints in Sequence 1

Sequence 2

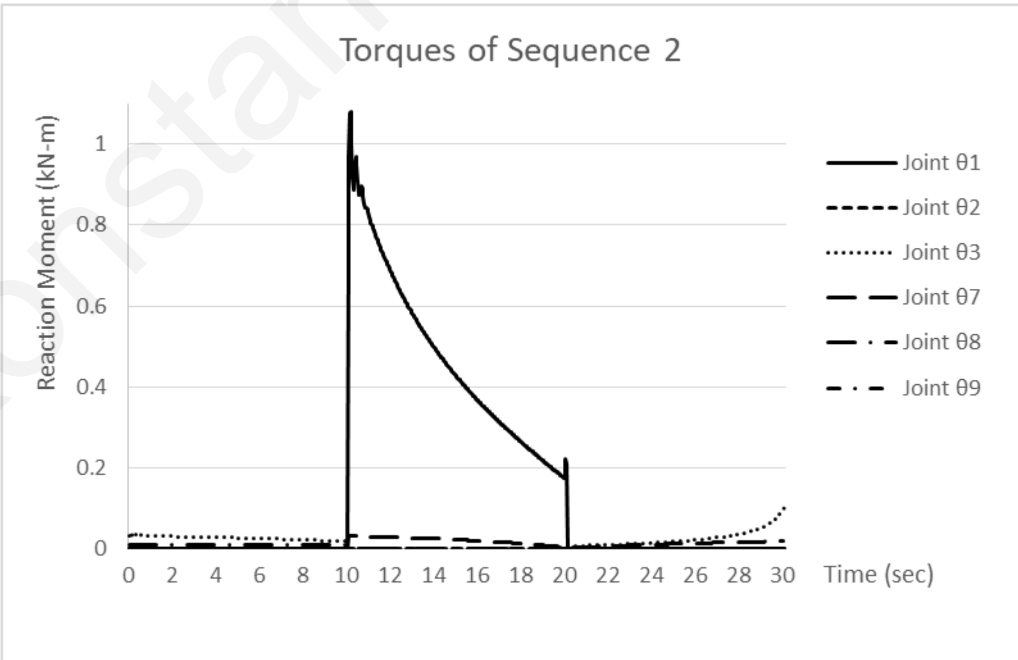

Graph 5.2: Brake torques of all Joints in Sequence 2

Konstantinos Petrou

Sequence 3

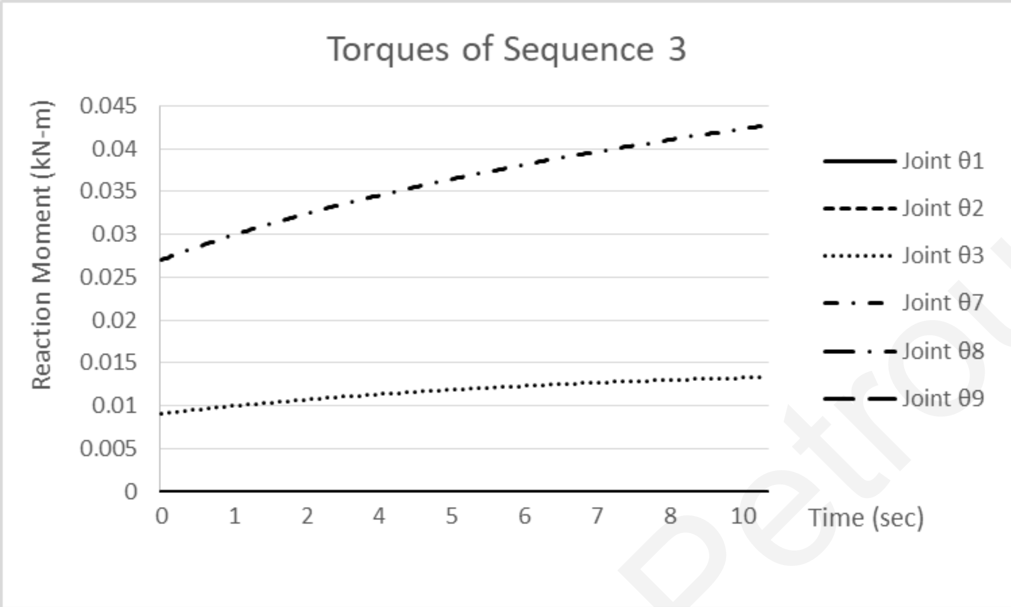

Graph 5.3: Brake torques of all Joints in Sequence 3

Table 5.1 shows the maximal brake torques on the joints, in each sequence. The maximum brake torques are registered in Sequence 2 and the minimum, in Sequence 3. The respective highest maximum value in Sequence 1 is about 7.7 kN-cm. In Sequence 2 and 3, the highest values amount to 108 kN-cm and 4.3 kN-cm, respectively. Moreover, in Sequence 2 is present the highest value of braking torques.

Table 5.1: Maximal brake torques

	Joint 1 θ_1 [kN.cm]	Joint 2 θ_2 [kN.cm]	Joint 3 θ_3 [kN.cm]	Joint 7 θ_7 [kN.cm]	Joint 8 θ_8 [kN.cm]	Joint 9 θ_9 [kN.cm]	Max Torque [kN.cm]
Seq. 1	0.0756	0	2.475	7.734	0	0.199	7.734
Seq. 2	107.944	0	10.220	3.111	0.913	0	107.944
Seq. 3	0	0	1.331	4.269	0	0	4.269

The required displacements of the sliding block have been recorded in Table 5.2. The maximum displacement in Sequences 1 and 2 is around 80 cm and 95 cm, respectively. In Sequence 3, the respective value amounts to 115 cm. Thus, Sequence 3 has the highest value of the sliding block displacement, in contrast to Sequence 1, which has the lowest.

Konstantinos Petrou

Table 5.2: Maximal displacement of sliding block

	Displacement STEP 1 [cm]	Displacement STEP 2 [cm]	Displacement STEP 3 [cm]	Maximum Displacement [cm]
Seq. 1	51.64	78.64	-	78.64
Seq. 2	47.86	94.07	37.70	94.07
Seq. 3	115	-	-	115

Konstantinos Petrou

Chapter 6

6 ACTUATION USING WIND ENERGY

The Dual Crank-Slider Mechanism with the actuator on the slider moves horizontally or vertically. The operation of the actuator requires power consumption to achieve their target positions. For reduced use of fossil fuels is proposed an idea to move the mechanism with a more energy efficient and environmental finally system. The movement of the mechanism is suggested to be done with a wind system with the help of fins. An aerodynamics analysis is followed with same basic equations to perform control in the case of the horizontal movement of the actuator.

6.1 Aerodynamics Background

Drag is the aerodynamic force that opposes motion through the air. It is generated by the difference in velocity between the solid object and the fluid. The drag is define as aerodynamic friction, and one of the sources of drag is the friction between the molecules of the air and the solid surface (Hall 2015a).

Drag depends on the density of the air, the square of the velocity, the air's viscosity and compressibility, the size and shape of the body, and the body's inclination to the flow. In general, the dependence on body shape, inclination, air viscosity, and compressibility is very complex, so it is simplified with an equation with dependence by a single variable. This variable is called the drag coefficient, designated "Cd" and it is almost always determined experimentally. For given air conditions, shape, and inclination of the object, we must determine a value for Cd to determine drag. The drag equation is:

$$\mathrm{D} = Cd * \frac{\rho * V^2}{2} * A$$

Where,

D: drag, Cd: coefficient, ρ: density, V: velocity, A: reference area

The area (A) in the drag equation is given as a reference area. The drag as being a resistance to flow, a more logical choice would be the frontal area of the body that is perpendicular to the flow direction. And finally, if compared with the lift coefficient, should be used the same wing area used to derive the lift coefficient. In practice, drag coefficients are reported based on a wide variety of object areas. In the report, it must be determined which area is used, since it may need to convert the drag coefficient using the ratio of the areas (Hall 2015b).

The relationship between drag coefficient and Reynolds number is shown in the diagram below.

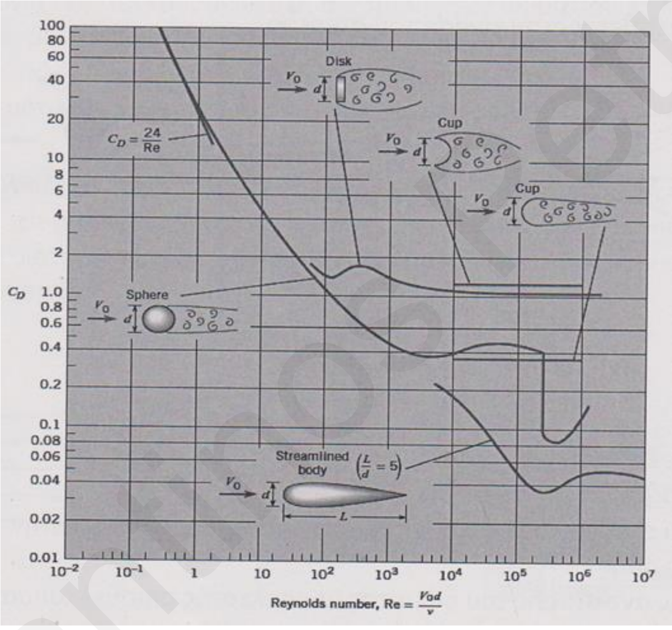

Graph 6.1: Diagram of the relationship between drag coefficient and Reynolds number Frank M. White, Fluid

Lift acts perpendicular to the flow direction. It contrasts with the drag force, which is the force parallel to the flow direction. Lift conventionally acts in an upward direction in order to counter the force of gravity, but it can act in any direction at right angles to the flow. Lift occurs when a moving flow of gas on a solid object according to Newton's Third Law (action and reaction). For lift to be generated, the solid body must be in contact with the fluid (Hall 2015c).

Lift depends on the density of the air, the square of the velocity, the air's viscosity and compressibility, the surface area over which the air flows, the shape of the body, and the body's inclination to the flow. In general, the dependence on body shape, inclination, air viscosity, and compressibility is very complex, so it is simplified by an equation with dependence by a single variable. This variable is called the “lift coefficient”, designated "Cl" and in general, this coefficient is determined experimentally. The lift equation is:

$$\mathrm{L} = Cl * \frac{\rho * V^2}{2} * A$$

Where,

L: lift, Cl: coefficient, ρ: density, V: velocity, A: wing area

For given air conditions, shape, and inclination of the object, we must determine a value for Cl to determine lift. For some simple flow conditions and geometries and low inclinations, aerodynamicists can determine the value of Cl mathematically. The lift coefficient is a dimensionless coefficient that relates the lift generated by a lifting body to the fluid density around the body, the fluid velocity and an associated reference area. The Cl is a function of the angle of the body to the flow, its Reynolds number and it’s Mach number. The relationship between section lift coefficient and angle of attack and shown in the diagram below (Hall 2015d).

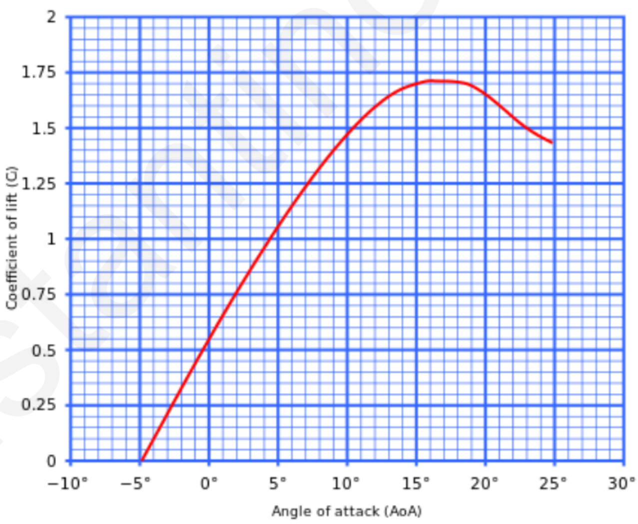

Graph 6.2: A typical curve showing section lift coefficient versus angle of attack (Wikipedia 2020)

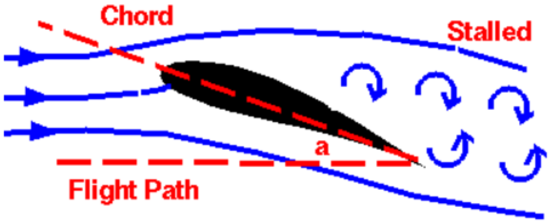

Figure 6.1: Angle of attack (Hall 2018)

6.1.1 Proposed Solution for reduced Energy Consumption

It is proposed a construction solution based on similar examples applied on ships that use sails (fins) for assistance in their horizontal motion in a natural way. Then, it will be checked whether the specific hybrid example can be applied in this construction study of the Dual Crank-Slider Mechanism for its horizontal movement with the help of air in Cyprus and Europe. The wind helps the movement of the structure and electrical energy (motor) is used to rotate the fins, in order to change the direction of movement of the slider. A preliminary analysis is performed and a conceptual design is presented.

6.1.1.1 Example of Wind System

Wind assisted propulsion is the practice of decreasing the fuel consumption of a merchant vessel through the use of sails or some other wind capture device. The design of the specific wind system features four vertical rotating cylinders driven by electro motors which, together with the wind, provide 10 times the thrust of conventional sails. Thus, this system can also be implemented in the study mechanism. That is, with the help of the wind the mechanism will be a more energy efficient system.

Figure 6.2: Wind-assisted shipping (Seaspout 2012)

6.1.2 Meteorological Data

Initially, a review was made in the regions of Cyprus and Europe for wind speeds which exist at an altitude of ten meters. This way a check was made if the proposed solution can be supported and in which regions. The map of Cyprus in Fig. 6.3 highlights mean

Konstantinos Petrou

annual wind speeds at an altitude of ten meters. From the map can be identified the velocities with the highest percentages that exist and the maximum speeds. With these data were calculated the lift and drag forces for specific angles of the fins to check whether is feasible to apply the proposed wind system.

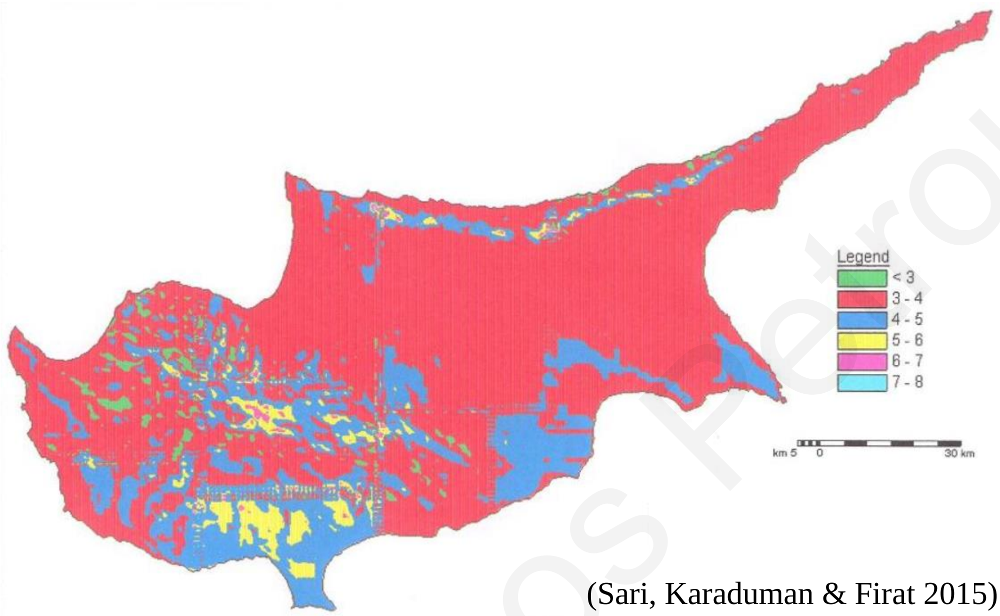

(Sari, Karaduman & Firat 2015)

Figure 6.3: Mean annual wind speeds at an altitude of ten meters in Cyprus

Next to the legend is the speeds by colour, with the highest speeds being in light blue and the smaller ones in green colour. Speeds are calculated in meters per second (m/s). For most areas (red area) in Cyprus it seems that the speeds are about 3-4 m/s. In Limassol dominates mainly the blue and to a lesser extent the yellow color, that is 4-5 m/s and 5-6 m/s, respectively. In general, the green appears in some areas near Morphou and pink least in Kyrenia, while the light blue is not visible in any area.

The map of Europe shows the wind speed in kilometers per hour (km/h) at an altitude of ten meters. According to the colors in the caption to the right of the map, it seems that a large percentage in Europe has wind speeds from 5-45 km/h. Also, it is noticed that there are more intense colors, in certain areas and therefore higher speeds. Converting velocities to the same units (m/s) so that they can be compared, common wind speeds in Europe are in the range of 1.4 – 12.5 m/s.

Konstantinos Petrou

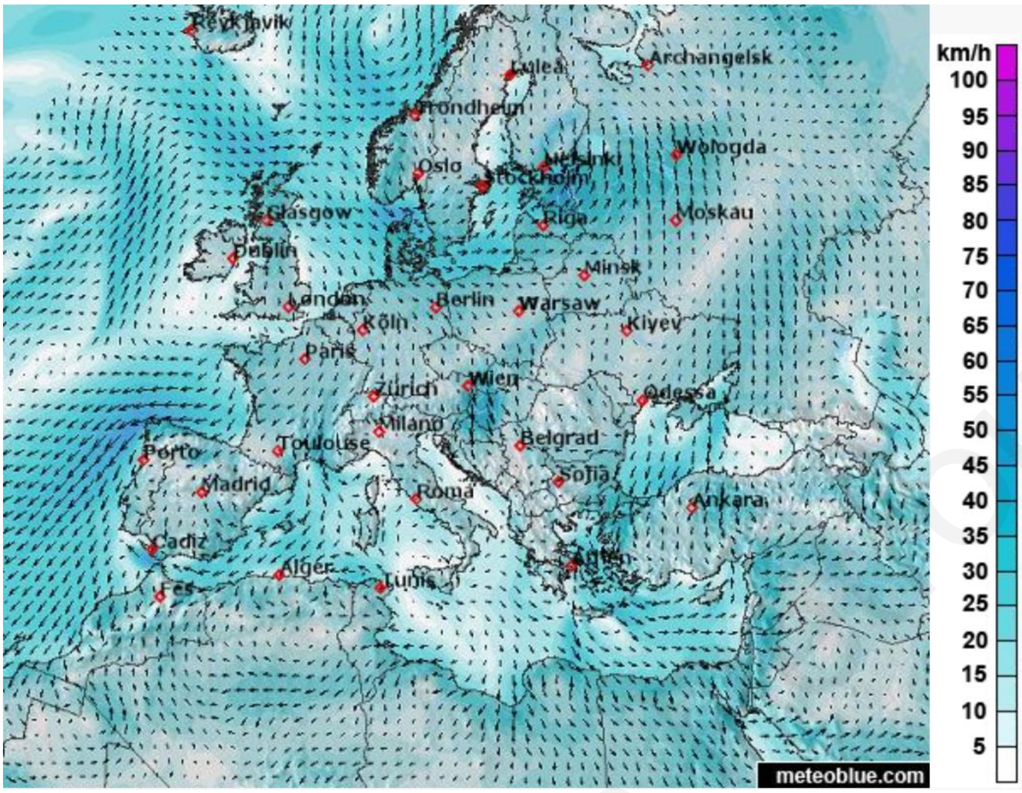

Figure 6.4: Mean annual wind speeds at an altitude of ten meters in Europe (Meteoblue 2020)

It is therefore observed that in general, in areas in Europe the winds reach higher speeds than in Cyprus. Studying the two maps of Cyprus and Europe, lift and drag forces are calculated for a range of speeds and a comparison is made in which regions this system can be applied. The speeds used to calculate the forces are 3.5, 4.5 and 5.5 m/s, where are the highest percentages prevailing in Cyprus and 15, 30 and 45 km/h (4.2, 8.3 and 12.5 m/s) for Europe.

After the meteorological review of Cyprus and Europe maps for the air speed, the Drag and Lift forces can be calculated. At first, the speeds presented in higher percentages in each map are selected for the calculation of the forces. Subsequently, it is calculated the projection area that the air is directed to for specific angles. The angles that were used for the calculation of the areas and forces are 5^o, 15^o and 25^o. So, the speeds and its angles of the fin were determined and the coefficient of drag and lift can be calculated with the help of graphs. The lift coefficient was calculated based on the angle as shown in Fig. 6.1, while the drag coefficient was calculated based on the Reynolds number. After calculating the Reynolds number, the Graph 6.1 was used to calculate the drag coefficient. In Graph 6.2 is used the shape of the corresponding fin as used on the proposed wind system. So, the coefficients of drag and lift were determined for each speed and then the corresponding forces were calculated. Below, the Lift and Drag forces are shown for three different angles (Nancy Hall 2015e; Wikipedia 2020; Nancy Hall 2018).

Table 6.1: Forces Lift and Drag in Cyprus and Europe for each fin, for three different angles

		Lift (N)			Drag (N)		
	Velocity (m/s)	Angle 5°	Angle 15°	Angle 25°	Angle 5°	Angle 15°	Angle 25°
Cyprus	3.5	5.67	13.12	16.00	0.35	0.50	0.72
	4.5	9.38	21.69	26.43	0.45	0.64	0.91
	5.5	14.00	32.40	39.48	0.60	0.86	1.23
Europe	4.2	8.17	18.89	23.02	0.47	0.67	0.95
	8.3	31.90	73.78	89.90	1.22	1.74	2.48
	12.5	72.35	167.34	203.91	2.62	3.74	5.34

Also, after the forces were calculated based on the speeds with the highest percentages on the maps, the maximum speeds that exist in both Cyprus and Europe were checked.

Table 6.2: Maximum forces Lift and Drag in Cyprus and Europe for each fin, for three different angles

		Lift (N)			Drag (N)		
	Velocity (m/s)	Angle 5°	Angle 15°	Angle 25°	Angle 5°	Angle 15°	Angle 25°
Cyprus	7.0	22.69	52.48	63.95	0.86	1.23	1.76
Europe	23.6	257.90	596.50	726.80	9.30	13.30	19.05

Based on the above results, it is clear that as the air velocity increases, the forces are greater. Also, as the fins angle increases, the forces seem to increase. This is expected since with the increase of the angle, the projection area increases. Still, it is observed that the Lift forces are much larger than the Drag forces. This is positive as the Drag force does not contribute towards the movement of the structure. These remarks are clearly demonstrated in the diagrams below.

Konstantinos Petrou

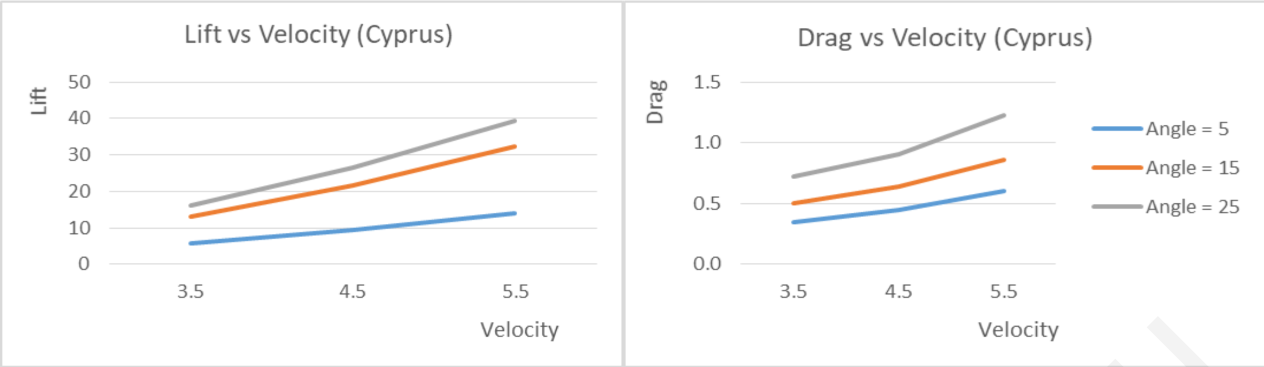

Graph 6.4: Forces Lift and Drag in Cyprus for each fin, for three different angles

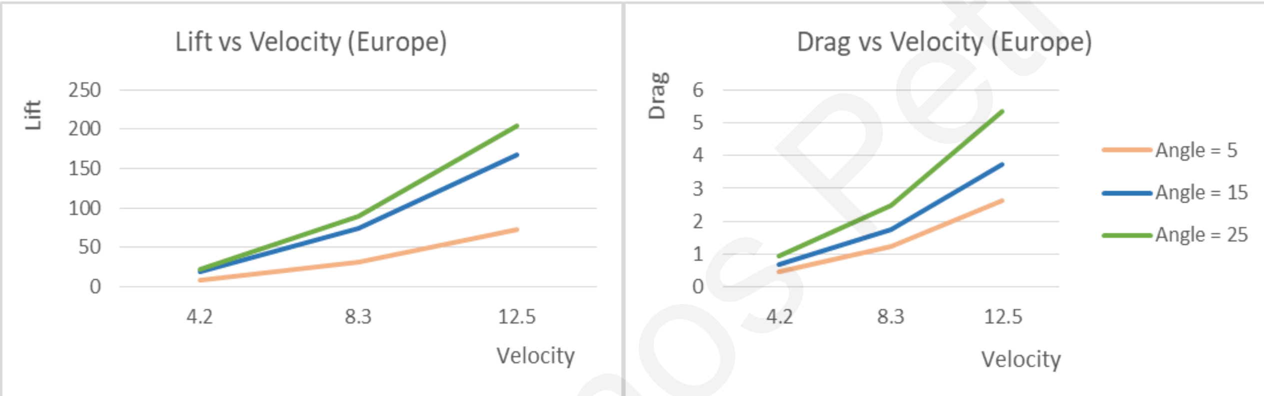

Graph 6.3: Forces Lift and Drag in Europe for each fin, for three different angles

Observing tables and graphs, the best scenario to move the structure is when, the fins angle is 25^o since it provides the biggest lift forces. Nevertheless, this angle has given the biggest drag forces, but the drag forces are much smaller than lift forces. Also, greater force result when the structure is located in the areas with the biggest speeds. Therefore, the wind system would give better results for the movement of the structure in the mountainous areas of Cyprus and in north Europe with fins angle 25^o.

After the forces were checked for different projection areas (depending on the angle of the fin) of the fins, follows the construction of a 3D model in Solidworks of the proposed system. Initially, the fin was made with symmetrical shape with a ratio of dimensions of length and width equal to five, as shown in Graph 6.1.

Konstantinos Petrou

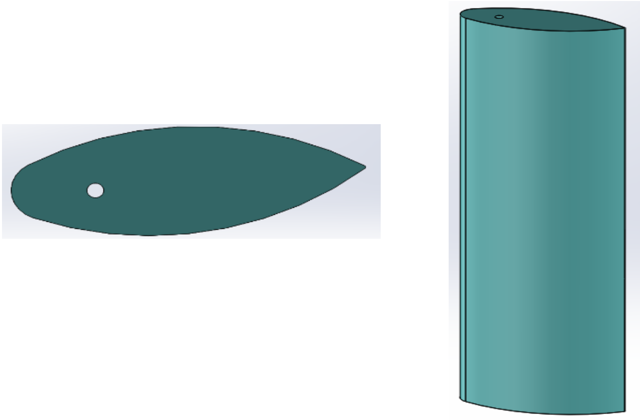

Figure 6.5: Type of fin

Then, the proposed mechanism was designed which allows the fins to rotate. One central axis was placed where it is connected to bearings with the fin and a gears system under the base. Four fins were included in the construction, so that the lift force increases by four times and the structure can move with the help of the wind (shown in Fig. 6.6).

Figure 6.6: Assembly of four fins on the central base

Each fin is connected to a central axis according to the above and it is connected between them with gears, so that with the movement of one, to move all the rest in parallel. The movement to change their angle is done with a motor that it is placed on one of the fins. The consumed energy of the motor is negligible, since the movement of the fins angles are minimal.

Konstantinos Petrou

The connection at the bottom of the base (see in Fig. 6.7) can be done in different ways. That is, the fins not only can be rotated using gears, but they can be connected with a combination of chain and sprockets or with a belt and pulleys. The base of system has a base at the bottom for the mounting of the motor (shown in Fig. 6.8).

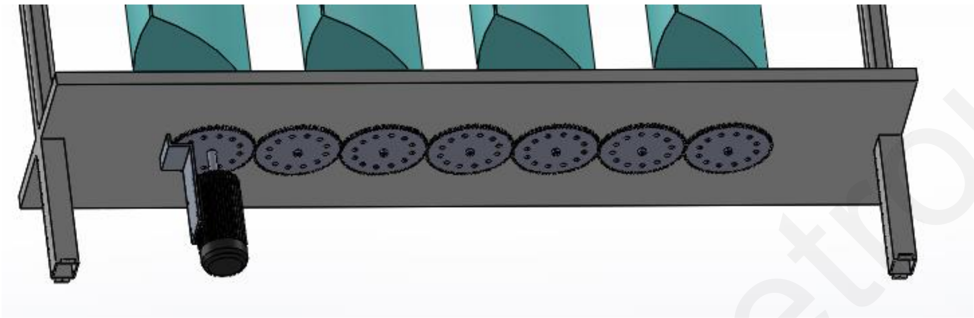

Figure 6.7: Gear connection for parallel drive, motor for fins drive and base connections

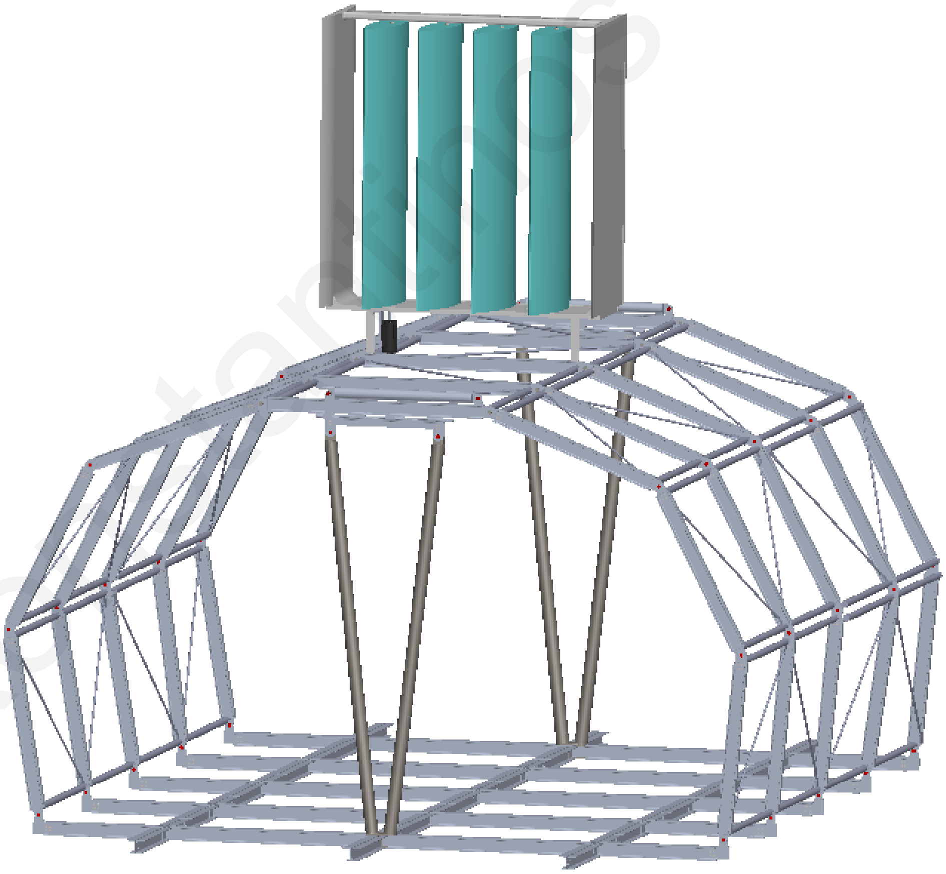

Figure 6. 8: Aerodynamic system assembled in the construction (conceptual design)

Konstantinos Petrou

Chapter 7

7 SOLAR GAIN AND LIGHTING SIMULATIONS

The selection of an appropriate building shape can be on the basis of external conditions. The solar gain and lighting condition inside the building is one of the factors that may drive reconfigurations.

Solar gain is the increase in thermal energy of a space or structure as it absorbs incident solar radiation. The amount of solar gain a space experiences is a function of the total incident solar irradiance and of the ability of any intervening material to transmit or resist the radiation. Objects struck by sunlight absorb its visible irradiation, increase in temperature, and then re-radiate that heat. The transparent building materials, such as glass, allow visible light to pass through almost unimpeded, once that light is converted to long-wave infrared radiation by materials indoors. The trapped heat thus causes solar gain via a phenomenon known as the "greenhouse effect". In buildings, excessive solar gain can lead to overheating within a space, but it can also be used as a passive heating strategy when heat is desired. Passive solar heating is a design strategy that attempts to maximize the amount of solar gain in a building when additional heating is desired. Reconfigurable buildings have the potential to take a form for maximum solar gain in winter and minimum solar gain in summer (Wikipedia 2021a).

The source of all daylight is the Sun. The proportion of direct to diffuse light impacts the amount and quality of daylight. Daylighting is the practice of placing windows, skylights, other openings, and reflective surfaces so that sunlight can provide effective internal lighting. Particular attention is given to daylighting while designing a building when the aim is to maximize visual comfort or to reduce energy use. Energy savings can be achieved from the reduced use of artificial lighting or from passive solar heating (Wikipedia 2021b).

The analysis of the solar gain and lighting conditions in relation to the motion of the sun will be investigated using software simulations in relation to the proposed reconfigurable structure and its reconfiguration capabilities. This further high lights the importable of reconfigurable buildings.

The structures were first checked for their functionality. The systems are closed everywhere with metal plates of thickness 2 mm and between them there is an

Konstantinos Petrou

insulating material, of thickness 90 mm. The structure floor is wooden and there are two single clear windows, of thickness 3 mm, one on each side.

Firstly, the analysis results take place in the climatic conditions of Larnaca, Cyprus with latitude: 34.923 and Longitude: 33.634, where for almost eight months of the year the sky is clear and there is high solar radiation.

According to the Department of Meteorology of Cyprus, the region of Larnaca has mild winters and warm to hot summers, with temperatures ranging from 7 °C to 33 °C, respectively. Also, the sunhours do not touch rates under the 180 hours during the winter months (Weather and Climate 2021).

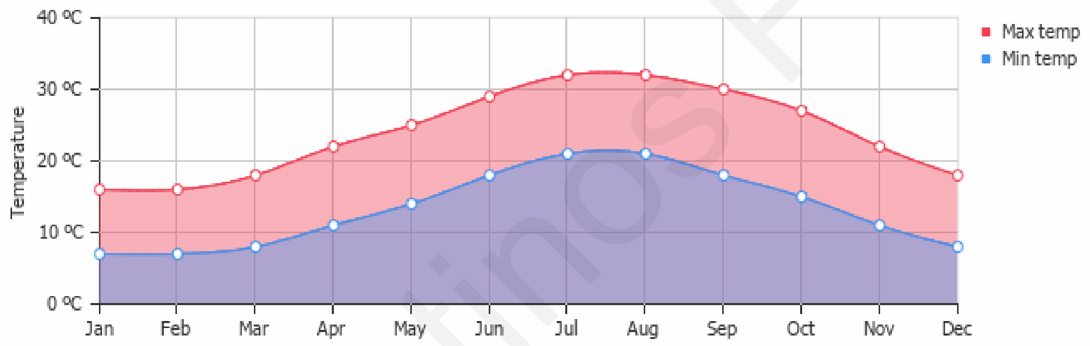

Graph 7.1: Average min and max temperatures in Larnaca, Cyprus

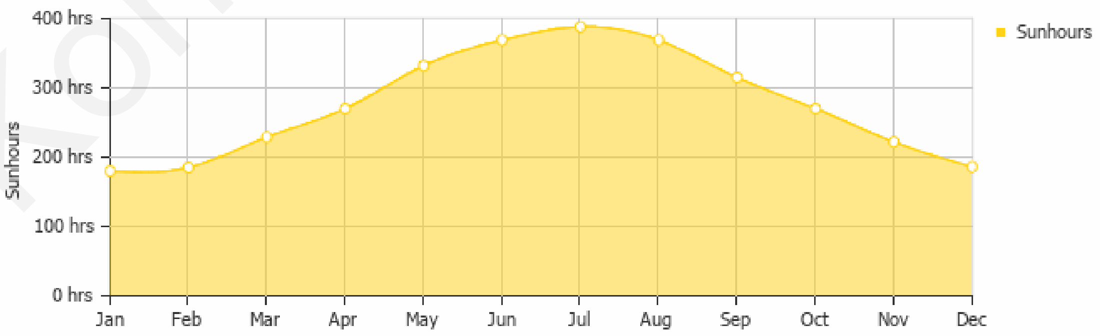

Graph 7.2: Average sunhours over the year in Larnaca, Cyprus

Konstantinos Petrou

The model was designed in the 3D drawing interface in the dynamic simulation software Energy Plus through the platform Design Builder and then all the data needed for the simulation were entered into the database (building materials, location). All HVAC systems and artificial lighting were deactivated. First of all, was designed in the drawing interface the initial position of the model and then the three target positions.

Through the simulation analysis, solar gain measurements and lighting results are presented. The incidence of solar radiation in the structures affect both measurements.

After the meteorological analysis of the area, the diagrams of the incidence of solar radiation in the structures (initial position and in three target positions) are presented in the morning (8:00 am), at noon (12:00 pm) and in the afternoon (15:00 pm). The case study refers to the solstices that occur annually, on the 21st of December, 21st of March, 21 space June and the 21st of September (see Fig. 7.1 – Fig. 7.16).

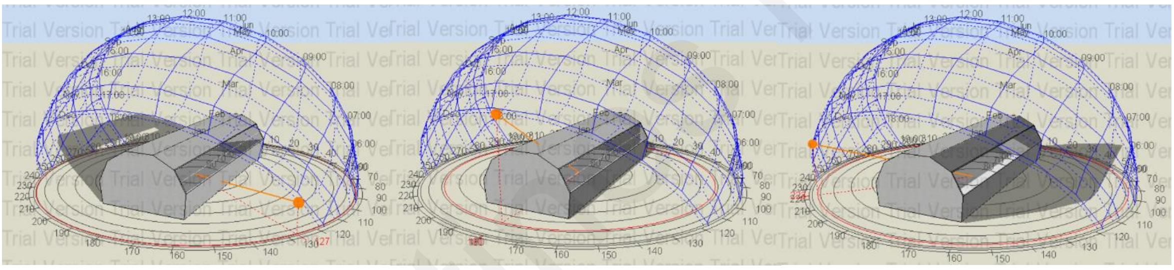

8:00 am 12:00 pm 15:00 pm

Figure 7.1: Incidence of solar radiation in the initial position on the 21^{st} of December

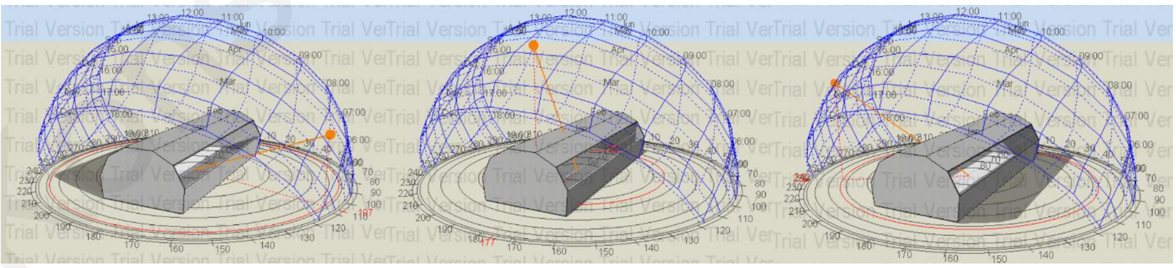

8:00 am 12:00 pm 15:00 pm

Figure 7.2: Incidence of solar radiation in the initial position on the 21^{st} of March

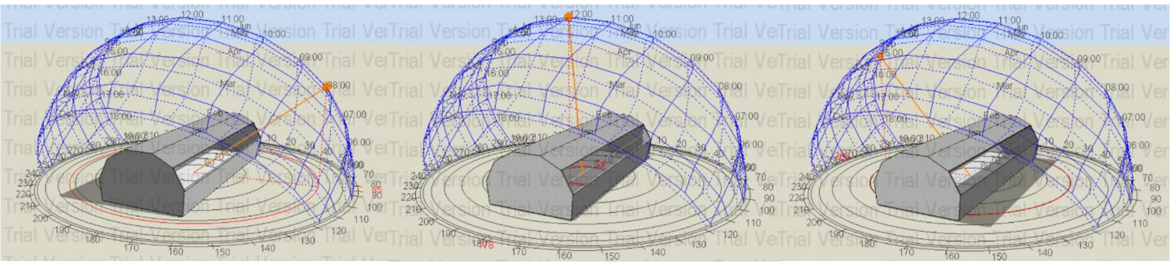

8:00 am 12:00 pm 15:00 pm

Figure 7.3: Incidence of solar radiation in the initial position on the 21st of June

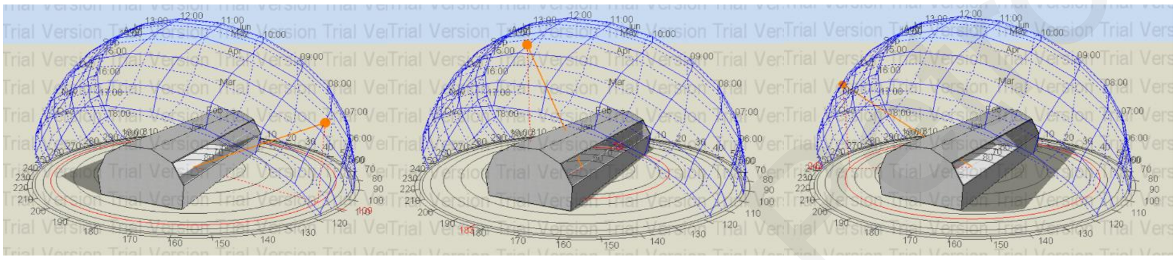

8:00 am 12:00 pm 15:00 pm

Figure 7.4: Incidence of solar radiation in the initial position on the 21st of September

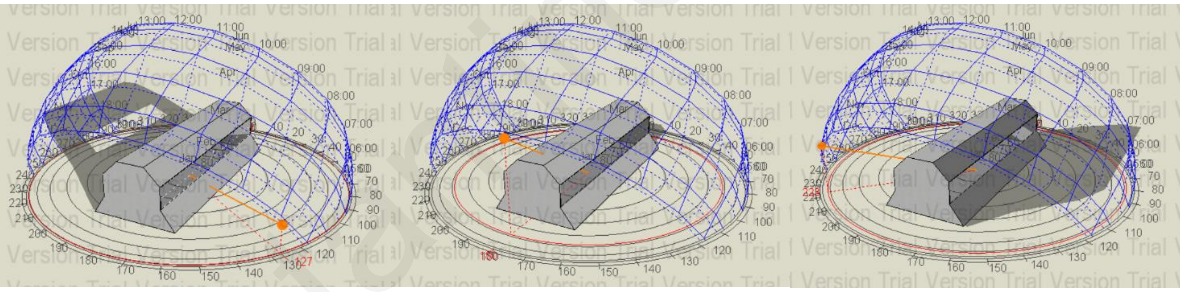

8:00 am 12:00 pm 15:00 pm

Figure 7.5: Incidence of solar radiation in the target position 1 on the 21st of December

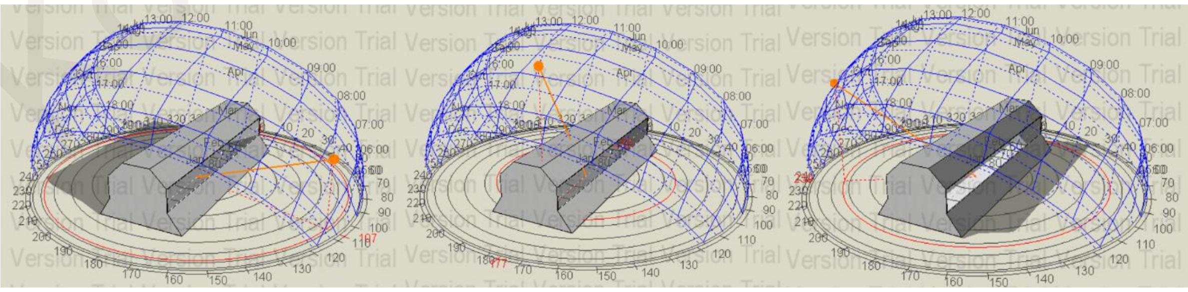

8:00 am 12:00 pm 15:00 pm

Figure 7.6: Incidence of solar radiation in the target position 1 on the 21st of March

Konstantinos Petrou

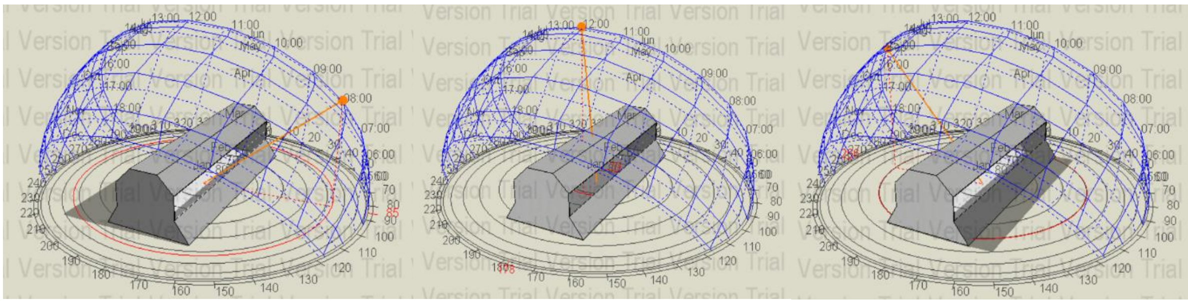

8:00 am 12:00 pm 15:00 pm

Figure 7.7: Incidence of solar radiation in the target position 1 on the 21st of June

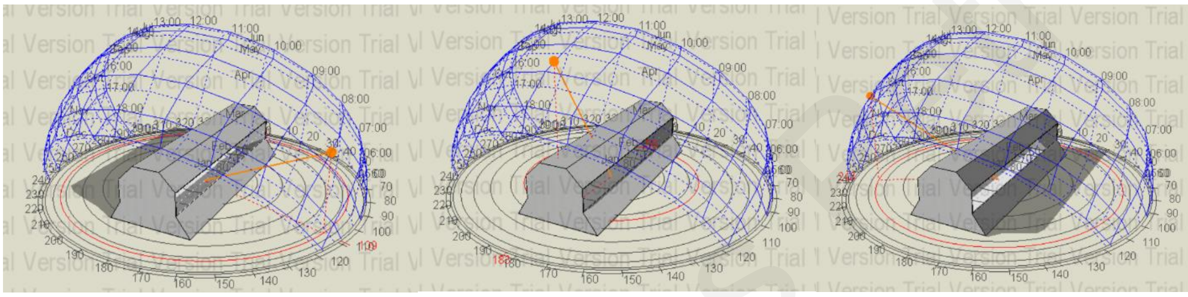

8:00 am 12:00 pm 15:00 pm

Figure 7.8: Incidence of solar radiation in the target position 1 on the 21st of September

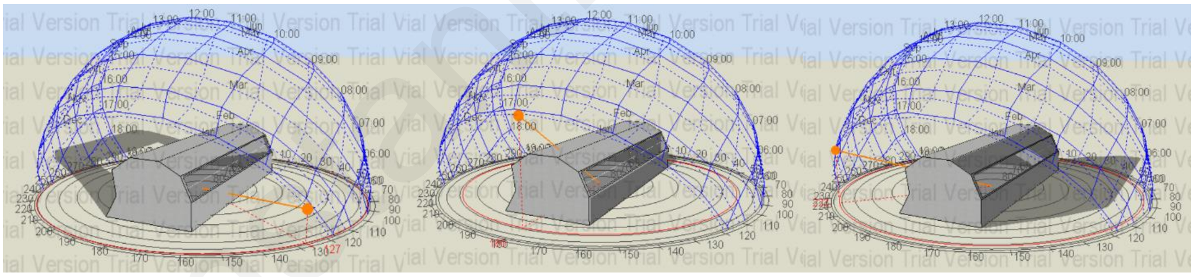

8:00 am 12:00 pm 15:00 pm

Figure 7.9: Incidence of solar radiation in the target position 2 on the 21st of December

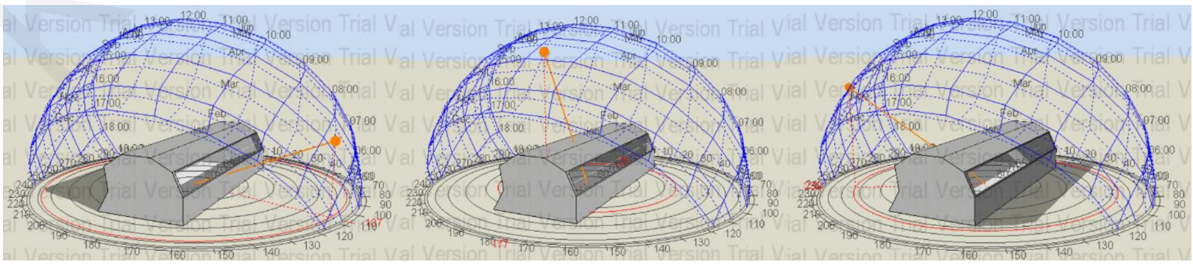

8:00 am 12:00 pm 15:00 pm

Figure 7.10: Incidence of solar radiation in the target position 2 on the 21st of March

Konstantinos Petrou

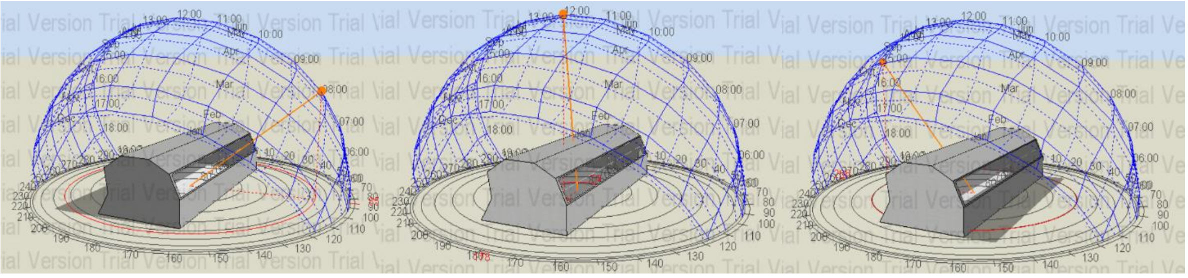

8:00 am 12:00 pm 15:00 pm

Figure 7.11: Incidence of solar radiation in the target position 2 on the 21st of June

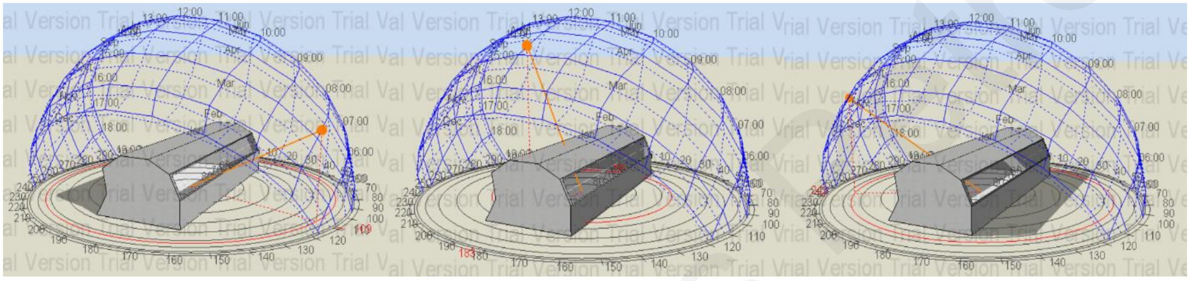

8:00 am 12:00 pm 15:00 pm

Figure 7.12: Incidence of solar radiation in the target position 2 on the 21st of September

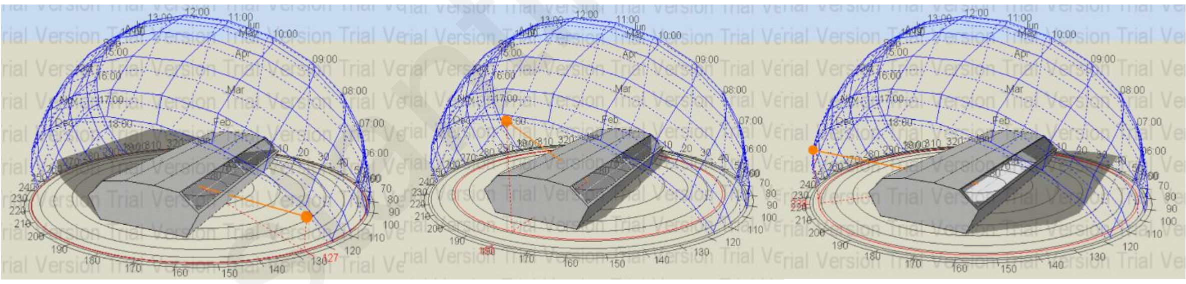

8:00 am 12:00 pm 15:00 pm

Figure 7.13: Incidence of solar radiation in the target position 3 on the 21st of December

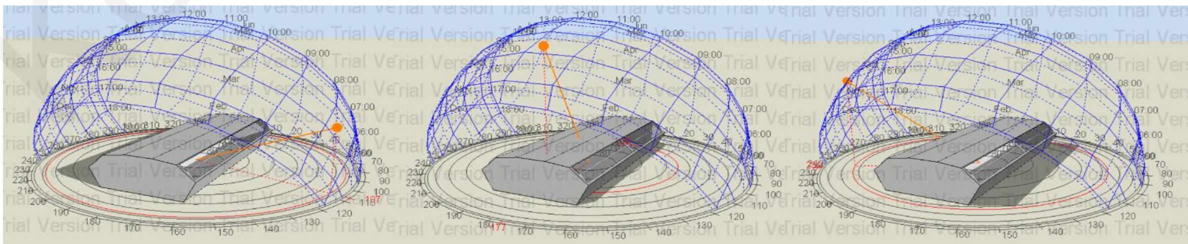

8:00 am 12:00 pm 15:00 pm

Figure 7.14: Incidence of solar radiation in the target position 3 on the 21st of March

Konstantinos Petrou

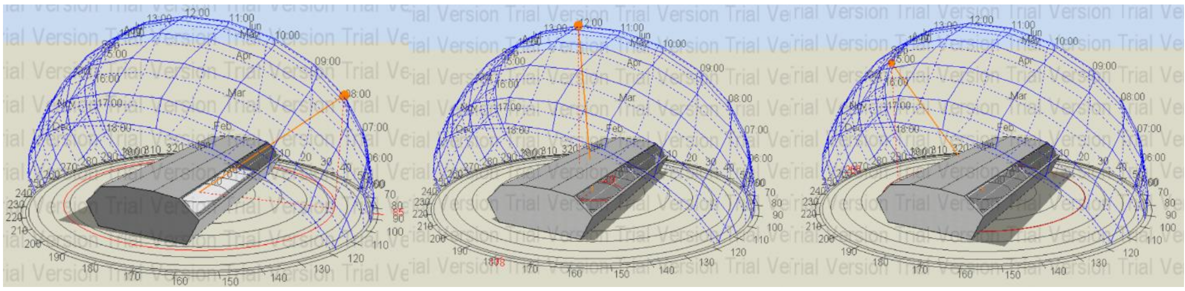

8:00 am　　　　12:00 pm　　　　15:00 pm

Figure 7.15: Incidence of solar radiation in the target position 3 on the 21st of June

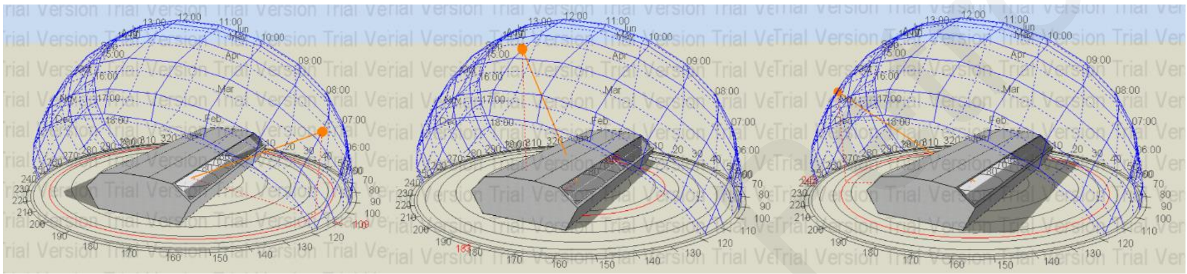

8:00 am　　　　12:00 pm　　　　15:00 pm

Figure 7.16: Incidence of solar radiation in the target position 3 on the 21st of September

Furthermore, the structures were checked as above in a vertical orientation (0^o site orientation) and when they are in horizontal orientation (90^o site orientation). Shown below are the diagrams of the incidence of solar radiation in the structures (initial position and in three target positions) in the morning (8:00 am), at noon (12:00 pm) and in the afternoon (15:00 pm). The case study refers to the solstices that occur annually, on the 21st of December, 21st of March, 21st of June and the 21st of September and when the structure is in horizontal orientation (see Fig.7.17 – Fig 7.32).

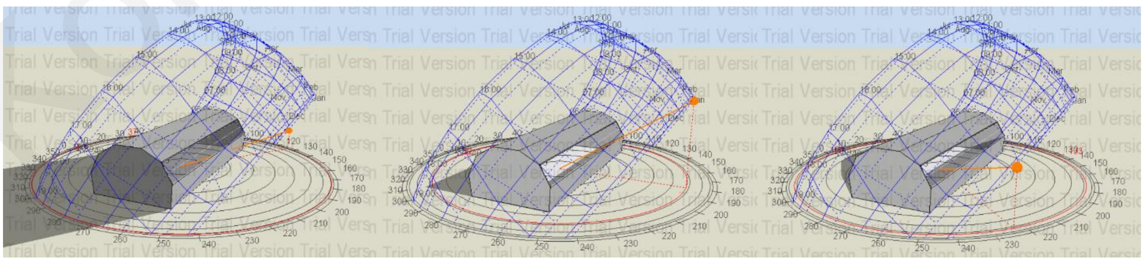

8:00 am　　　　12:00 pm　　　　15:00 pm

Figure 7.17: Incidence of solar radiation in the initial position on the 21st of December

Konstantinos Petrou

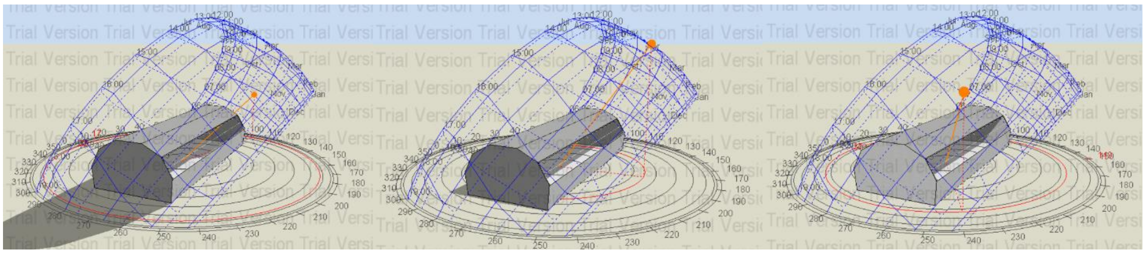

8:00 am | 12:00 pm | 15:00 pm

Figure 7.18: Incidence of solar radiation in the initial position on the 21st of March

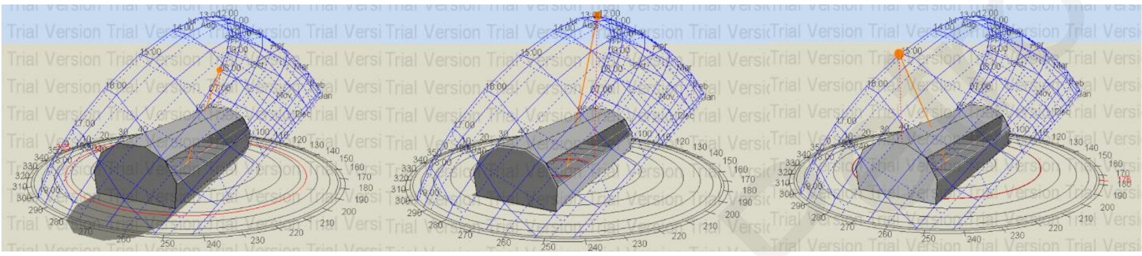

8:00 am | 12:00 pm | 15:00 pm

Figure 7.19: Incidence of solar radiation in the initial position on the 21st of June

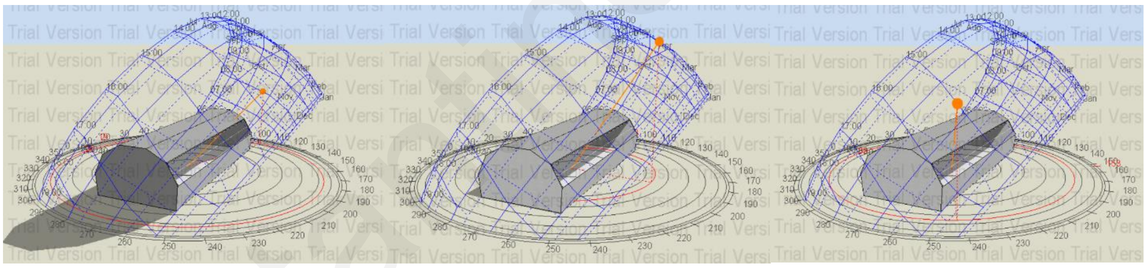

8:00 am | 12:00 pm | 15:00 pm

Figure 7.20: Incidence of solar radiation in the initial position on the 21st of September

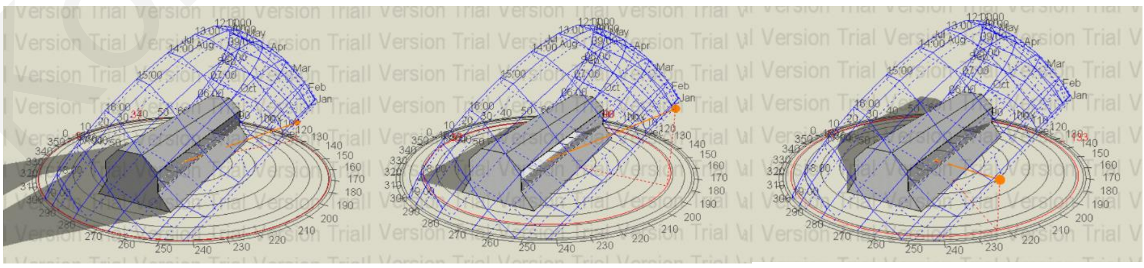

8:00 am | 12:00 pm | 15:00 pm

Figure 7.21: Incidence of solar radiation in the target position 1 on the 21st of December

Konstantinos Petrou

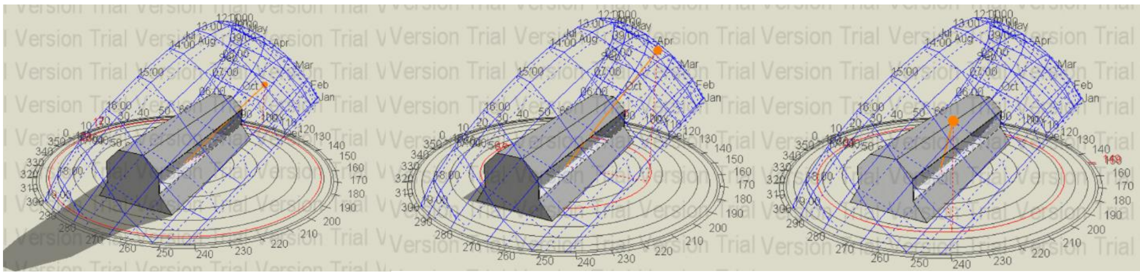

8:00 am 12:00 pm 15:00 pm

Figure 7.22: Incidence of solar radiation in the target position 1 on the 21st of March

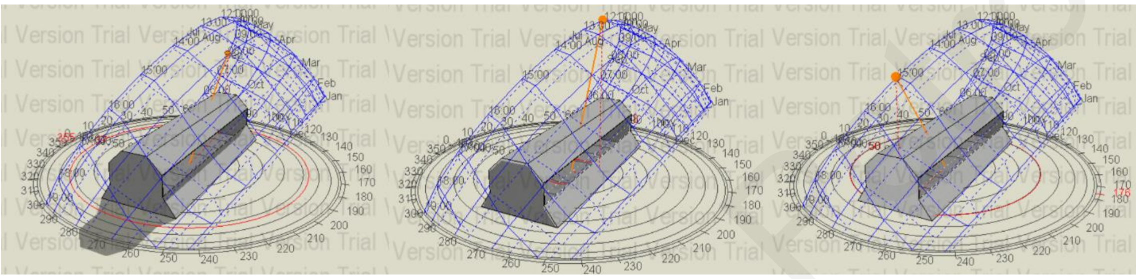

8:00 am 12:00 pm 15:00 pm

Figure 7.23: Incidence of solar radiation in the target position 1 on the 21st of June

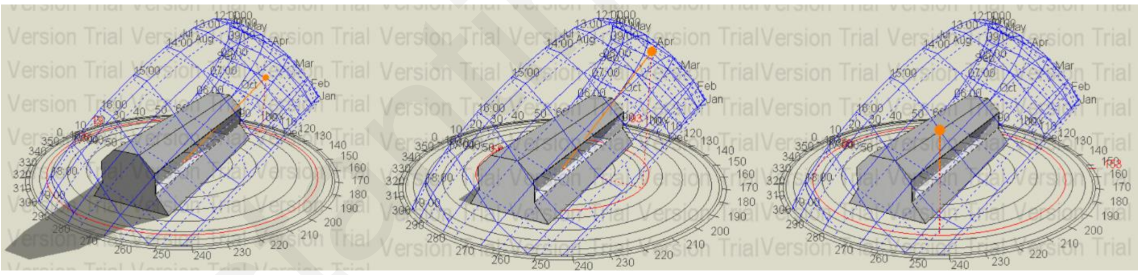

8:00 am 12:00 pm 15:00 pm

Figure 7.24: Incidence of solar radiation in the target position 1 on the 21st of September

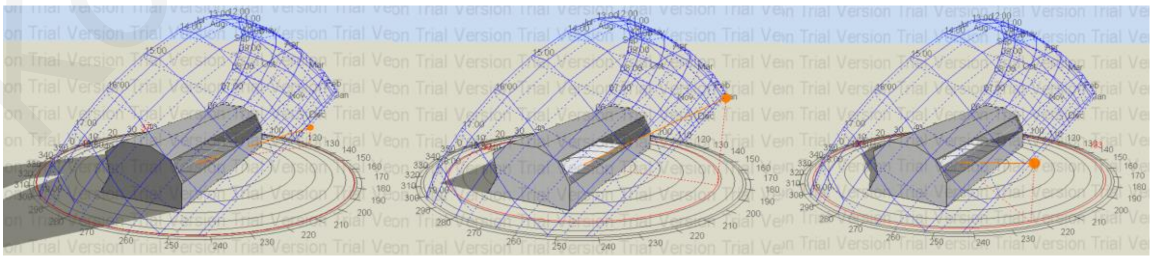

8:00 am 12:00 pm 15:00 pm

Figure 7.25: Incidence of solar radiation in the target position 2 on the 21st of December

Konstantinos Petrou

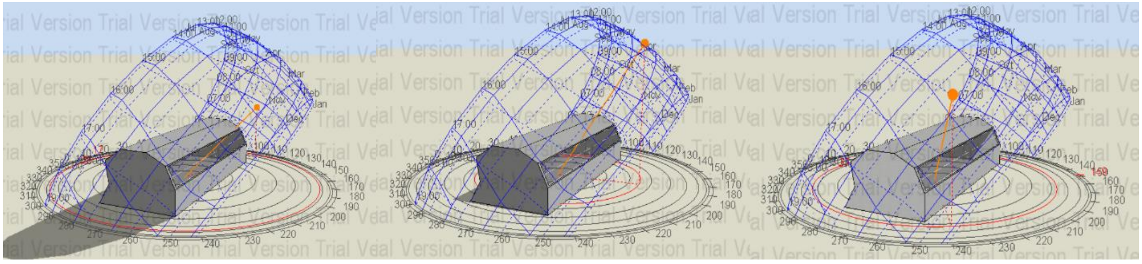

8:00 am 12:00 pm 15:00 pm

Figure 7.26: Incidence of solar radiation in the target position 2 on the 21st of March

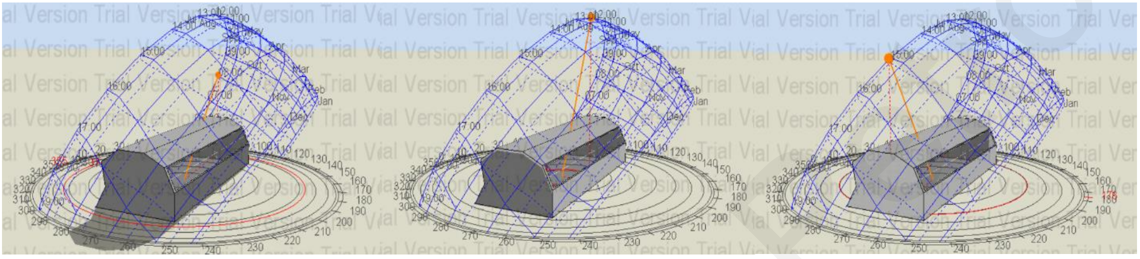

8:00 am 12:00 pm 15:00 pm

Figure 7.27: Incidence of solar radiation in the target position 2 on the 21st of June

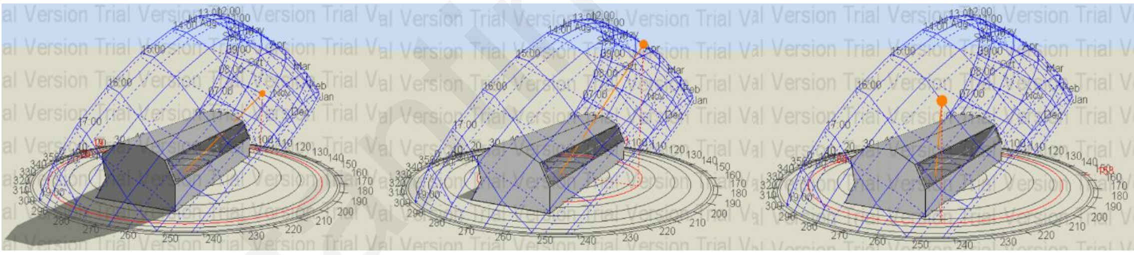

8:00 am 12:00 pm 15:00 pm

Figure 7.28: Incidence of solar radiation in the target position 2 on the 21st of September

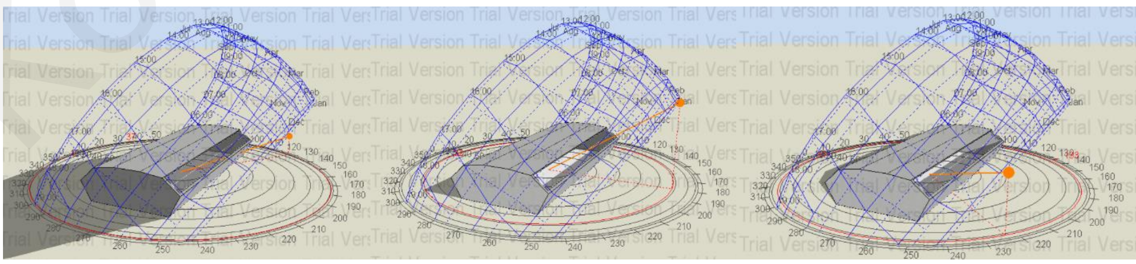

8:00 am 12:00 pm 15:00 pm

Figure 7.29: Incidence of solar radiation in the target position 3 on the 21st of December

Konstantinos Petrou

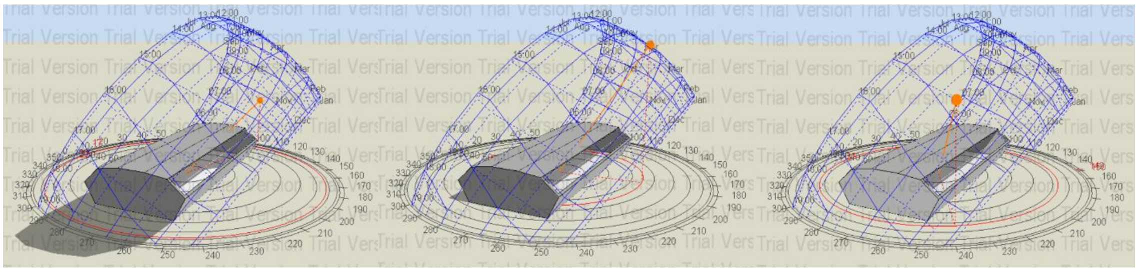

8:00 am 12:00 pm 15:00 pm

Figure 7.30: Incidence of solar radiation in the target position 3 on the 21st of March

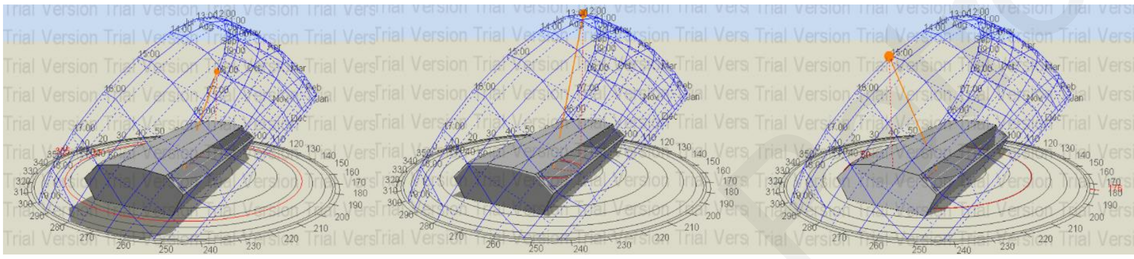

8:00 am 12:00 pm 15:00 pm

Figure 7.31: Incidence of solar radiation in the target position 3 on the 21st of June

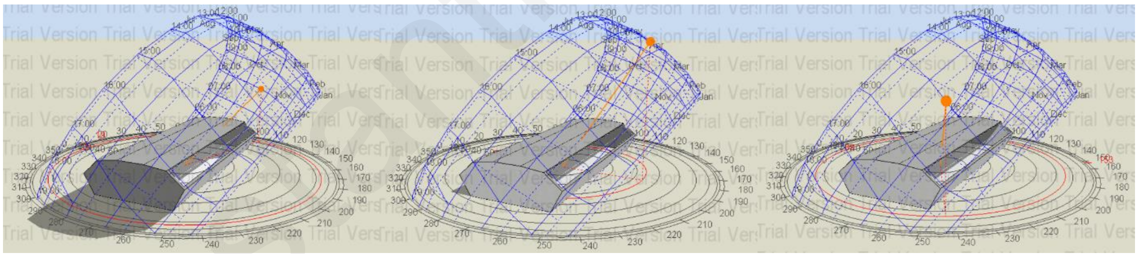

8:00 am 12:00 pm 15:00 pm

Figure 7.32: Incidence of solar radiation in the target position 3 on the 21st of September

7.1 Solar Gain Results

Clearly, the selection of an appropriate building shape can be on the basis of external conditions. One of these conditions as mentioned above is the solar gain in the building. Reconfigurable buildings have the potential to take a form for maximum solar gain in winter and minimum solar gain in summer. Thus, the results of the Design Builder software were studied, so that a suitable position is chosen for each period, winter (December – February), summer (May – September) and intermediate (March – April

Konstantinos Petrou

and October – November). The check was performed for all four orientations (site orientation 0°, 90°, 180° and 270°).

Observing the Table 7.1 and graph 7.3, the most favorable position of the structures for winter with maximum solar gain is the initial position. In summer the minimum solar gain corresponds to the target position 1 and in the intermediate period the best forms are target positions 2 and 3, except in November where it is the target positions 1 and 3. In the intermediate period can be selected one of the two forms that they were mentioned depending on the needs of the building.

Table 7.1: Annually solar gain results for all positions (site orientation 0°)

Position	Solar Gain [kWh] - Site Orientation 0°											
	January	February	March	April	May	June	July	August	September	October	November	December
Initial	3466	4083	5753	6968	8162	9023	9201	8672	7272	5551	3913	3273
Target 1	2761	3219	4344	5162	5871	6449	6584	6305	5439	4261	3089	2611
Target 2	2713	3193	4437	5282	6090	6680	6814	6460	5504	4285	3065	2564
Target 3	3359	3994	5821	7157	8549	9484	9668	9018	7413	5543	3816	3168
Most Favorable	Initial	Initial	2 or 3	2 or 3	1	1	1	1	1	2 or 3	1 or 3	Initial

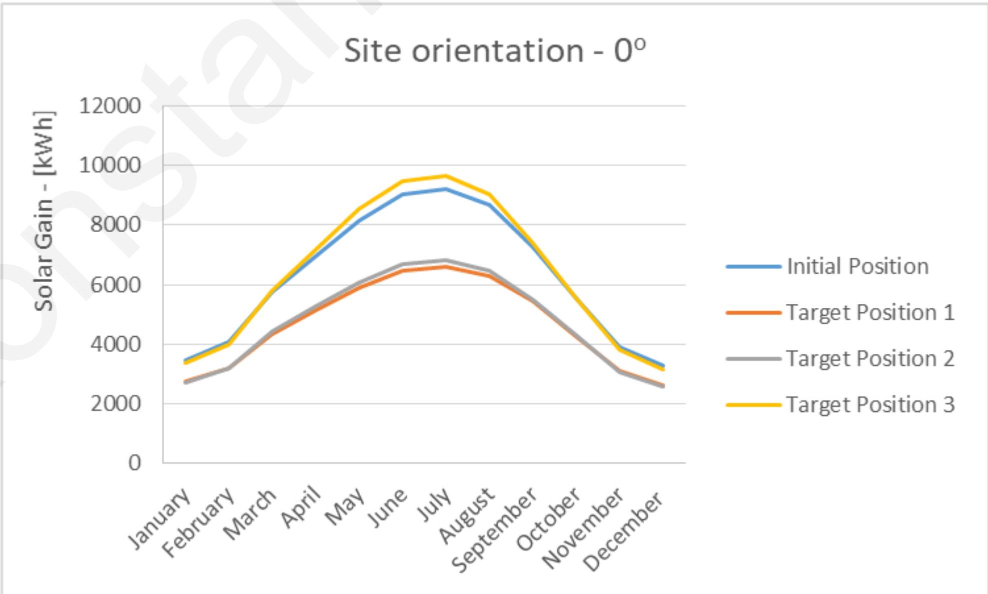

Graph 7.1: Annual configuration of solar gain in the structures

Konstantinos Petrou

From the Table 7.2 and Graph 7.4, the best position of the structures for winter with maximum solar gain is the initial position and summer with minimum solar gain is the target position 1. In the intermediate period for months March and April the most favorable forms are the initial position and the target position 2 and in the months October and November are the target position 2 and 3, depending on the needs of the building.

Table 7.2: Annually solar gain results for all positions (site orientation 90^o)

Position	Solar Gain [kWh] - Site Orientation 90^o											
	January	February	March	April	May	June	July	August	September	October	November	December
Initial	4369	4481	5326	5668	6437	6912	6966	6493	6135	5800	4790	4389
Target 1	3914	3806	4042	3740	3378	3113	3210	3585	4355	4749	4240	4008
Target 2	3978	4053	4768	4938	4924	4843	5090	5464	5691	5348	4400	4016
Target 3	3661	3909	5359	6611	8070	8938	9070	8276	6614	5196	4023	3620
Most Favorable	Initial	Initial	Initial or 2	Initial or 2	1	1	1	1	1	2 or 3	2 or 3	Initial

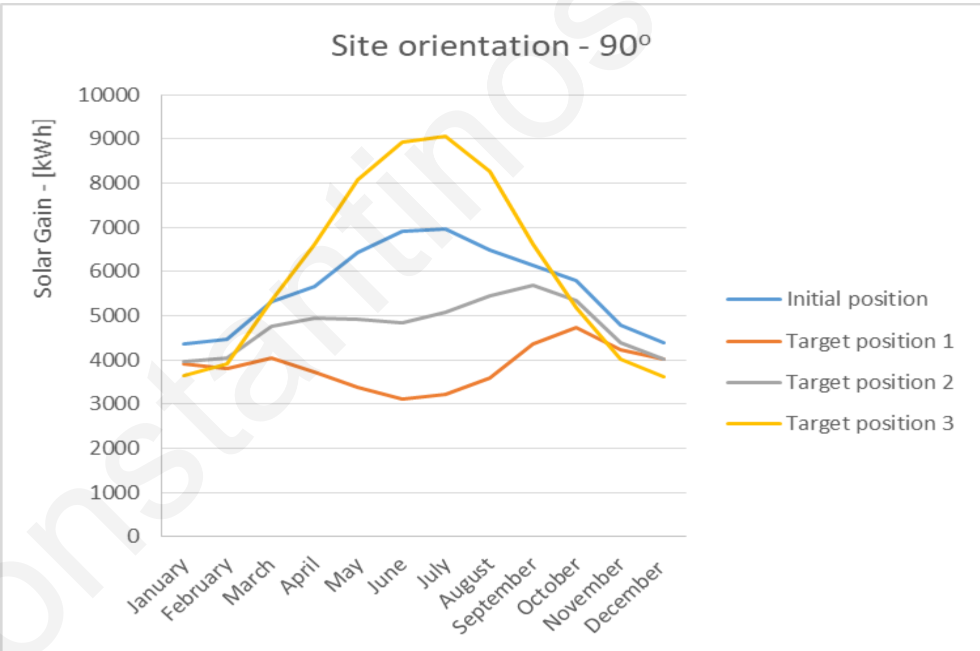

Graph 7.2: Annual configuration of solar gain in the structures

Studying the Table 7.3 and Graph 7.5, the best position of the structures for winter with maximum solar gain is the initial position and summer with minimum solar gain is the target position 1. In the intermediate period the best form for month March are initial position and target position 1, April are initial position and target position 2, October

Konstantinos Petrou

are target position 2 and 3 and November are the target position 1 and 3, depending on the needs of the building.

Table 7.3: Annually solar gain results for all positions (site orientation 180°)

Position	Solar Gain [kWh] - Site Orientation 180°											
	January	February	March	April	May	June	July	August	September	October	November	December
Initial	3466	4083	5753	6968	8162	9023	9201	8672	7272	5551	3913	3273
Target 1	2761	3219	4344	5162	5871	6449	6584	6305	5439	4261	3089	2611
Target 2	2722	3174	4330	5226	6030	6667	6804	6480	5511	4244	3039	2573
Target 3	3359	3994	5821	7157	8549	9484	9668	9018	7413	5543	3816	3168
Most Favorable	Initial	Initial	Initial or 1	Initial or 2	1	1	1	1	1	2 or 3	1 or 3	Initial

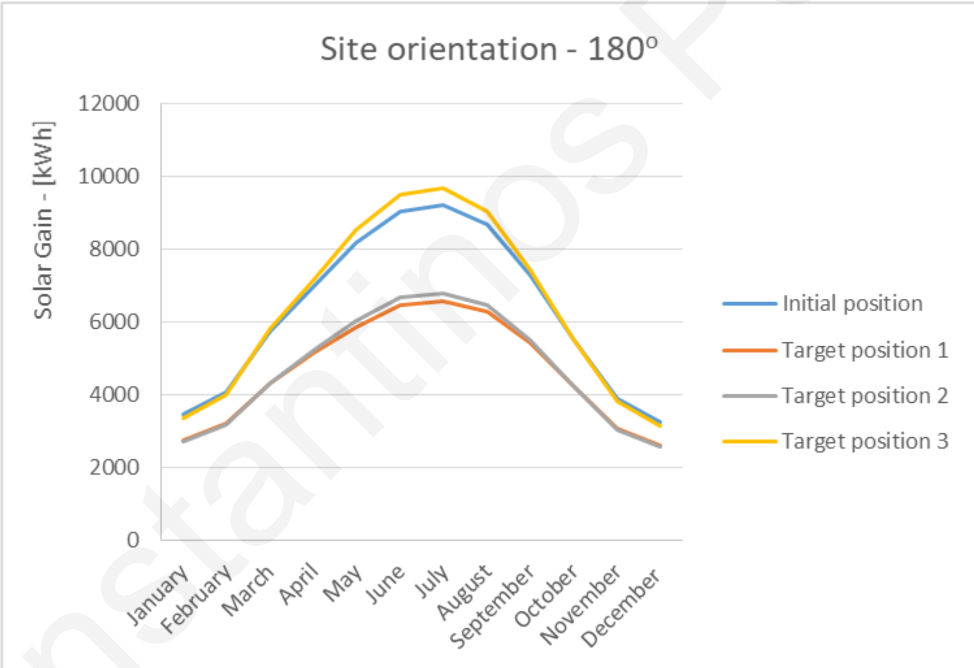

Graph 7.3: Annual configuration of solar gain in the structures

From the Table 7.4 and Graph 7.6, the most favorable position of the structures for winter with maximum solar gain is the initial position and summer with minimum solar gain is the target position 1. In the intermediate period the best form for month March and April are the initial position and the target position 1. In the months October and November are target position 1 and 3. In the intermediate period can be selected one of the two forms that they were mentioned depending on the needs of the building.

Table 7.4: Annually solar gain results for all positions (site orientation 270°)

Position	Solar Gain [kWh] - Site Orientation 270°											
	January	February	March	April	May	June	July	August	September	October	November	December
Initial	4369	4481	5326	5668	6437	6912	6966	6493	6135	5800	4790	4389
Target 1	3914	3806	4042	3740	3378	3113	3210	3585	4355	4749	4240	4008
Target 2	3339	3200	3274	3012	3414	3755	3576	2970	3185	3803	3553	3425
Target 3	3661	3909	5359	6611	8070	8938	9070	8276	6614	5196	4023	3620
Most Favorable	Initial	Initial	Initial or 1	Initial or 1	1	1	1	1	1	1 or 3	1 or 3	Initial

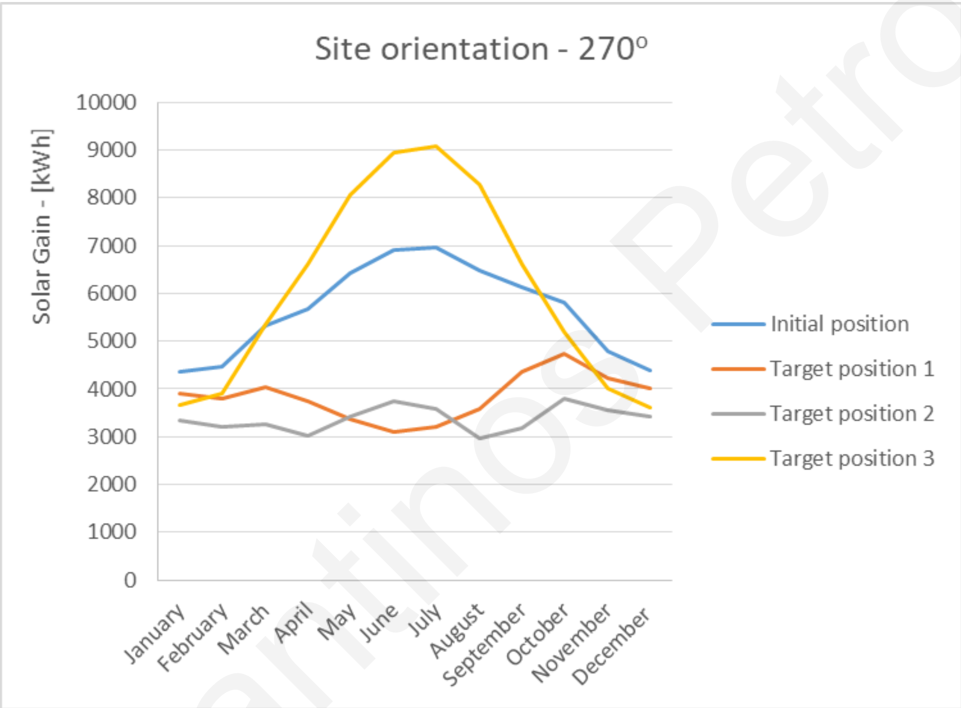

Graph 7.4: Annual configuration of solar gain in the structures

Observing the solar gain measurements and the above tables, all the options (initial and targets) are useful because they are the most favorable positions for different periods. Also the symmetrical positions have the same measurements in the site orientation 0° and 180° and in the site orientation 90° and 270°. Moreover, the target position 2 is a different structure from target positions 1 and 3, so they were studied separately. So it was studied the horizontal structures (initial and target 2 positions) and vertical structures (initial, target 1 and 3 positions) separately to identify the most favorable positions for each period.

Konstantinos Petrou

7.1.1 Horizontal Structure

Firstly, the measurements of the horizontal structure were checked for all orientations (site orientation 0°, 90°, 180° and 270°), since it is a non-symmetrical form.

In horizontal structure there are two options for each period, the most favorable position of the structure in site orientation 0° for winter with maximum solar gain is the initial position. The summer with minimum solar gain is the target position 2. In the intermediate period the best form are initial position and target position 2 that can be selected one of these forms that they were mentioned depending on the needs of the building.

Table 7.5: Annually solar gain results for horizontal structure (site orientation 0°)

Position	Solar Gain [kWh] - Site Orientation 0°											
	January	February	March	April	May	June	July	August	September	October	November	December
Initial	3466	4083	5753	6968	8162	9023	9201	8672	7272	5551	3913	3273
Target 2	2713	3193	4437	5282	6090	6680	6814	6460	5504	4285	3065	2564
Most Favorable	Initial	Initial	Initial or 2	Initial or 2	2	2	2	2	2	Initial or 2	Initial or 2	Initial

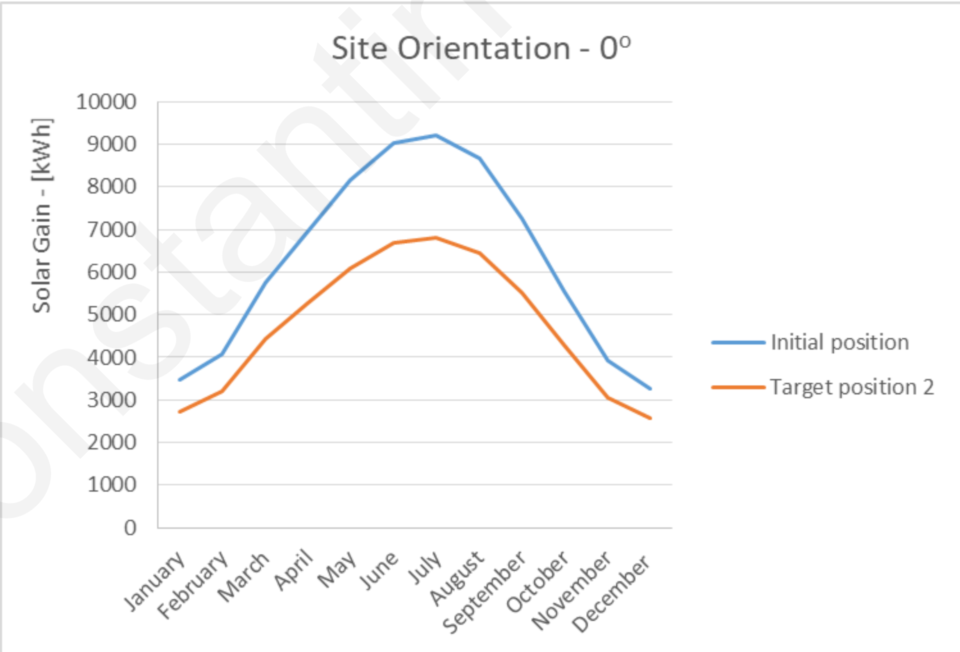

Graph 7.5: Annual configuration of solar gain in the horizontal structure

Observing the table and graph, the most favorable position of the structures for winter with maximum solar gain is the initial position. The summer with minimum solar gain is the target position 2. In the intermediate period the best form are initial position and

Konstantinos Petrou

target position 2. In the intermediate period can be selected one of the two forms that they were mentioned depending on the needs of the building.

Table 7.6: Annually solar gain results for horizontal structure (site orientation 90°)

Position	Solar Gain [kWh] - Site Orientation 90°											
	January	February	March	April	May	June	July	August	September	October	November	December
Initial	4369	4481	5326	5668	6437	6912	6966	6493	6135	5800	4790	4389
Target 2	3978	4053	4768	4938	4924	4843	5090	5464	5691	5348	4400	4016
Most Favorable	Initial	Initial	Initial or 2	Initial or 2	2	2	2	2	2	Initial or 2	Initial or 2	Initial

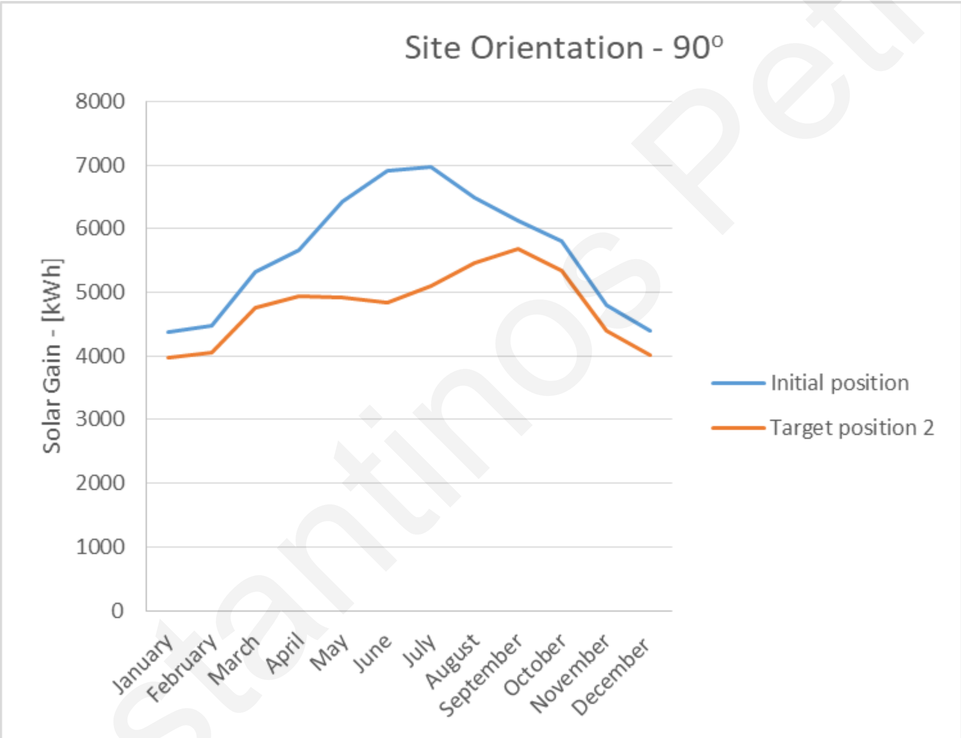

Graph 7.6: Annual configuration of solar gain in the horizontal structure

From the table and graph, the most favorable position of the structures for winter with maximum solar gain is the initial position. The summer with minimum solar gain is the target position 2. In the intermediate period can be selected one of the two forms (initial position and target position 2), if the building needs heating selected the initial position, if it needs cooling selected the target position 2 so that there is thermal comfort.

Table 7.7: Annually solar gain results for horizontal structure (site orientation 180^o)

Position	Solar Gain [kWh] - Site Orientation 180°											
	January	February	March	April	May	June	July	August	September	October	November	December
Initial	3466	4083	5753	6968	8162	9023	9201	8672	7272	5551	3913	3273
Target 2	2722	3174	4330	5226	6030	6667	6804	6480	5511	4244	3039	2573
Most Favorable	Initial	Initial	Initial or 2	Initial or 2	2	2	2	2	2	Initial or 2	Initial or 2	Initial

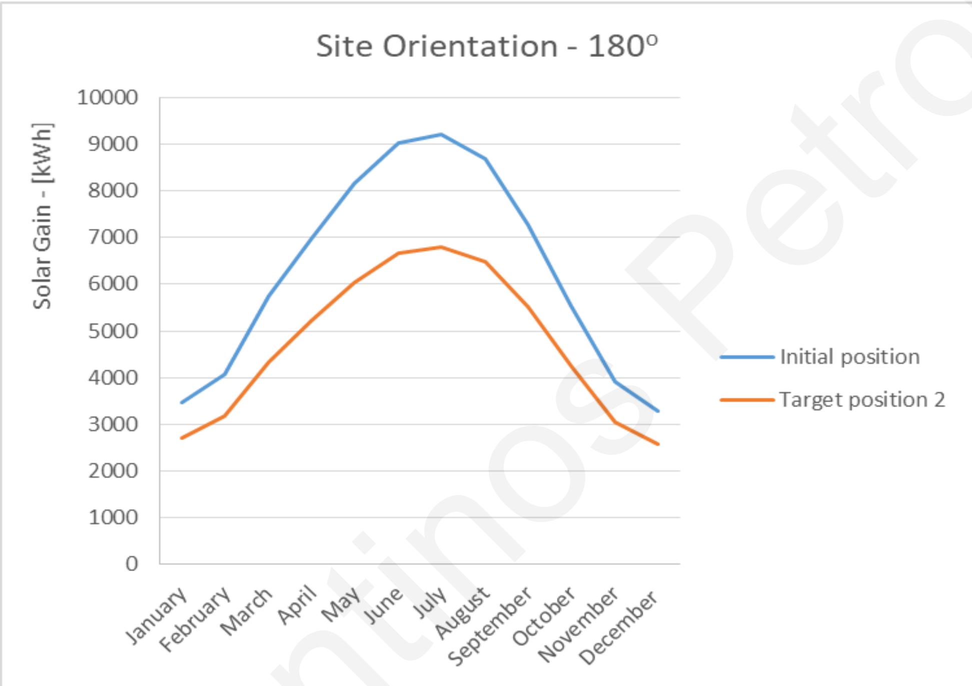

Graph 7.7: Annual configuration of solar gain in the horizontal structure

Studying the table and graph, the most favorable position of the structures for winter with maximum solar gain is the initial position and the summer with minimum solar gain is the target position 2. In the intermediate period the best form are initial position and target position 2 where it can be selected one of the two forms that they were mentioned depending on the needs of the building.

Table 7.8: Annually solar gain results for horizontal structure (site orientation 270^o)

Position	Solar Gain [kWh] - Site Orientation 270°											
	January	February	March	April	May	June	July	August	September	October	November	December
Initial	4369	4481	5326	5668	6437	6912	6966	6493	6135	5800	4790	4389
Target 2	3339	3200	3274	3012	3414	3755	3576	2970	3185	3803	3553	3425
Most Favorable	Initial	Initial	Initial or 2	Initial or 2	2	2	2	2	2	Initial or 2	Initial or 2	Initial

Konstantinos Petrou

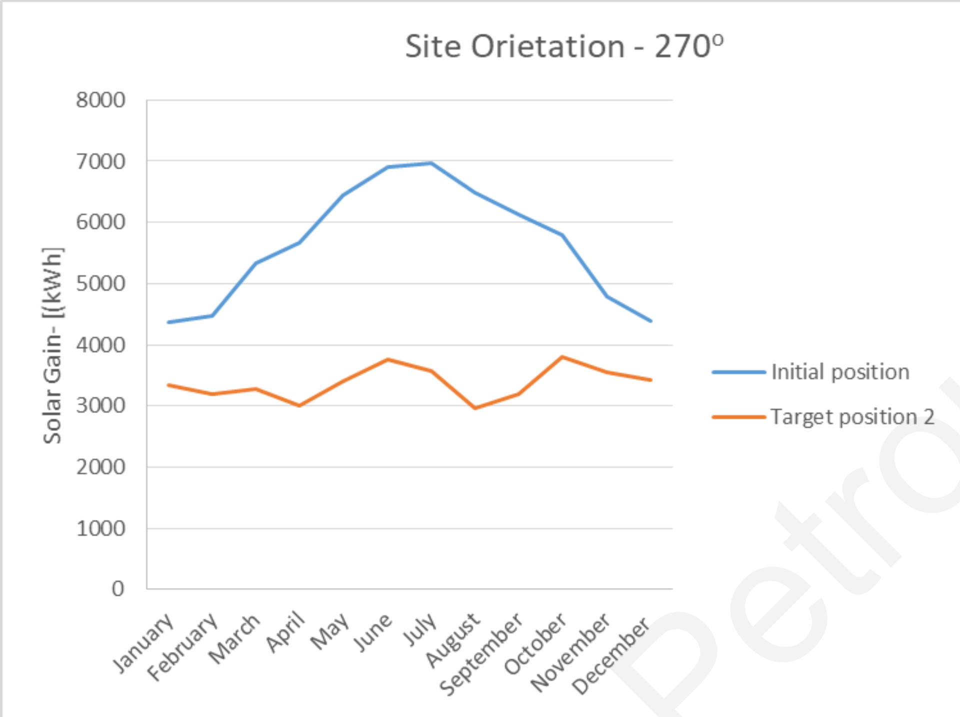

Graph 7.8: Annual configuration of solar gain in the horizontal structure

7.1.2 Vertical Structure

Subsequently, the measurements of the vertical structures were checked for two orientations, site orientation 0^o and 90^o, since it is a symmetrical form and it had same values with site orientations 180^o and 270^o, respectively.

In the vertical structures there are more options such as initial position, target position 1 and 3 for each period. The most favorable position of the structure in site orientation 0^o for winter with maximum solar gain is the initial position. The summer with minimum solar gain is the target position 1. In the intermediate period the best forms are initial position for months March and April and target position 3 for months October and November. These are the options for each period, so that there is thermal comfort.

Table 7.9: Annually solar gain results for vertical structures (site orientation 0^o)

Position	Solar Gain [kWh] - Site Orientation 0°											
	January	February	March	April	May	June	July	August	September	October	November	December
Initial	3466	4083	5753	6968	8162	9023	9201	8672	7272	5551	3913	3273
Target 1	2761	3219	4344	5162	5871	6449	6584	6305	5439	4261	3089	2611
Target 3	3359	3994	5821	7157	8549	9484	9668	9018	7413	5543	3816	3168
Most Favorable	Initial	Initial	Initial	Initial	1	1	1	1	1	3	3	Initial

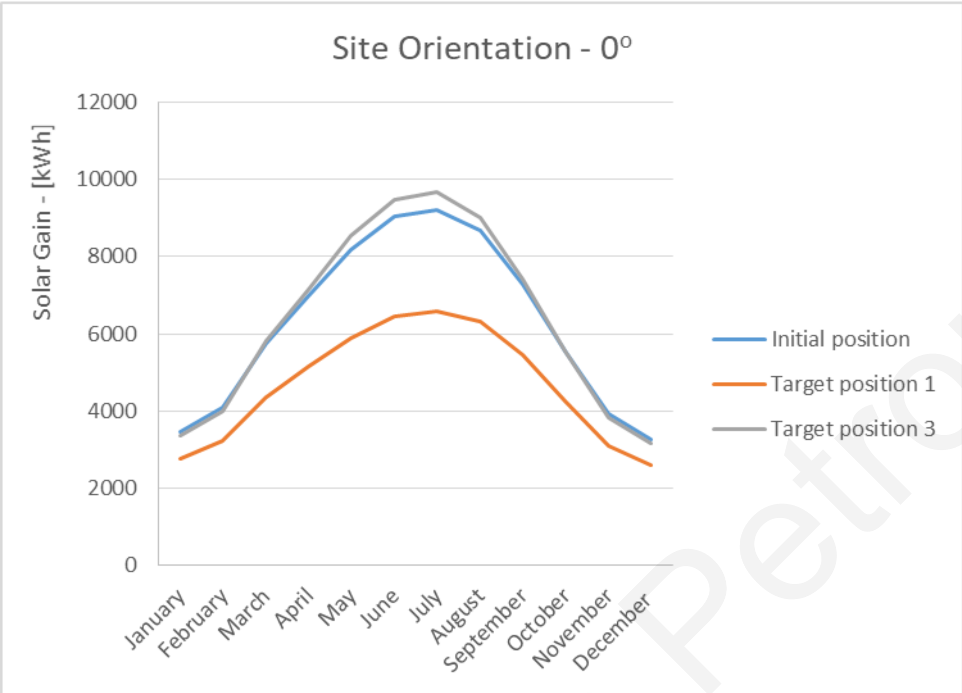

Graph 7.9: Annual configuration of solar gain in the vertical structure

From the table and graph, the most favorable position of the structure in site orientation 90° for winter with maximum solar gain is the initial position. The summer with minimum solar gain is the target position 1. In the intermediate period the best forms are initial position for months March and April, target position 3 for month October and target position 1 for month November. Annually, for each period selected one of the forms of the vertical structure depending on the needs of the building.

Table 7.10: Annually solar gain results for vertical structures (site orientation 90°)

Position	Solar Gain [kWh] - Site Orientation 90°											
	January	February	March	April	May	June	July	August	September	October	November	December
Initial	4369	4481	5326	5668	6437	6912	6966	6493	6135	5800	4790	4389
Target 1	3914	3806	4042	3740	3378	3113	3210	3585	4355	4749	4240	4008
Target 3	3661	3909	5359	6611	8070	8938	9070	8276	6614	5196	4023	3620
Most Favorable	Initial	Initial	Initial	Initial	1	1	1	1	1	3	1	Initial

Konstantinos Petrou

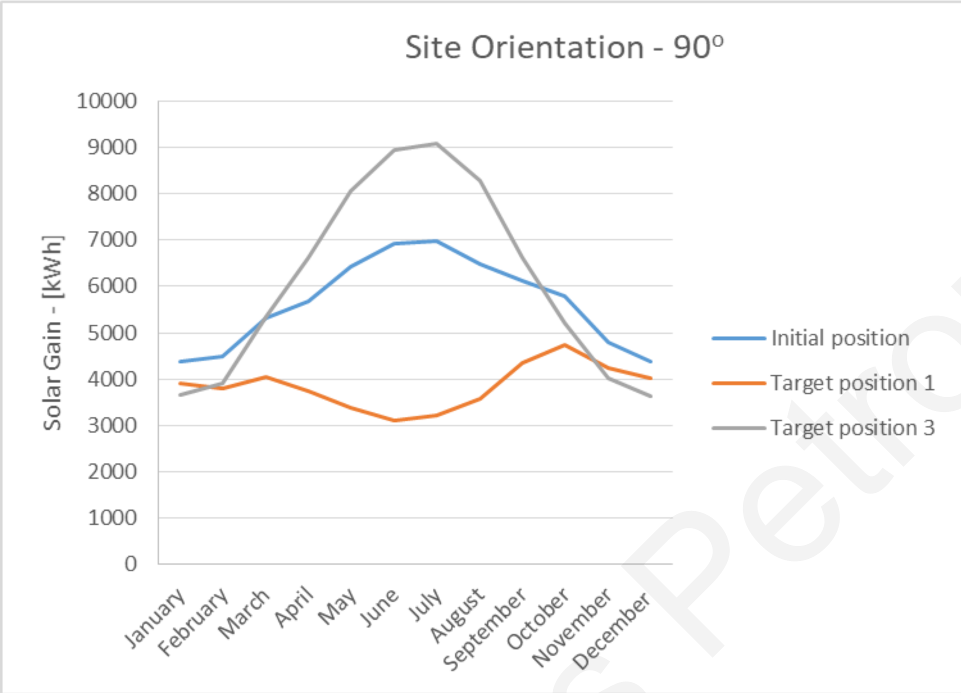

Graph 7.10: Annual configuration of solar gain in the vertical structures

Generally, all of the positions can positively affect the comfort in side a building depending on the season. Initially observing the overall comparison but also separately of the structures, the vertical structure gave better results than the horizontal structure. This is due to the fact that the vertical structure is the best form during the summer period which it is the lengthiest period annually in Cyprus. In the winter period the best form is the initial position, which it exists in both structures (vertical and horizontal structures). Finally, the vertical structures have a third option with an intermediate solar gain value suitable for the intermediate periods.

7.1.3Air Temperature

The average temperature of the zone air for each month is presented below for the four positions (initial, target 1, 2, and 3 position), in four orientations (site orientation 0°, 90°, 180° and 270°). The location is Larnaca, Cyprus and the simulation was done through the software Design Builder.

Table 7.11: Annually average air temperature (site orientation 0^o)

Position	Air Temperature [^{o}C] - Site Orientation 0^o											
	January	February	March	April	May	June	July	August	September	October	November	December
Initial	14.68	15.08	17.28	21.86	25.97	30.6	32.77	33.03	29.94	24.62	19.75	15.94
Target 1	14.65	14.09	16.97	21.38	25.23	29.62	31.87	32.24	29.41	24.38	19.69	15.96
Target 2	16.56	16.9	18.16	20.78	23.28	26.16	27.69	27.83	25.85	22.55	19.55	17.27
Target 3	16.49	16.88	18.43	21.35	24.22	27.29	28.72	28.69	26.4	22.78	19.51	17.13

Table 7.12: Annually average air temperature (site orientation 90^o)

Position	Air Temperature [^{o}C] - Site Orientation 90^o											
	January	February	March	April	May	June	July	August	September	October	November	December
Initial	15.12	15.18	16.92	20.98	24.93	29.21	31.41	31.66	29.13	24.68	20.21	16.46
Target 1	15.26	15.2	16.61	20.37	23.7	27.39	29.79	30.48	28.58	24.57	20.33	16.68
Target 2	17.03	17.12	18.13	20.48	22.65	25.11	26.76	27.2	25.8	22.95	20.12	17.82
Target 3	16.59	16.77	18.17	21.03	23.95	26.96	28.37	28.26	25.91	22.54	19.58	17.3

Table 7.13: Annually average air temperature (site orientation 180^o)

Position	Air Temperature [^{o}C] - Site Orientation 180^o											
	January	February	March	April	May	June	July	August	September	October	November	December
Initial	14.68	15.08	17.28	21.86	25.97	30.6	32.77	33.03	29.94	24.62	19.75	15.94
Target 1	14.65	14.09	16.97	21.38	25.23	29.62	31.87	32.24	29.41	24.38	19.69	15.96
Target 2	16.54	16.85	18.12	20.78	23.28	26.18	27.73	27.87	25.86	22.54	19.54	17.26
Target 3	16.49	16.88	18.43	21.35	24.22	27.29	28.72	28.69	26.4	22.78	19.51	17.13

Table 7.14: Annually average air temperature (site orientation 270^o)

Position	Air Temperature [^{o}C] - Site Orientation 270^o											
	January	February	March	April	May	June	July	August	September	October	November	December
Initial	15.12	15.18	16.92	20.98	24.93	29.21	31.41	31.66	29.13	24.68	20.21	16.46
Target 1	15.26	15.2	16.61	20.37	23.7	27.39	29.79	30.48	28.58	24.57	20.33	16.68
Target 2	16.78	16.78	17.54	19.69	22.05	24.67	26.19	26.11	24.64	22.27	19.71	17.6
Target 3	16.59	16.77	18.17	21.03	23.95	26.96	28.37	28.26	25.91	22.54	19.58	17.3

Konstantinos Petrou

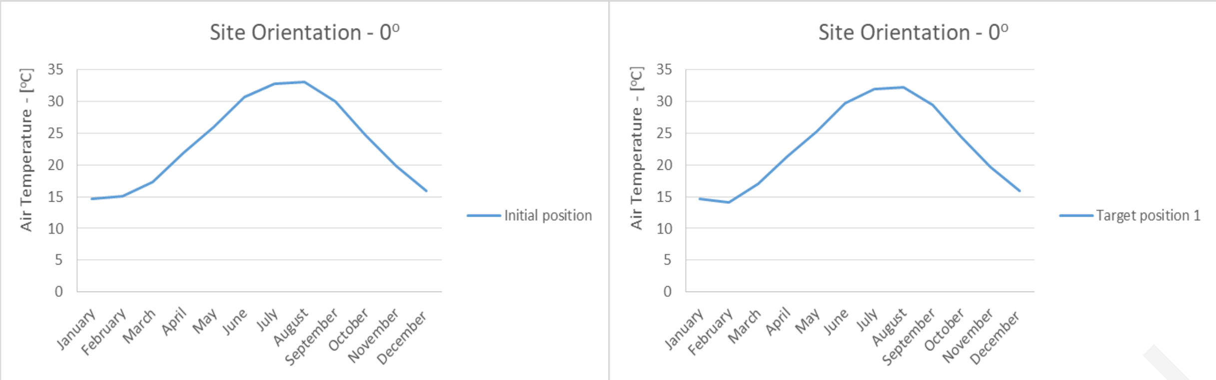

Graph 7.11: Annual configuration of air temperature in the initial and target position 1

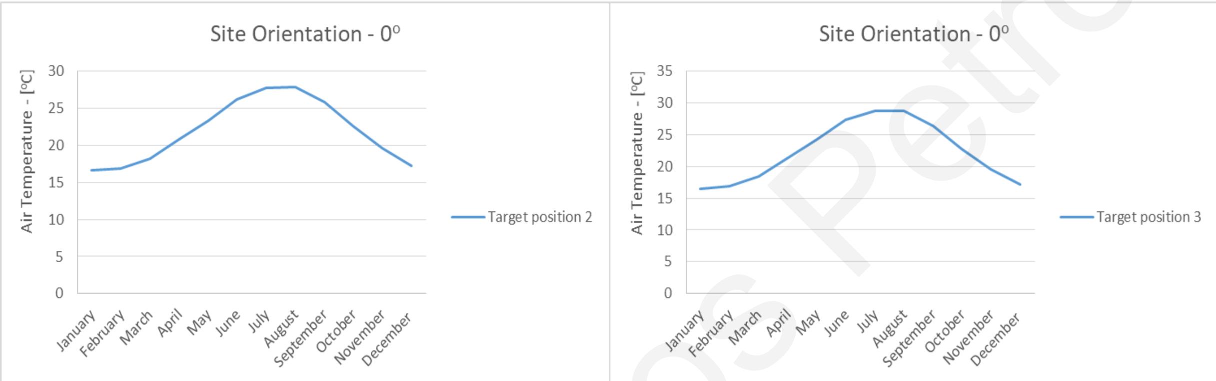

Graph 7.12: Annual configuration of air temperature in the target positions 2 and 3

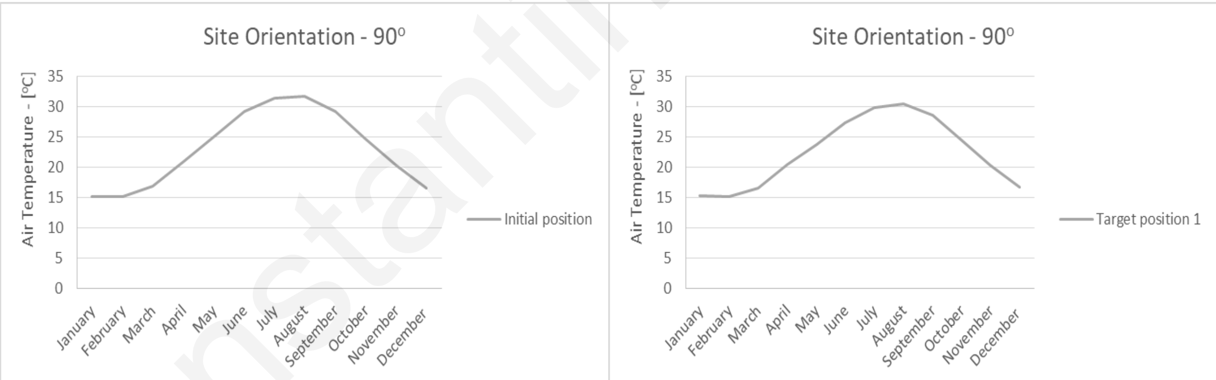

Graph 7.13: Annual configuration of air temperature in the initial and target position 1

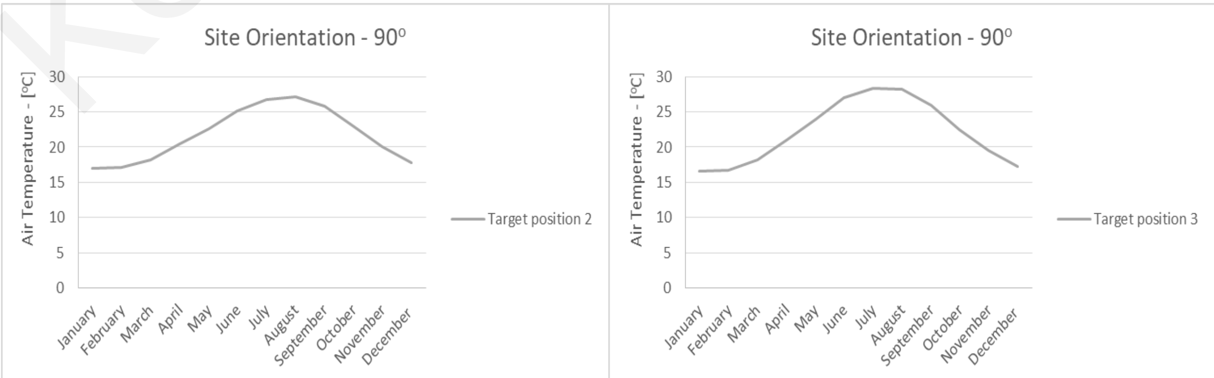

Graph 7.14: Annual configuration of air temperature in the target positions 2 and 3

Konstantinos Petrou

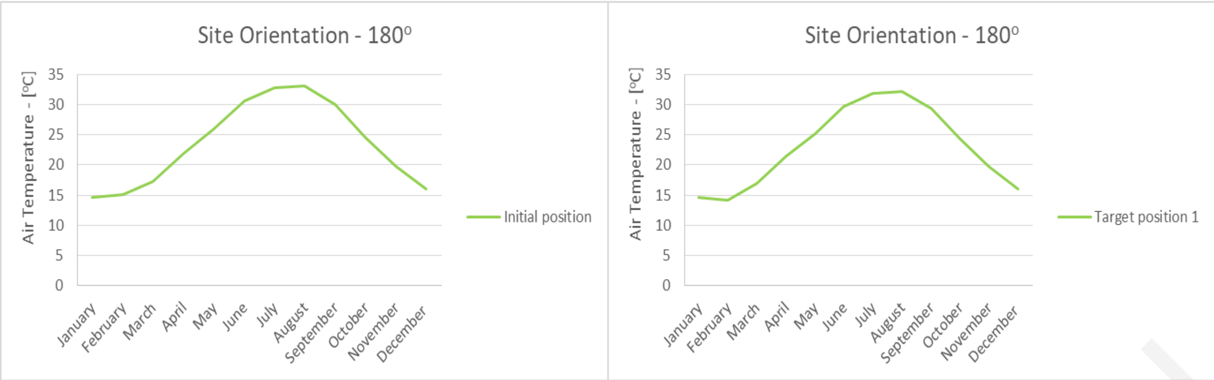

Graph 7.15: Annual configuration of air temperature in the initial and target position 1

Graph 7.16: Annual configuration of air temperature in the target positions 2 and 3

Graph 7.17: Annual configuration of air temperature in the initial and target position 1

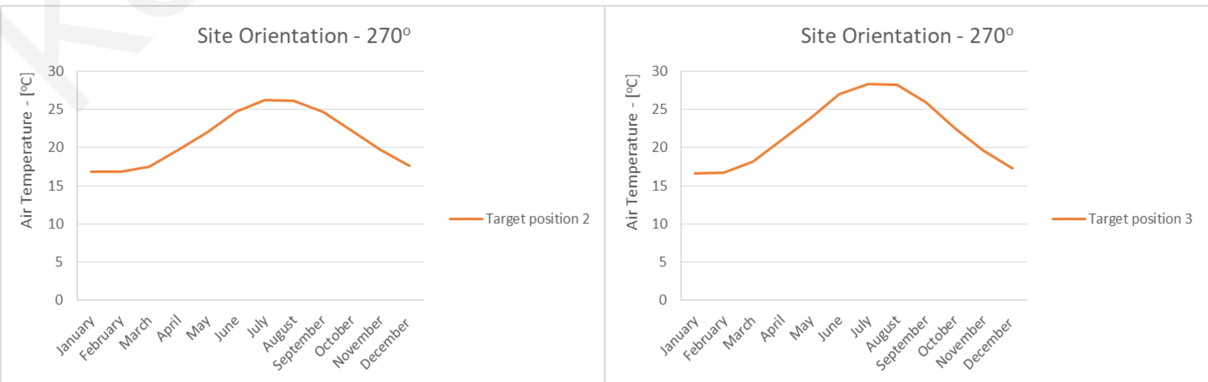

Graph 7.18: Annual configuration of air temperature in the target positions 2 and 3

Konstantinos Petrou

7.2 Lighting Results

Another external condition for the selection of an appropriate building shape is the lighting. Reconfigurable buildings have the potential to take a form that has the best lighting depending on the use of space. Thus, the results of the Design Builder software were studied, so that a suitable position is chosen for each use. The check was performed for all four orientations (site orientation 0°, 90°, 180° and 270°) in the horizontal structure and for two orientations (site orientation 0° and 90°) for vertical structure because it is symmetrical.

Climate-based daylight modelling (CBDM) is the prediction of illuminance on the working plane using realistic sun and sky conditions based on standardised climate data. In Design Builder, CBDM evaluations are carried out for a full year at a time-step of an hour in order to capture the daily and seasonal dynamics of natural daylight. The daylight illuminance map shows the distribution of natural daylight availability for the floor plan of the building for the sky conditions selected (location Larnaca, Cyprus). The daylight levels are shown in Lux and as percentages % daylight factors.

The lux is the SI derived unit of illuminance, measuring luminous flux per unit area. Daylight Factor is a ratio that represents the amount of illumination available indoors relative to the illumination present outdoors at the same time under overcast skies. In this case, the scale displays specific colours for maximum and minimum lighting areas, red and dark blue respectively (Advanced Buildings 2021; Wikipedia 2021c).

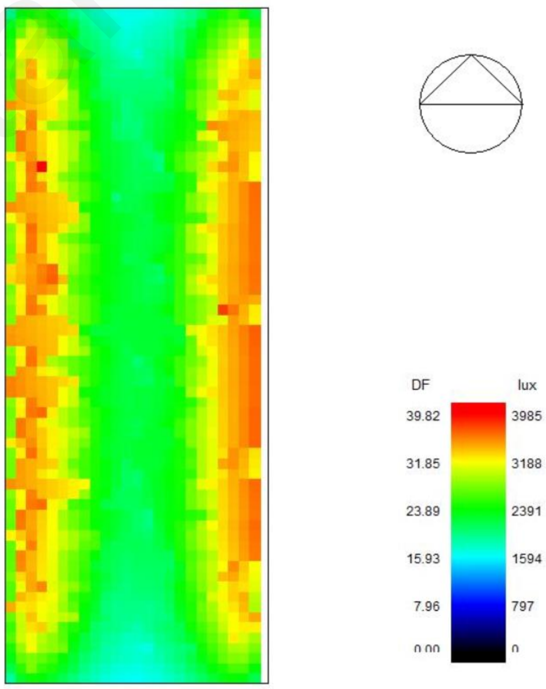

Figure 7.33: Configuration lighting of the initial position (site orientation 0°)

Konstantinos Petrou

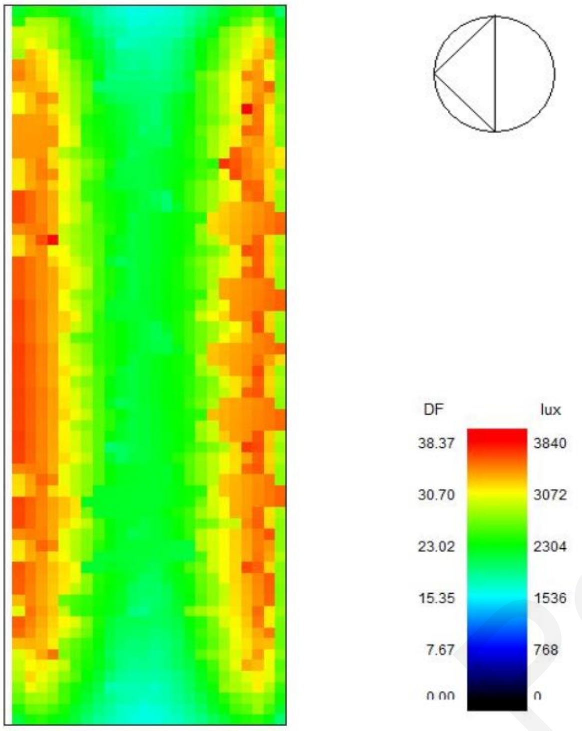

Figure 7.34: Configuration lighting of the initial position (site orientation 90°)

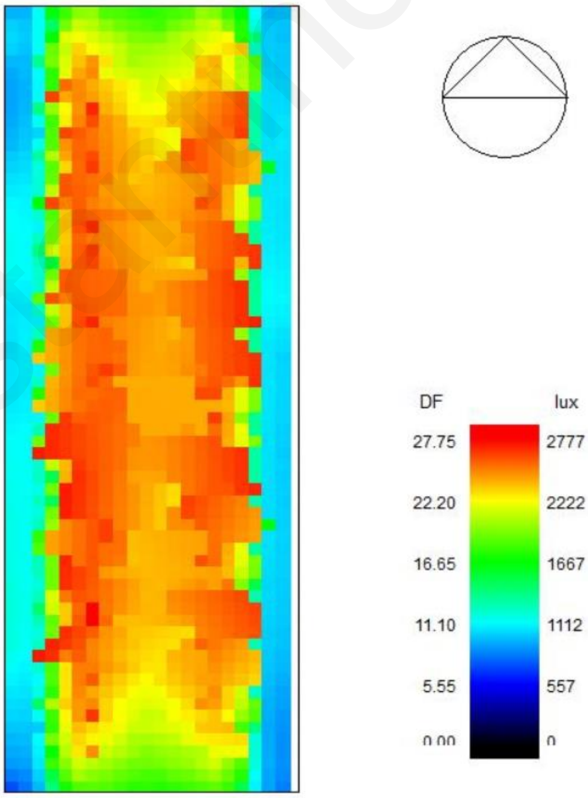

Figure 7.35: Configuration lighting of the target position 1 (site orientation 0°)

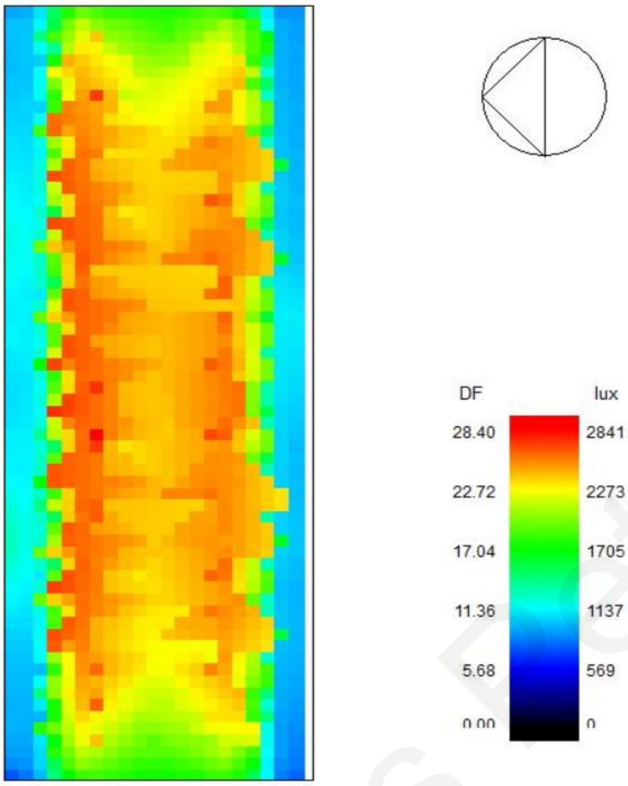

Figure 7.36: Configuration lighting of the target position 1 (site orientation 90°)

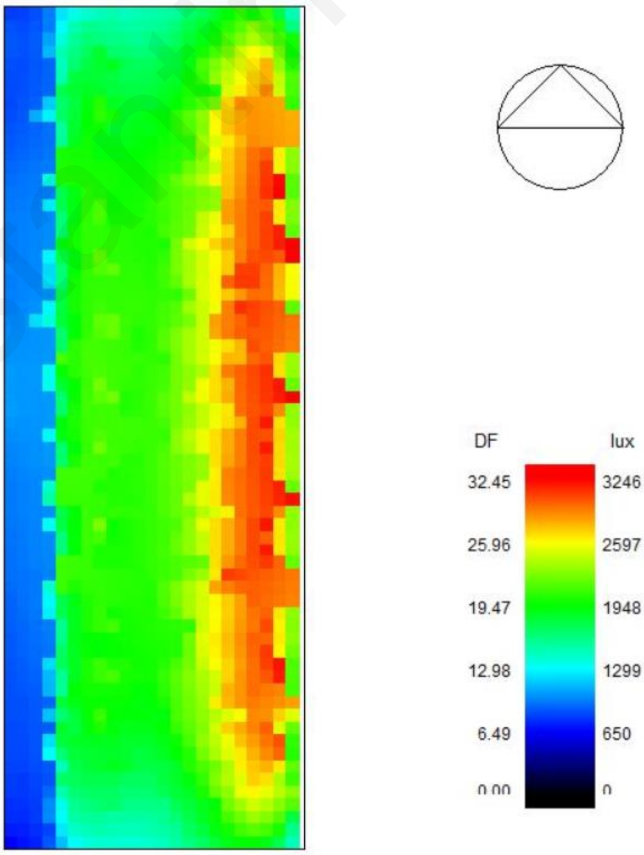

Figure 7.37: Configuration lighting of the target position 2 (site orientation 0°)

Konstantinos Petrou

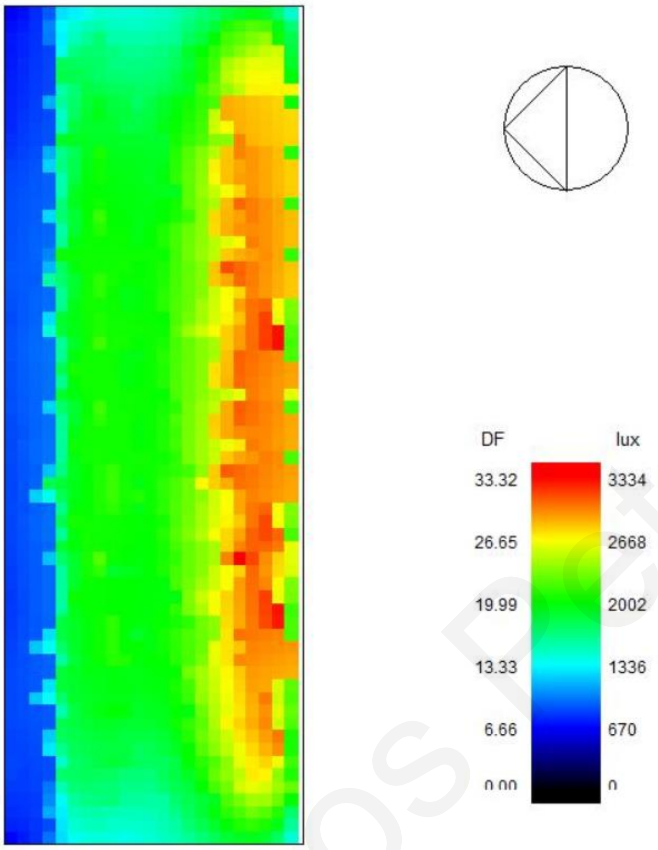

Figure 7.38: Configuration lighting of the target position 2 (site orientation 90^{o})

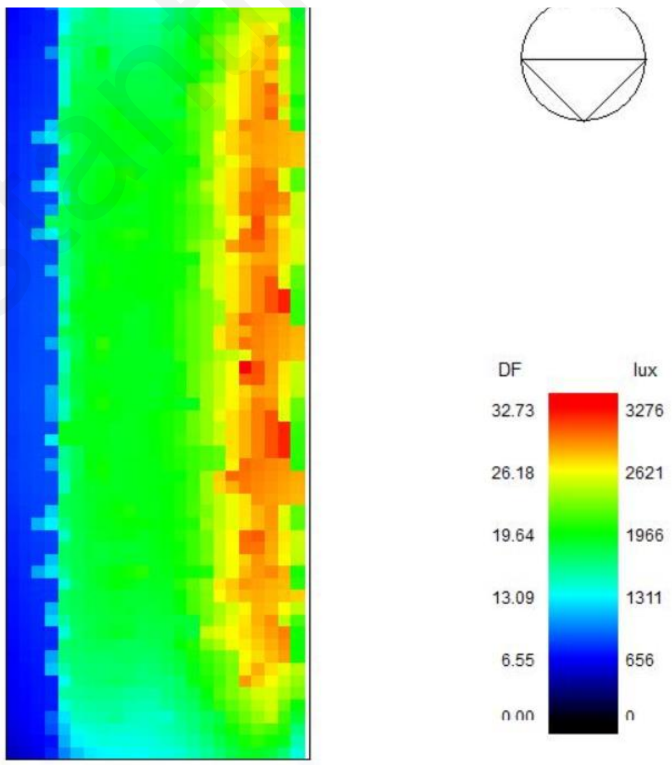

Figure 7.39: Configuration lighting of the target position 2 (site orientation 180^{o})

Konstantinos Petrou

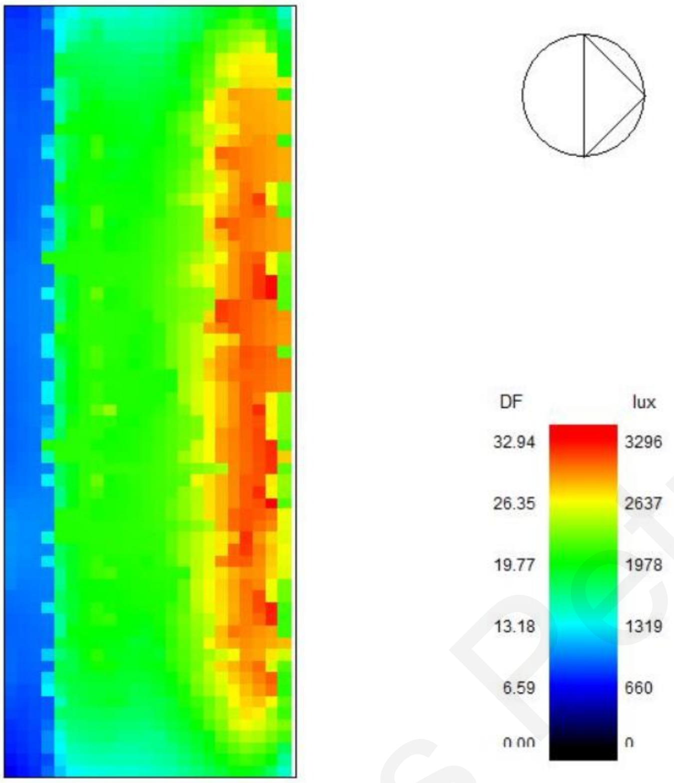

Figure 7.40: Configuration lighting of the target position 2 (site orientation 270º)

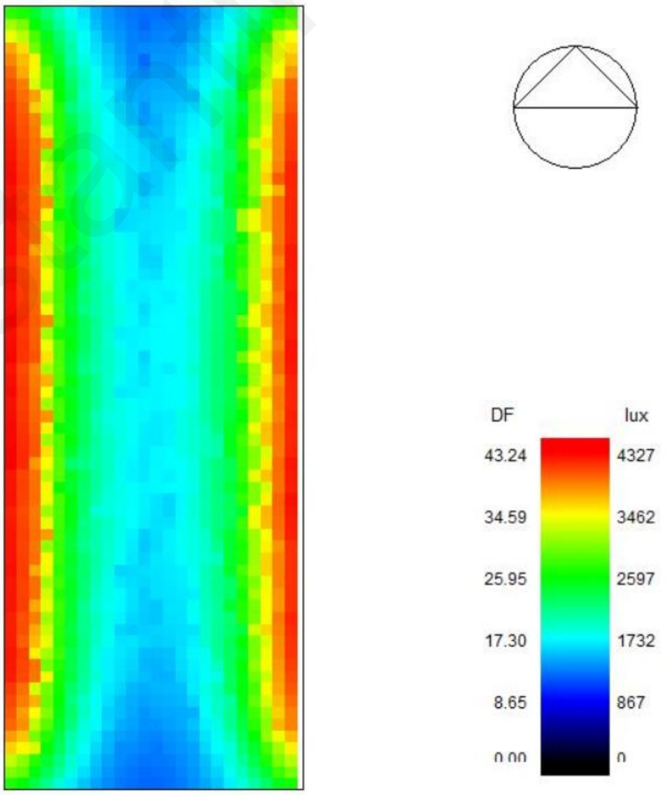

Figure 7.41: Configuration lighting of the target position 3 (site orientation 0º)

Konstantinos Petrou

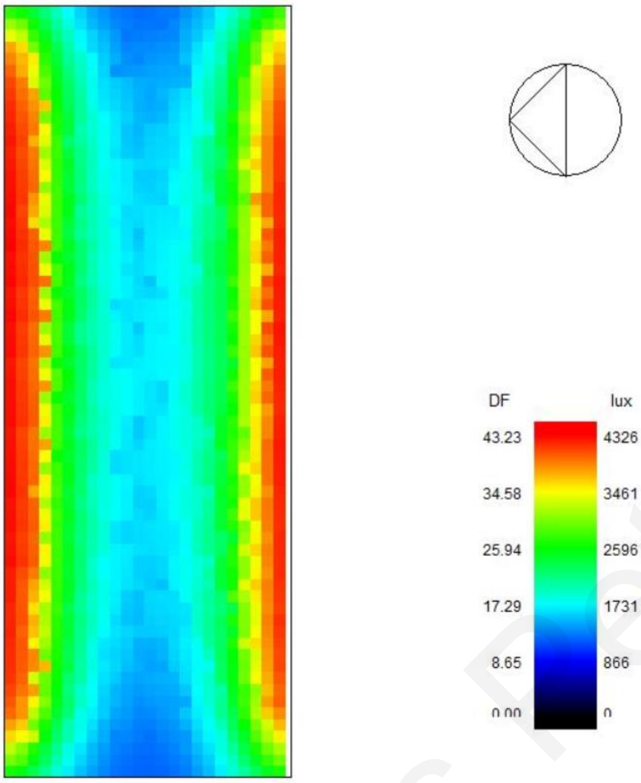

Figure 7.42: Configuration lighting of the target position 3 (site orientation 90°)

Observing the figures above, each position provides different lighting inside of the structure. Firstly, the initial position has bright lighting at the right and left of the structure on the large sides, where there are openings and seems to diffuse centrally. As to target position 1, the lighting dominates centrally inside of the structure. Concerning the target position 2 there is bright lighting only on the right and diffuse to the center. In the other side (left), the available lighting is minimal since the coloring is intense blue. Finally, the target position 3 presents lighting in the two sides, right and left, as in the initial position but in this case the lighting non diffuse centrally.

In the structures, the site orientation did not affect significantly the way the lighting is displayed internally. The orientation affected only the maximum illumination that occurs in the structures.

Based on the above, each position can be used for a different mode of the building and for a different configuration of the space. For example, the target position 2, where the lighting was only on the right side, it can work in events, theaters where they need lighting only for the speaker or the theater performance, respectively and not in the audience. Another example is in the case of an office where the office spaces will be configured peripherally or centrally, then it can be used target position 3 or initial position and target position 1, respectively.

Konstantinos Petrou

Chapter 8

CONCLUSIONS

The thesis focuses on reconfigurable buildings which provide many advantages compared to traditional fixed-shape ones. It focuses on the design and control of a proposed multilink, articulated reconfigurable structure and the investigation of its morphological and kinematic behavior. The reconfiguration approach refers to the "effective dual crank-slider" mechanism concept with horizontal or vertical actuation. In fact, a number of these planar linkages are used, which are connected together to create the building volume. Such structures can be used as temporary buildings for various uses. One of the design characteristics is modularity, which allows increasing the volume of the building. More members can be included in each planar linkage while more planar linkages can be used to increase the volume in the longitudinal direction.

The structural concept was presented and construction details were created using 3D CAD models (Solidworks). The models were also used for simulation studies to demonstrate the applicability of the concept and highlight relevant issues. The proposed control approach allows to modify the building structure to a 1-DOF system, which is done with the use of brakes on the system's joints. This allows to adjust each joint angle of the planar system from an initial to a target position. The reconfiguration procedure is multistep and allows flexibility in motion planning. It can be performed using alternative sequences and it is possible to select an optimal one to meet certain objectives, including energy efficiency. As part of kinematic investigations, the basic mechanisms were analyzed and their singular configurations were identified. These configurations need to be carefully considered in motion planning, along with other limitations that apply (e.g., limitations to motion due to neighboring structures in order to avoid collisions).

Two different actuation configurations were proposed related to a horizontal and a vertical motion of a linear actuator, respectively. These mechanisms may allow for symmetrical and non-symmetrical target positions. As part of the simulation studies, the brakes torques were calculated together with the actuator motions, providing an estimation of their required capacity and travel ranges. For the simulation studies all members were considered to be perfectly rigid. A further improvement to the model

Konstantinos Petrou

would be to include structural flexibility, calculate static deformations and consider their effect on the shape and the kinematics behavior of the mechanisms. The modeling of the joints may also become more accurate by considering friction, which in practice will affect the required control action and the energy consumption during reconfigurations. Energy consumption calculations during motion would also provide useful information in regard to the cost of operation of the reconfigurable building. Comparisons between the energy consumption and the potential energy gains, as well as other benefits due to reconfigurability will be more systematic.

An energy-efficient method for actuation was proposed, which allows exploitation of wind energy for actuation purposes. A preliminary concept was presented and its feasibility was investigated considering realistic wind conditions in Cyprus and other locations in Europe. Using basic aerodynamics, the generated lift and drag forces were considered.

Building reconfigurations may also be used towards improving the energy performance of the building and also improving the comfort levels. This was demonstrated using simulation studies on solar gain and lighting conditions inside the building, while considering the motion of the sun. For this purpose, the software Design Builder was used.

Future work may include a definition of the range of possible configurations and corresponding building envelopes, which will provide useful information while selecting appropriate configurations for the building. Further work is also required in relation to motion planning and specifically to the automated generation of the reconfiguration sequences. This may then be extended to the generation/ selection of optimal reconfiguration sequences, resulting to low energy consumption and reduced actuation effort. In terms of structural design, important issues to be further investigated include the modular design, foldability, transportability and self-erectability of the structure. Another direction for further investigations is the solar energy production with a photovoltaic system installed on the structure. System reconfigurations may significantly improve their efficiency by adjusting the orientation of the solar panels. Some other parameters related to occupants' comfort can also be investigated including shading and ventilation.

Perhaps a most important future step will be the experimental implementation to demonstrate the applicability of the proposed approaches and their benefits. Reconfigurable architecture is a new but very promising field.

Konstantinos Petrou

REFERENCES

1. Advanced Buildings 2021, ‘Daylight Factor _ Daylighting Pattern Guide’, <http://patternguide.advancedbuildings.net/ >.
2. Anastasiadou, I 2018, ‘NUMERICAL ANALYSIS OF HYBRID CABLE BENDING-ACTIVE ARCH SERIES’.
3. Dimitriou, P, Phocas, M.C & Christoforou, E.G 2020, ‘Kinematics and control approach for deployable and reconfigurable rigid bar linkage structures’, *Engineering Structures*, vol. 208, pp. 110-310.
4. Dorma 2002, ‘Rodan Load-bearing Transparency’,.
5. El-Haik, B & Roy, DM 2005, *Service Design for Six Sigma: A Road Map for Excellence*,.
6. Hall, N 2015a, ‘What is Drag?’, *Nasa*, pp. 1–2, accessed from <http://www.grc.nasa.gov/WWW/k-12/airplane/drag1.html>.
7. Hall, N 2015b, ‘The Drag equation’, *Nasa*, accessed from <https://www.grc.nasa.gov/www/k-12/airplane/drageq.html>.
8. Hall, N 2015c, ‘What is Lift_’, <https://www.nasa.gov/>.
9. Hall, N 2015d, ‘The Lift Equation’, <https://www.nasa.gov/>.
10. Hall, N 2015e, ‘L_D Ratio’, <https://www.nasa.gov/>.
11. Hall, N 2018, ‘Inclination Effects on Lift’, <https://www.nasa.gov/>.
12. Korkmaz, K & Akgun, Y 2011, ‘Simulation of a Novel Primary Element to Increase the Form Flexibility of Deployable Scissor Structures’.
13. Matheou, M, Arnos, S, Christoforou, E.G, Muller, A & Phocas, M.C 2013, ‘DRAFT: Towards realization of shape-controlled adaptab;e buildings following a robotics approach’.
14. Matheou, M, Phocas, M.C & Christoforou, E.G 2015, ‘Design,

Konstantinos Petrou

motion planning and control of a reconfigurable hybrid structure', *Engineering Structures*, vol. 101, pp. 376–385.

15. Meteoblue 2020, 'Χάρτες καιρού - Ευρώπη - meteoblue', <https://www.meteoblue.com/>.
16. Muller, A, Christoforou, E.G & Phocas, M.C 2012, 'Draft: Motion planning for shape-controlled adaptable buildings resembling topologically closed-loop robotic systems',.
17. Robert L. Norton 2008, 'Design of Machinery',4 ed. Mc Graw - Hill.
18. Rosenberg, D 2010, 'Indeterminate architecture: Scissor-pair transformable structures', *Footprint*, no. 6, pp. 19–39.
19. Sari, A, Karaduman, A & Firat, A 2015, 'Deployment Challenges of Offshore Renewable Energy Systems for Sustainability in Developing Countries', pp. 465–477.
20. Weather and Climate 2021, 'Climate and average monthly weather in Larnaca, Cyprus',< https://weather-and-climate.com/>.
21. Wikipedia 2009, 'Design For X', pp. 249–268, <https://en.wikipedia.org/wiki/Design_for_X#searchInput>.
22. Wikipedia 2020, 'Lift coefficient', <https://en.wikipedia.org/wiki/Lift_coefficient#p-search>.
23. Wikipedia 2021a, 'Solar gain', <https://en.wikipedia.org/wiki/Solar_gain#searchInput>.
24. Wikipedia 2021b, 'Daylighting', <https://en.wikipedia.org/wiki/Daylighting#searchInput>.
25. Wikipedia 2021c, 'Lux', <https://en.wikipedia.org/wiki/Lux#searchInput>.
26. Zakou, C 2016, 'DESIGN AND ANALYSIS OF AN ADAPTIVE BENDINGACTIVE GRIDSHELL', pp. 1–120.
27. Αθηνή, Σ 2017, 'ΠΡΟΣΑΡΜΟΣΤΙΚΟΣ ΦΟΡΕΑΣ ΑΠΟ ΨΑΛΙΔΩΤΑ ΚΑΙ ΚΑΛΩΔΙΩΤΑ ΕΥΚΑΜΠΤΑ ΣΤΟΙΧΕΙΑ',.

Konstantinos Petrou

APPENDIX

Appendix I – Senarios of Sequences 2 (Motion planning and scheduling tables)

Sequence 2a (S_{2a}):

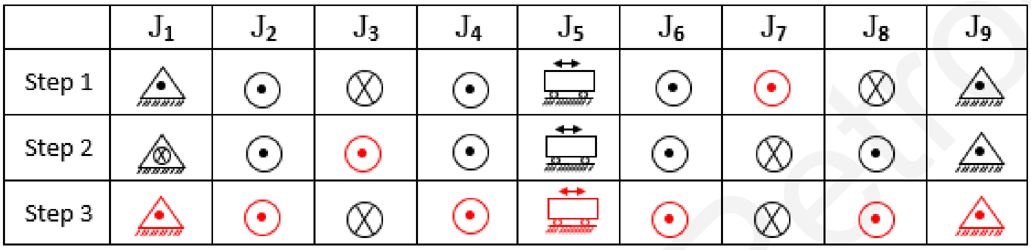

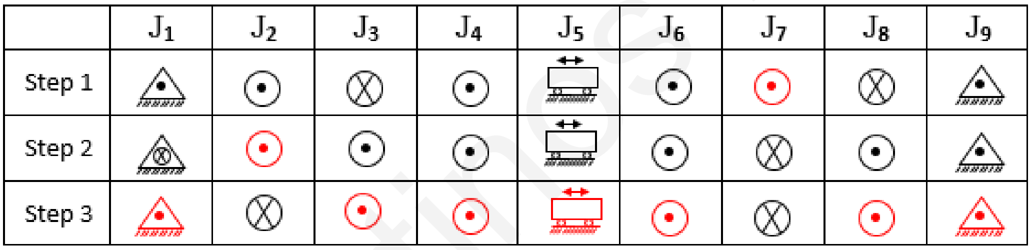

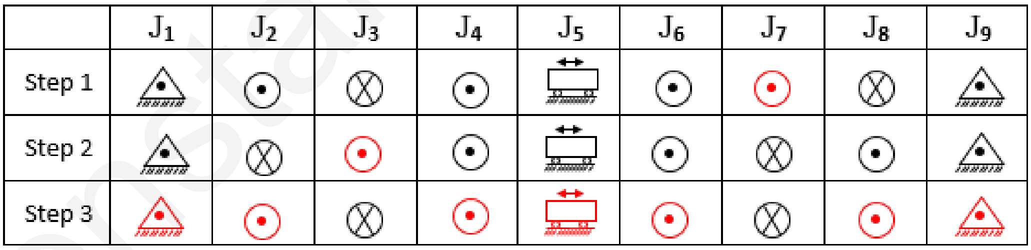

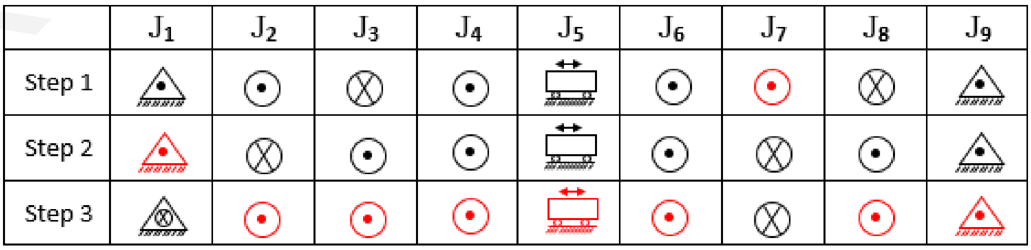

Konstantinos Petrou

<u>Sequence 2b (S_{2b}):</u>

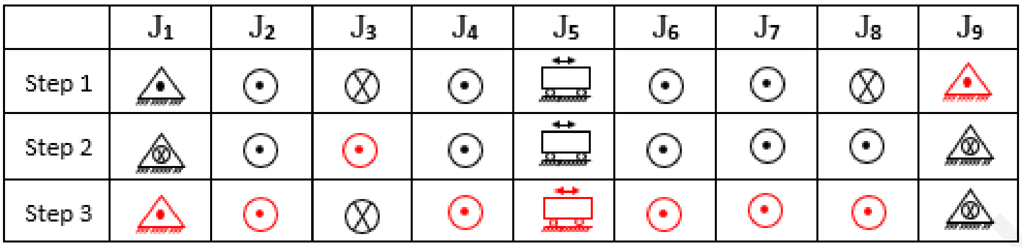

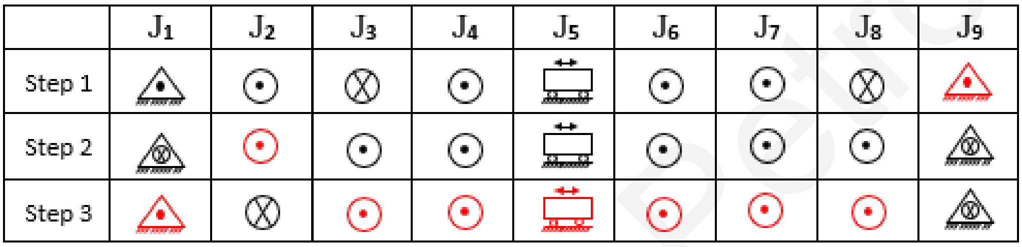

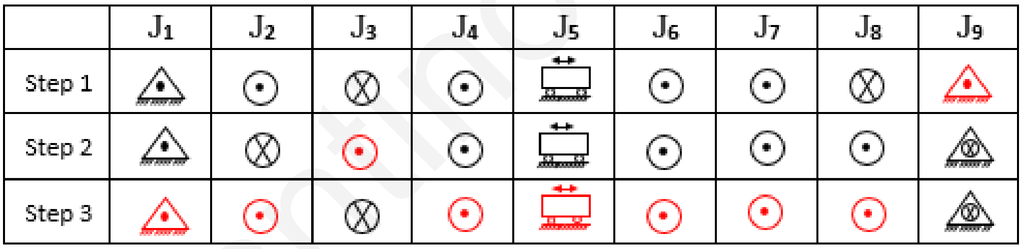

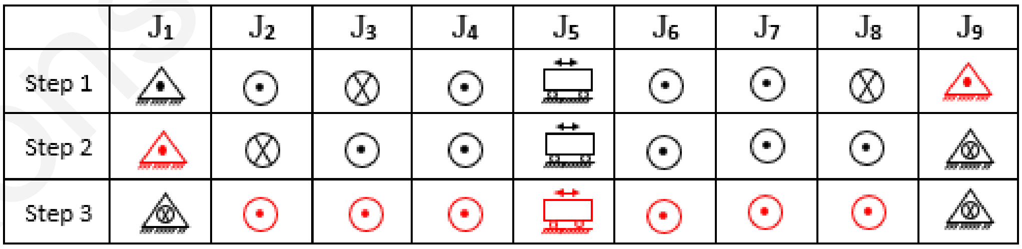

Konstantinos Petrou

Sequence 2c (S_{2c}):

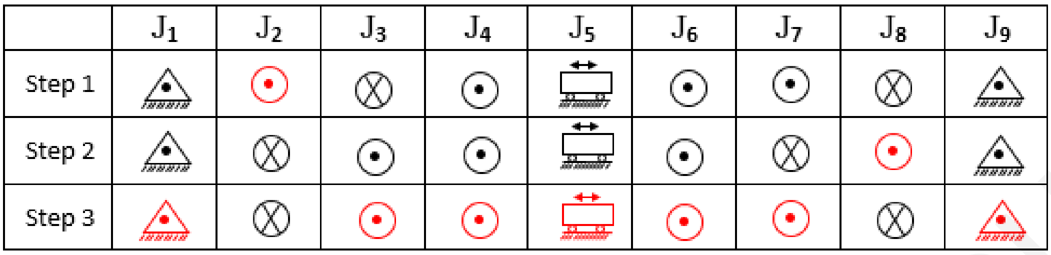

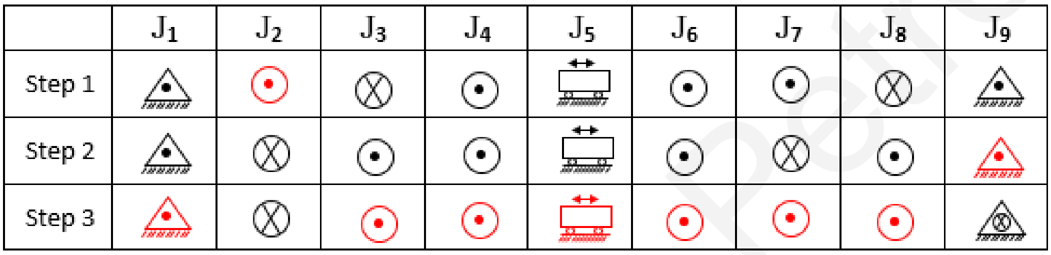

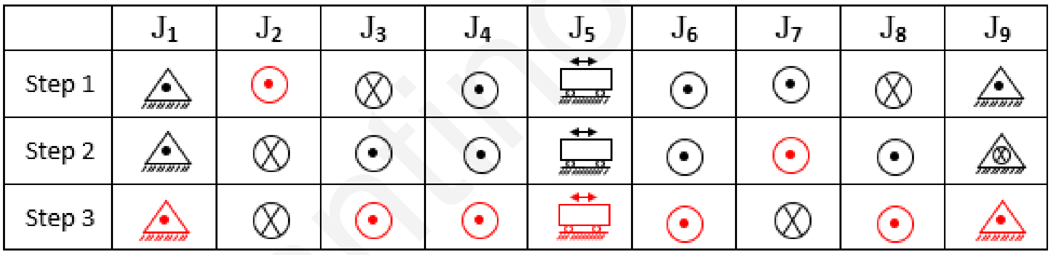

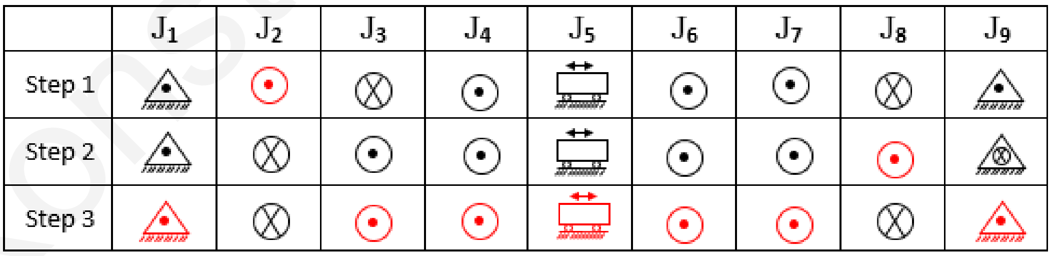

Konstantinos Petrou

Sequence 2d (S_{2d}):

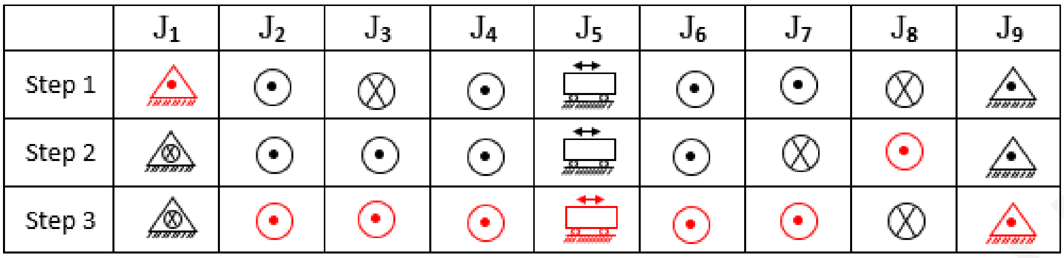

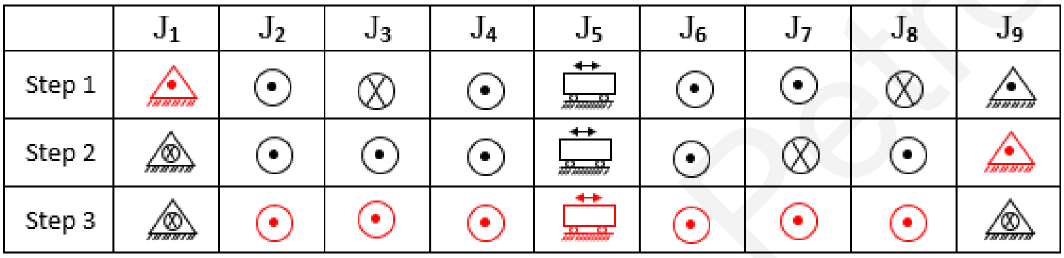

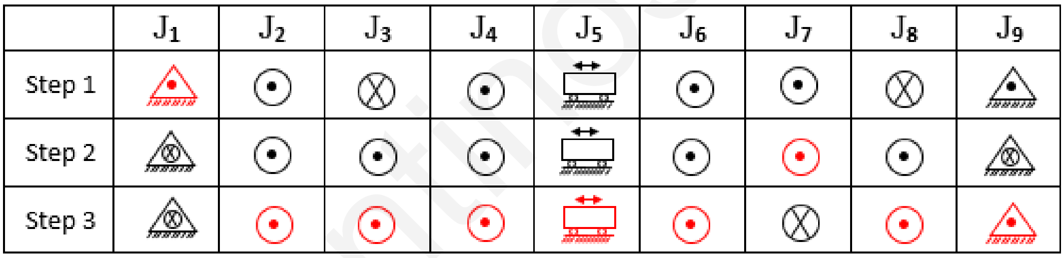

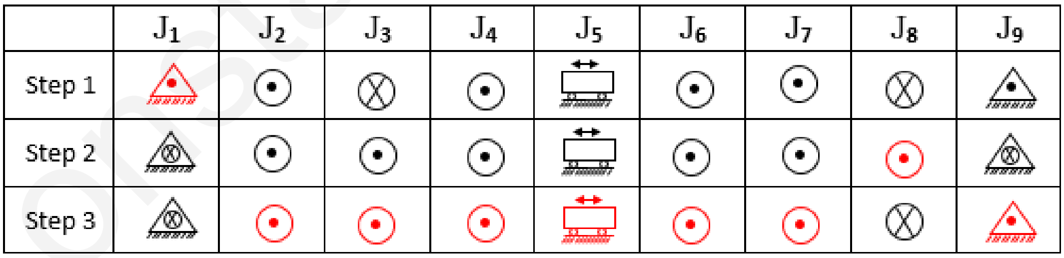

Konstantinos Petrou

Sequence 2e (S_{2e}):

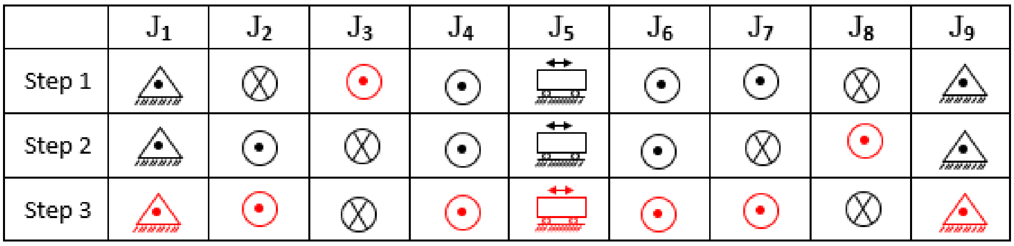

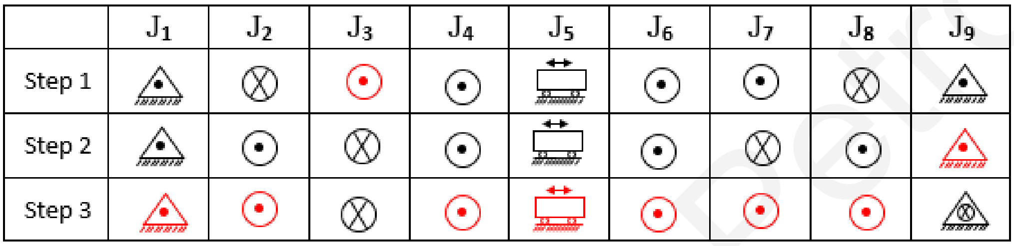

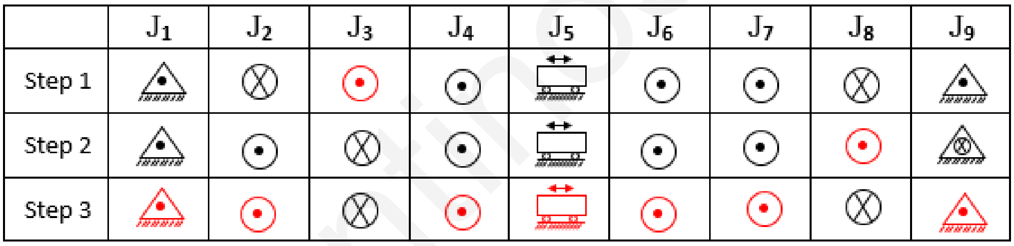

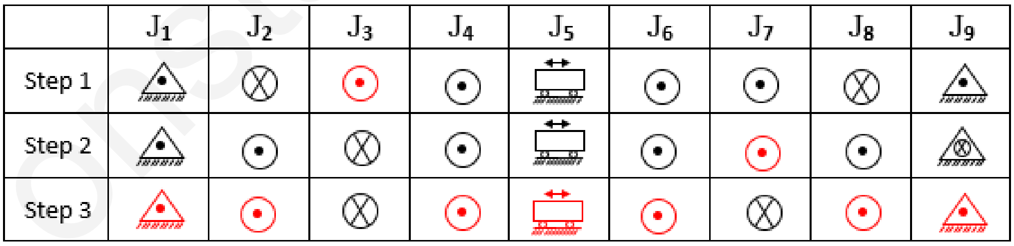

Konstantinos Petrou

Sequence 2f (S_{2f}):

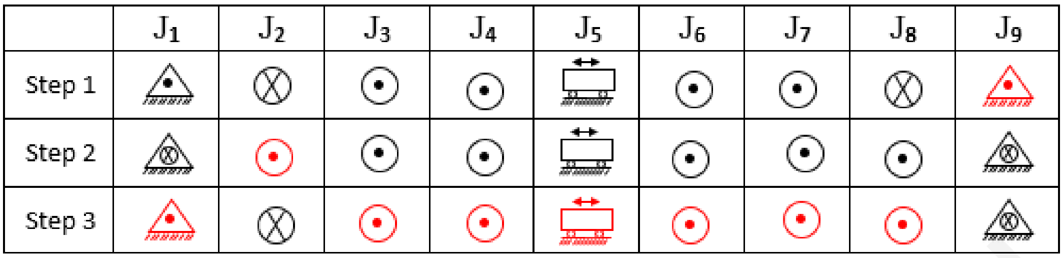

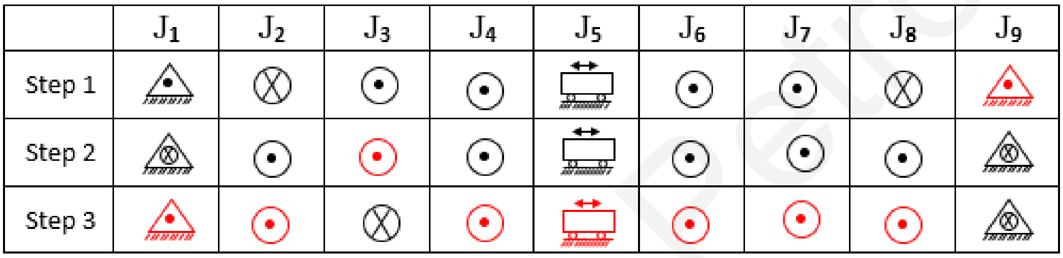

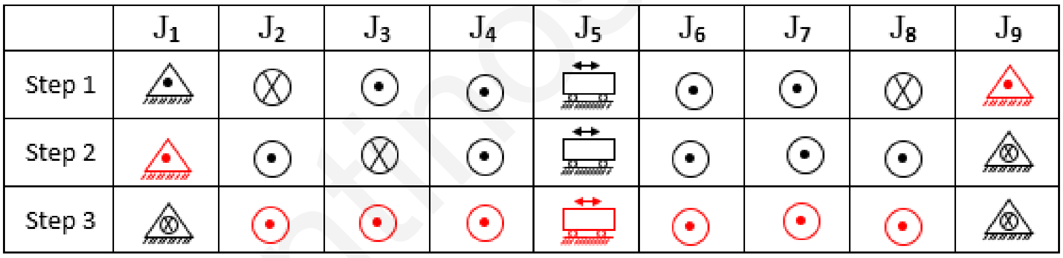

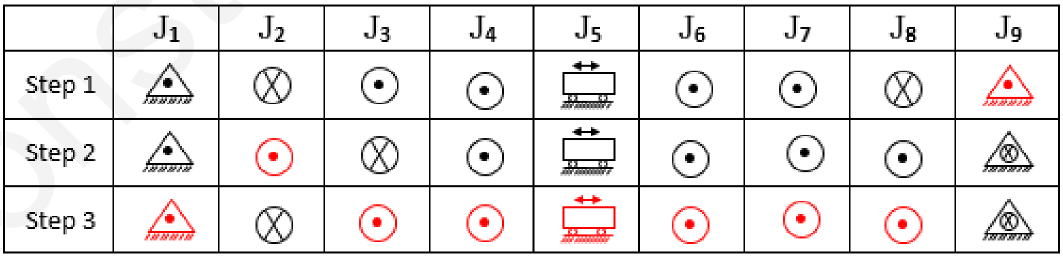

Konstantinos Petrou

Sequence 2g (S_{2g}):

	J_1	J_2	J_3	J_4	J_5	J_6	J_7	J_8	J_9
Step 1	△	⊗	⊙	⊙	↔▭	⊙	⊙	⊗	△
Step 2	△	⊙	⊗	⊙	↔▭	⊙	⊗	⊙	△
Step 3	△⊗	⊙	⊙	⊙	↔▭	⊙	⊗	⊙	△

	J_1	J_2	J_3	J_4	J_5	J_6	J_7	J_8	J_9
Step 1	△	⊗	⊙	⊙	↔▭	⊙	⊙	⊗	△
Step 2	△	⊙	⊗	⊙	↔▭	⊙	⊗	⊙	△
Step 3	△	⊗	⊙	⊙	↔▭	⊙	⊗	⊙	△

	J_1	J_2	J_3	J_4	J_5	J_6	J_7	J_8	J_9
Step 1	△	⊗	⊙	⊙	↔▭	⊙	⊙	⊗	△
Step 2	△⊗	⊙	⊙	⊙	↔▭	⊙	⊗	⊙	△
Step 3	△	⊗	⊙	⊙	↔▭	⊙	⊗	⊙	△

	J_1	J_2	J_3	J_4	J_5	J_6	J_7	J_8	J_9
Step 1	△	⊗	⊙	⊙	↔▭	⊙	⊙	⊗	△
Step 2	△⊗	⊙	⊙	⊙	↔▭	⊙	⊗	⊙	△
Step 3	△	⊙	⊗	⊙	↔▭	⊙	⊗	⊙	△

Konstantinos Petrou

Sequence 2h (S_{2h}):

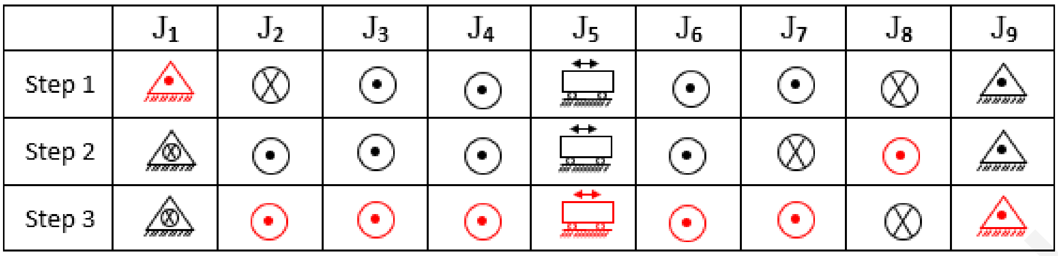

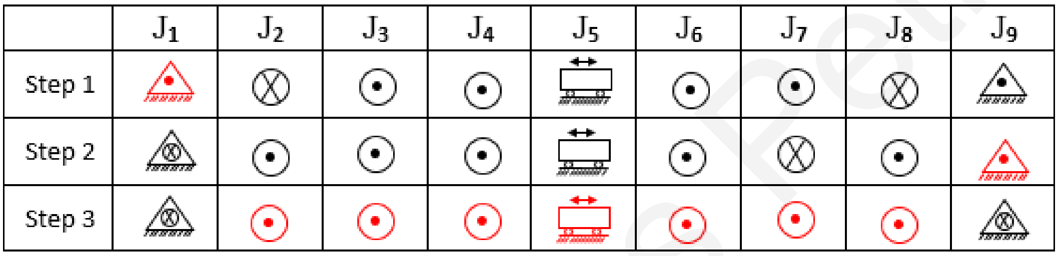

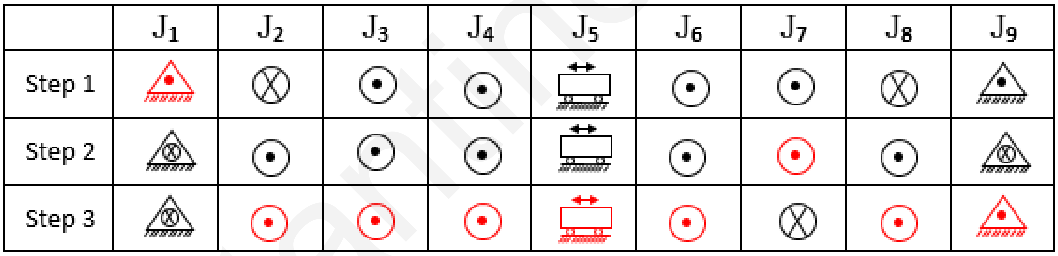

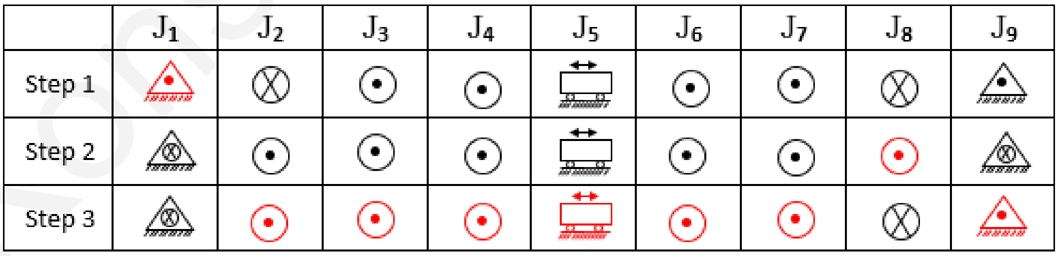

Konstantinos Petrou

Sequence 2i (S_{2i}):

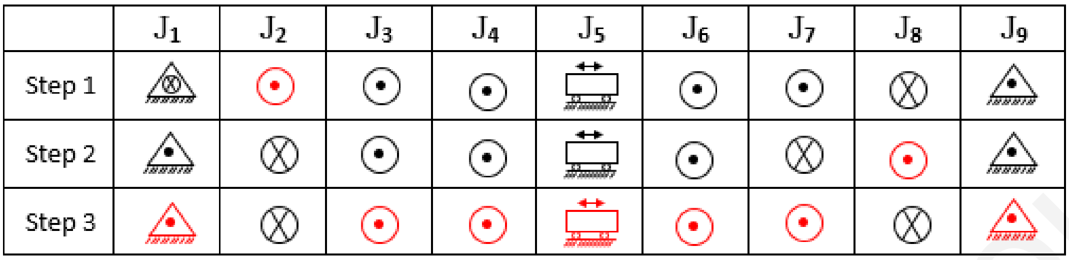

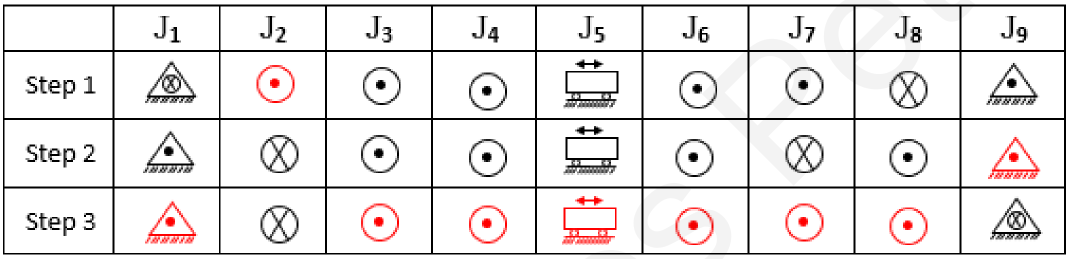

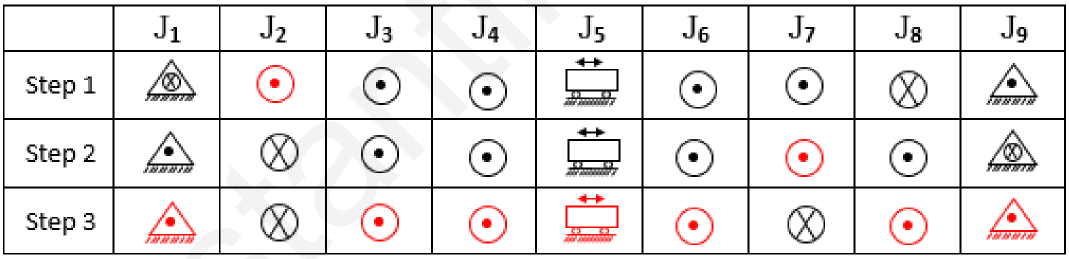

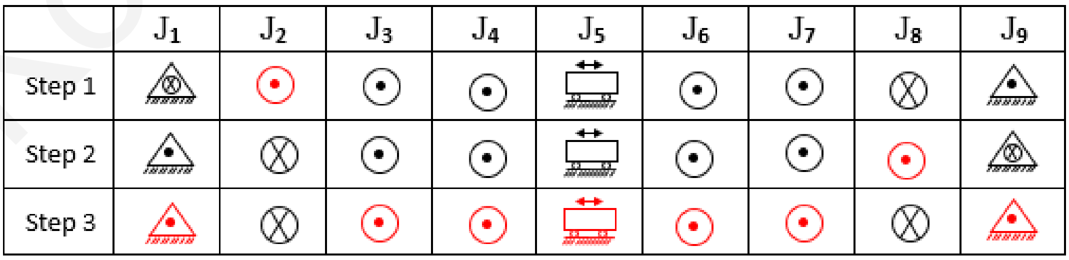

Konstantinos Petrou

Sequence 2j (S_{2j}):

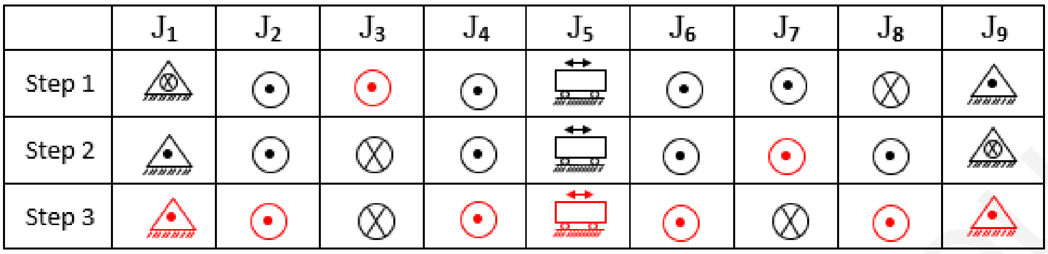

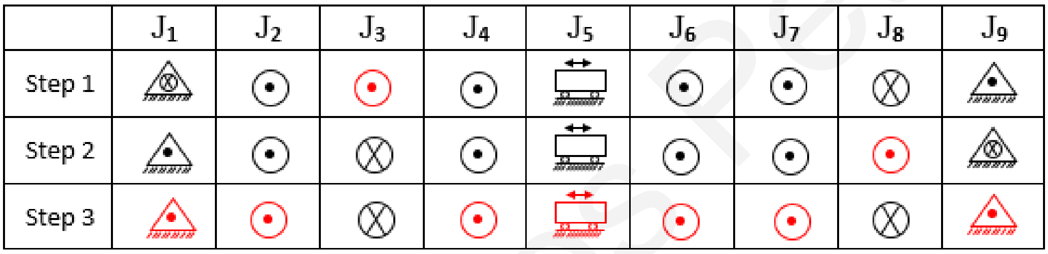

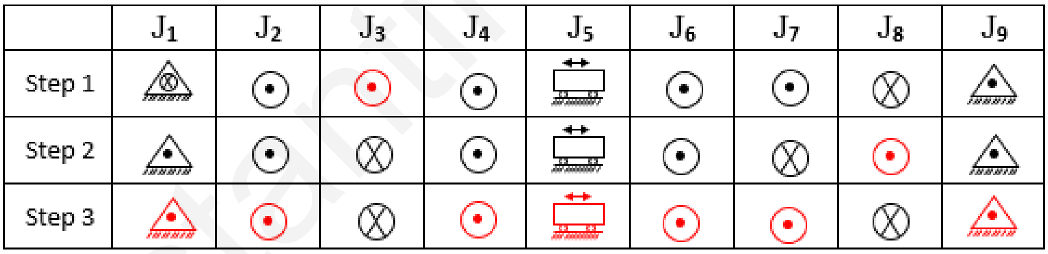

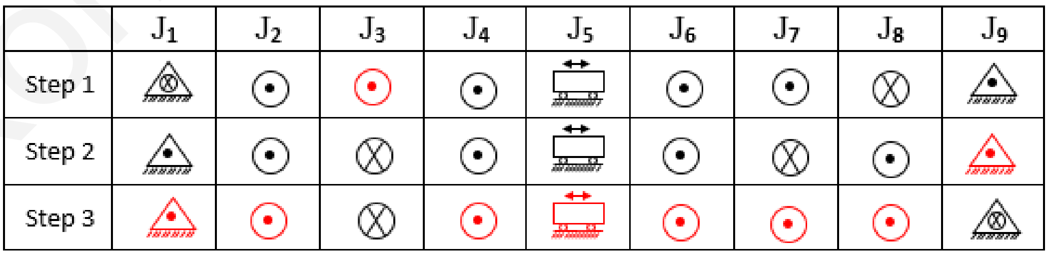

Konstantinos Petrou

Sequence 2k (S_{2k}):

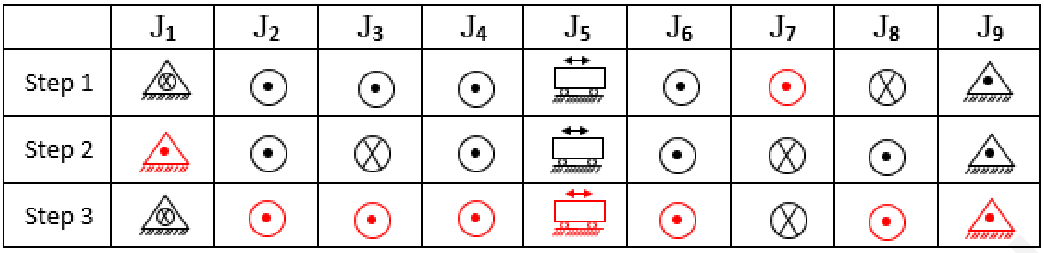

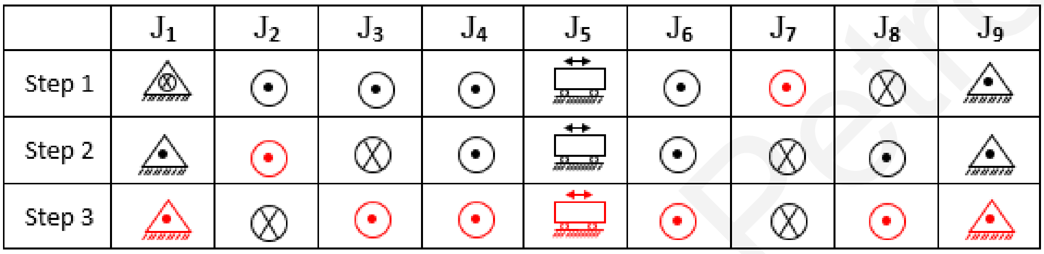

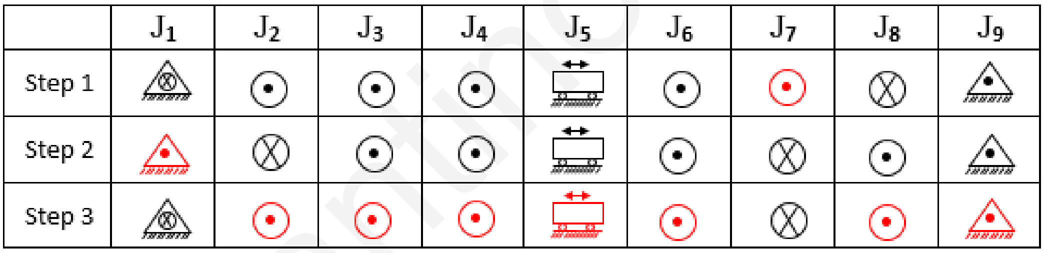

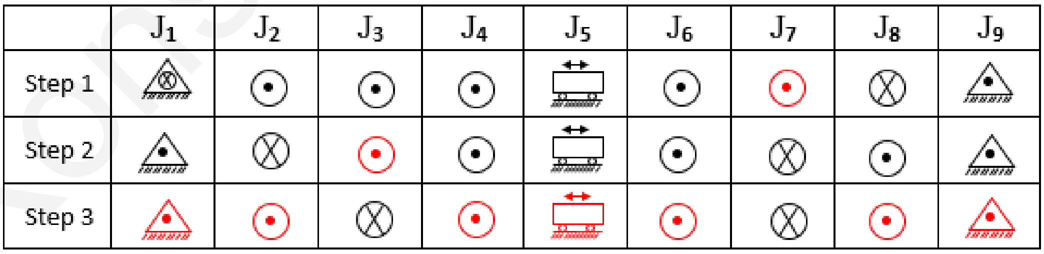

Konstantinos Petrou

Sequence 21 (S_{21}):

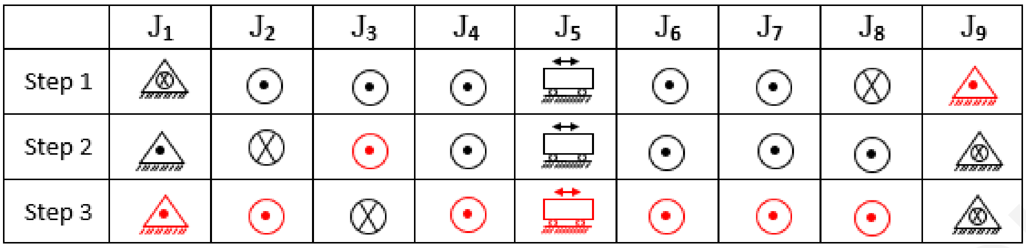

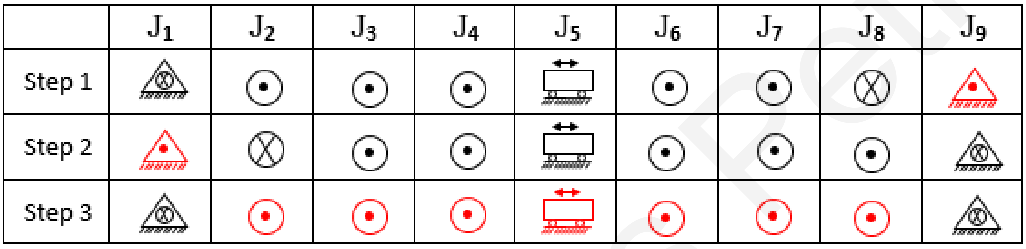

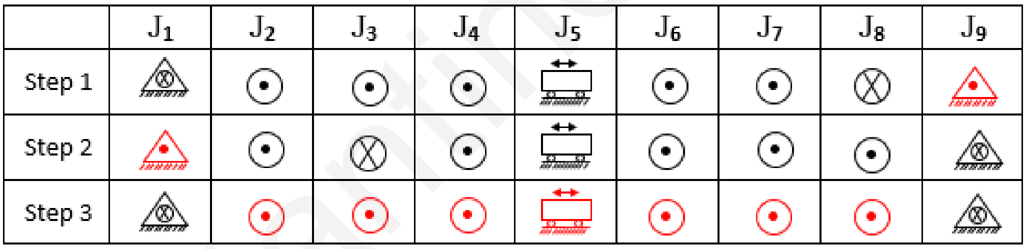

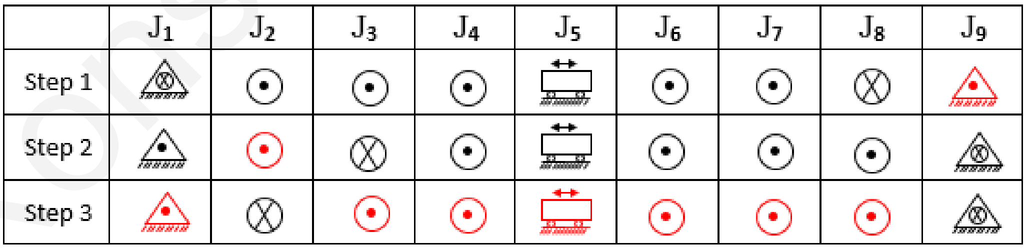

Konstantinos Petrou

Sequence 2m (S_{2m}):

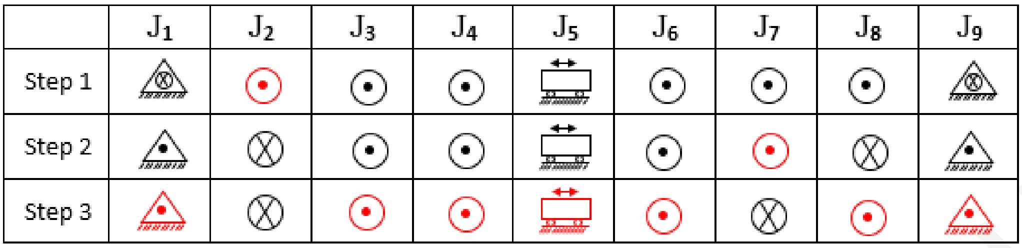

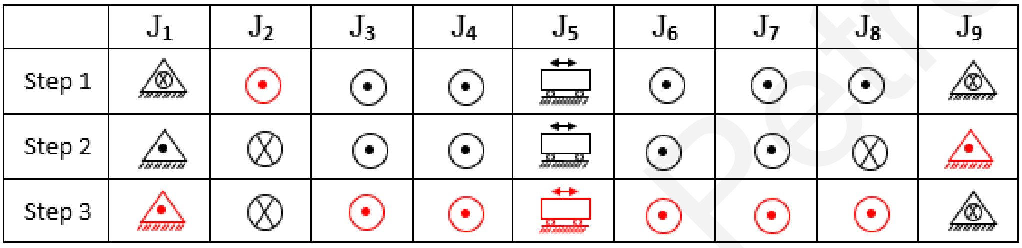

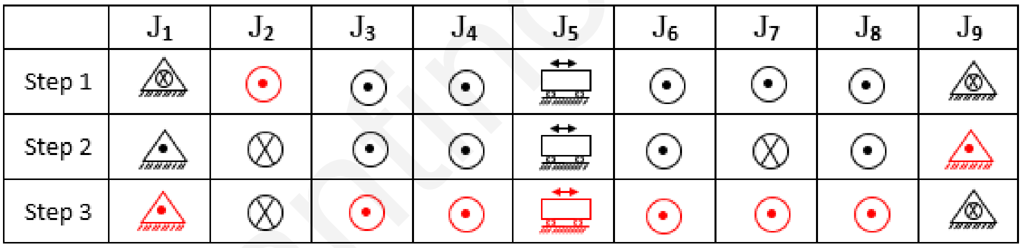

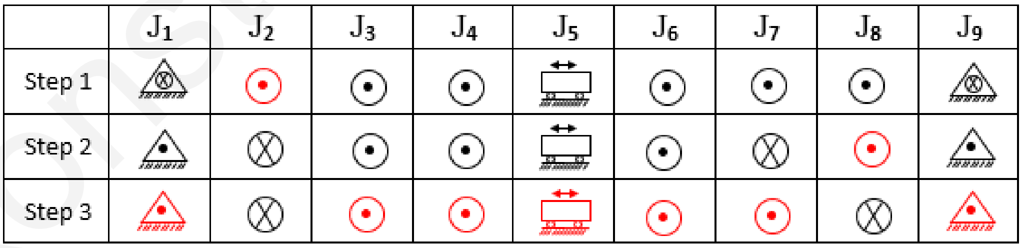

Konstantinos Petrou

Sequence 2n (S_{2n}):

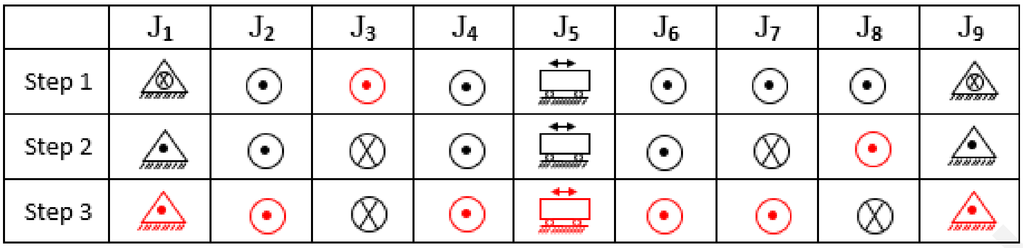

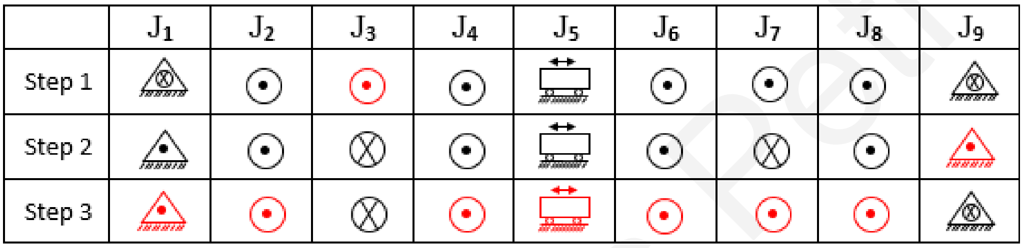

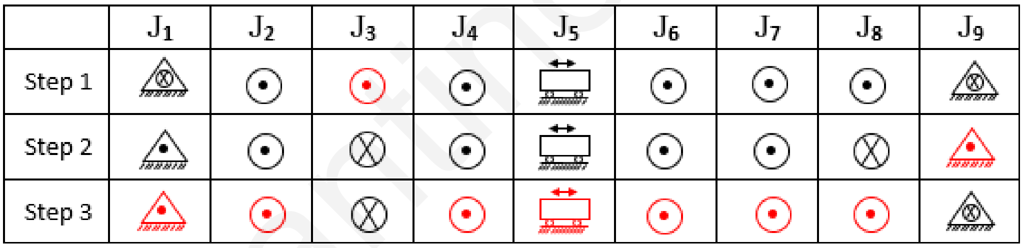

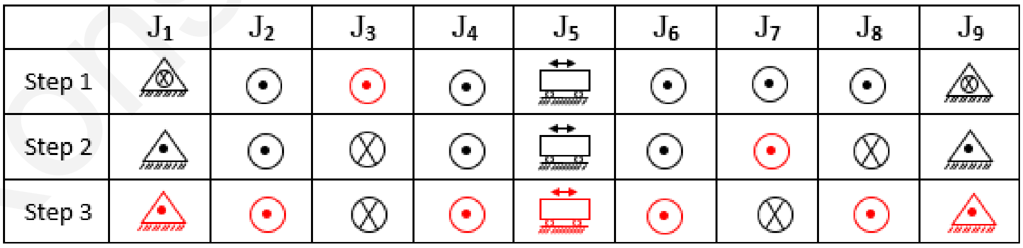

Konstantinos Petrou

Sequence 2o (S_{2o}):

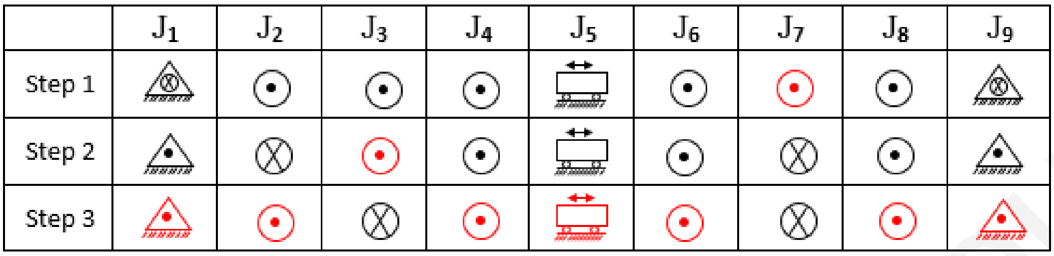

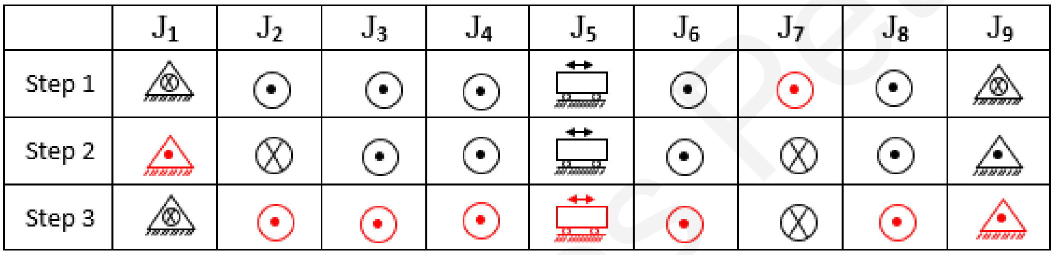

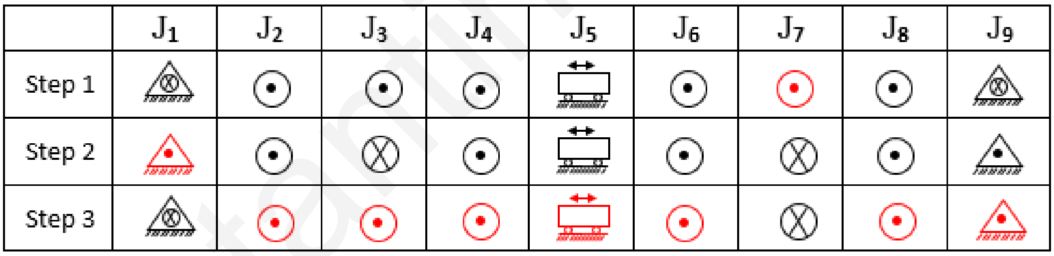

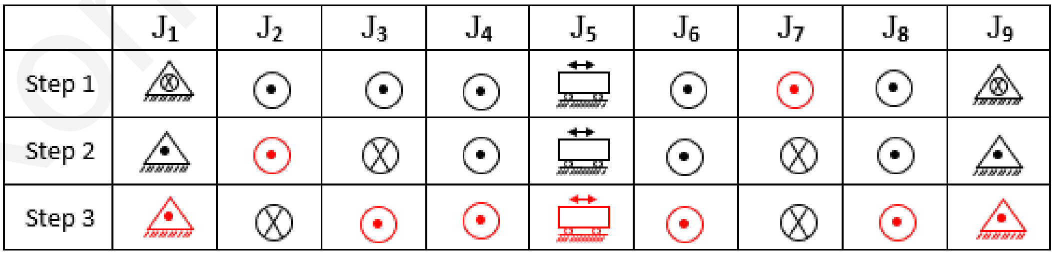

Sequence 2p (S_{2p}):

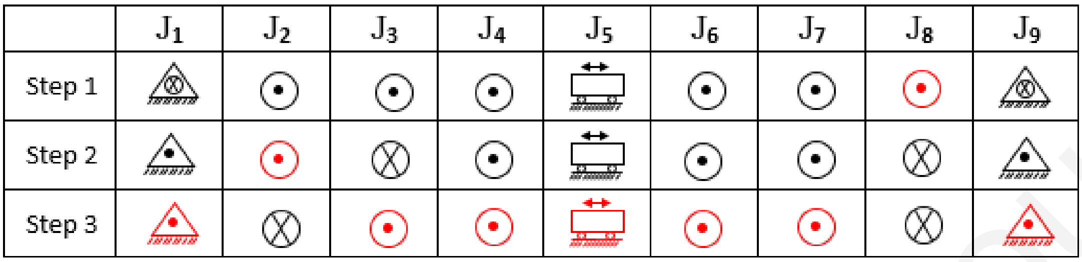

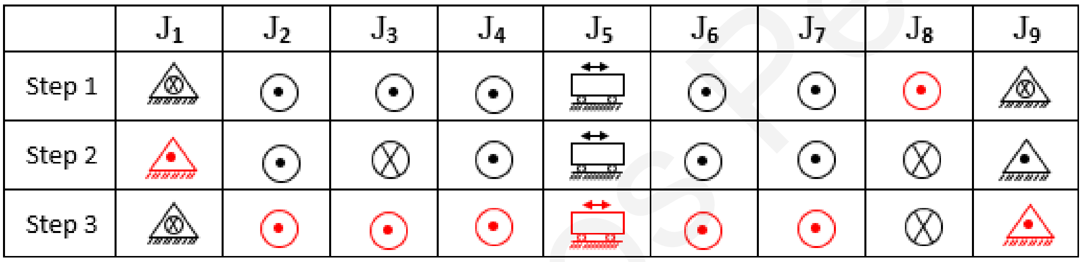

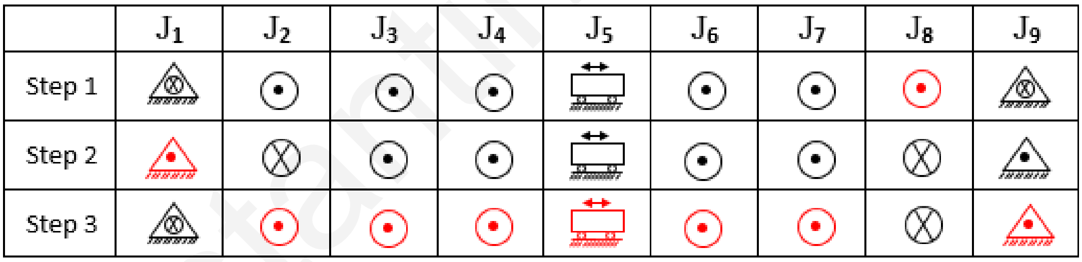

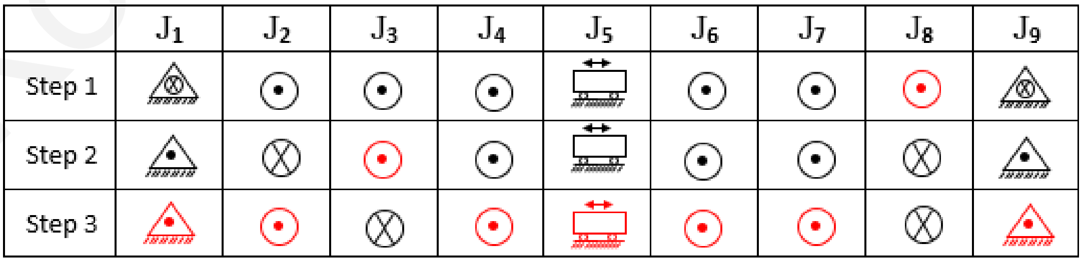

Sequence 2q (S_{2q}):

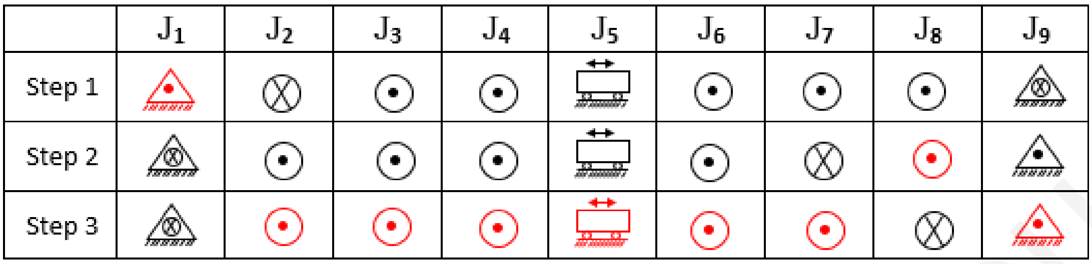

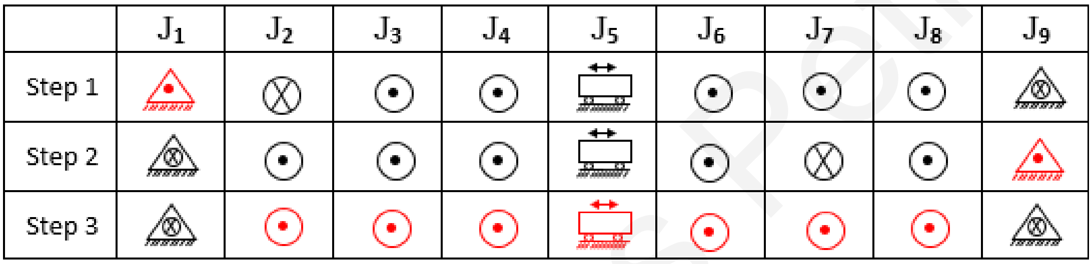

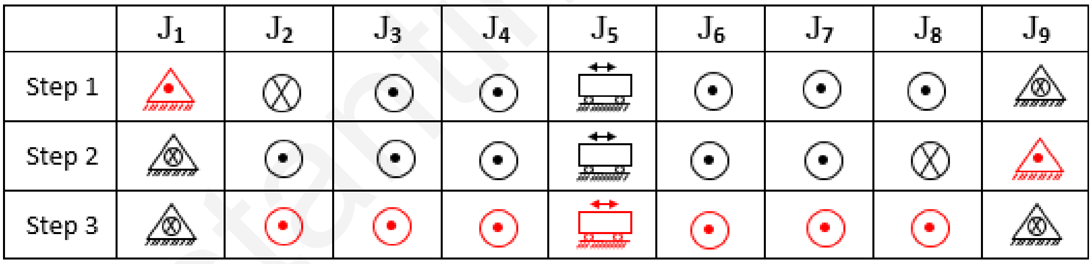

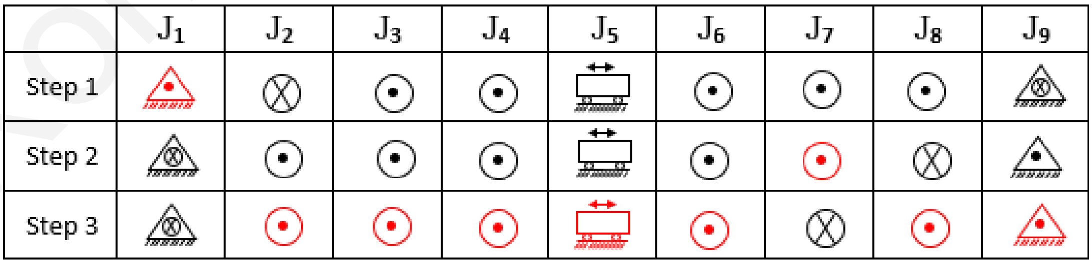

Konstantinos Petrou

Sequence 2r (S_{2r}):

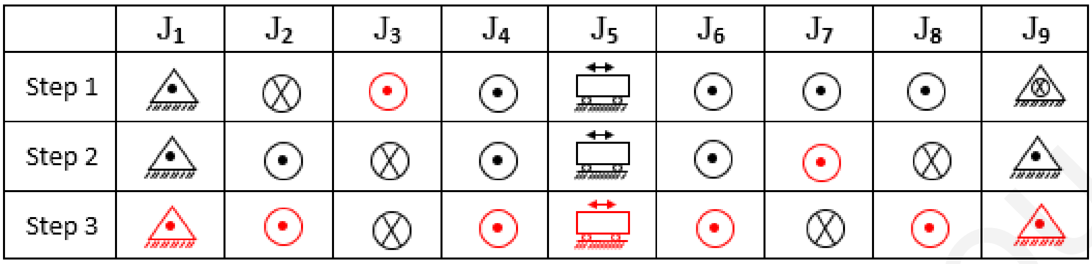

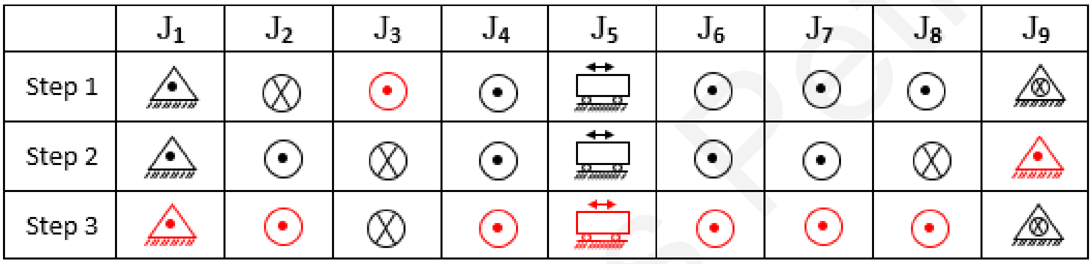

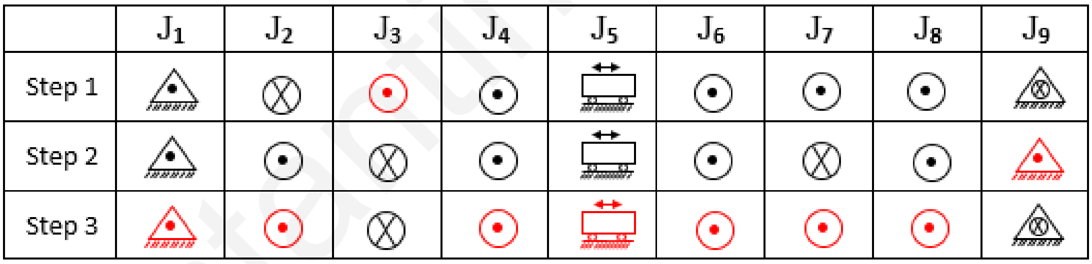

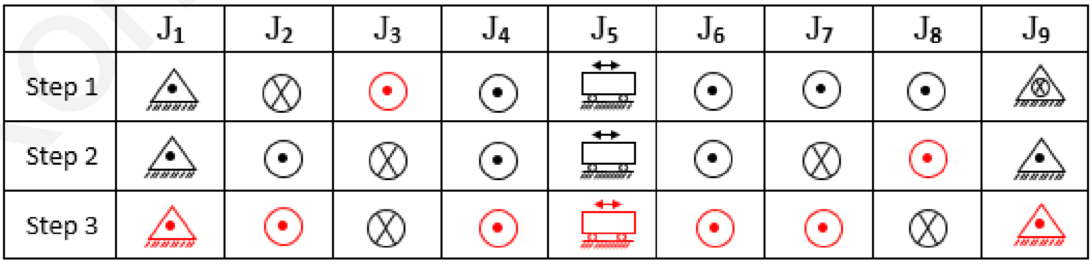

Konstantinos Petrou

Sequence 2s (S_{2s}):

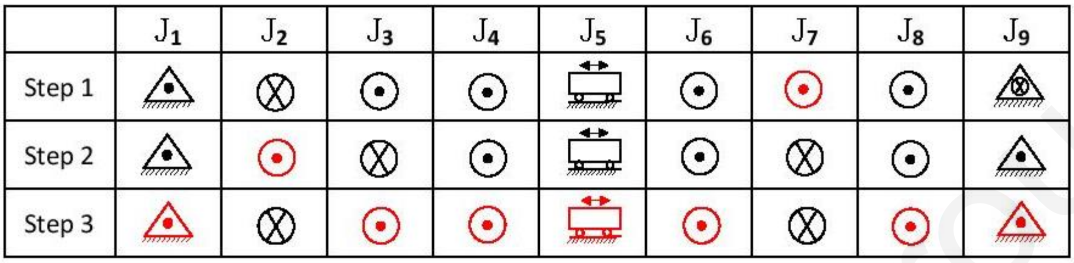

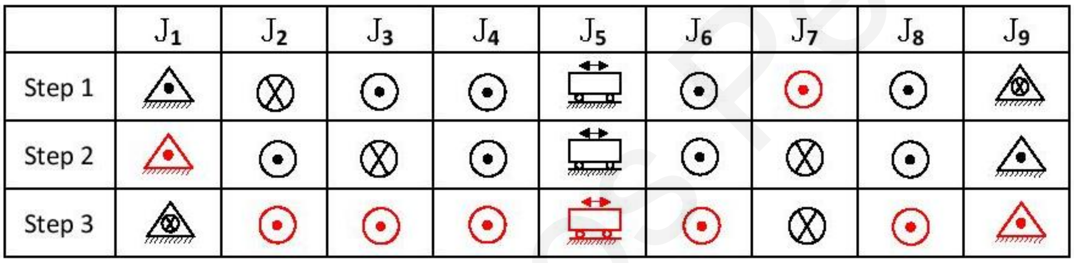

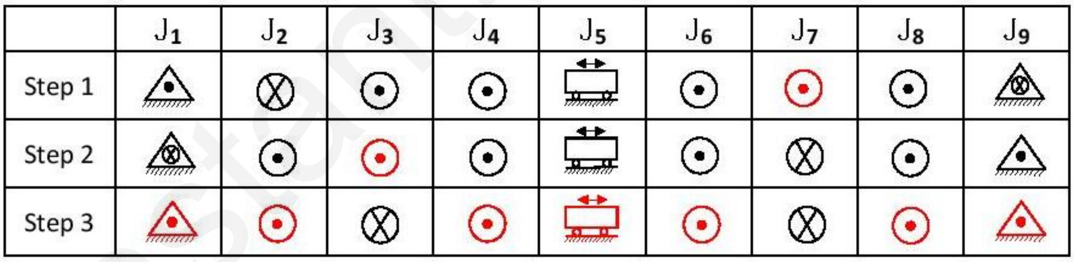

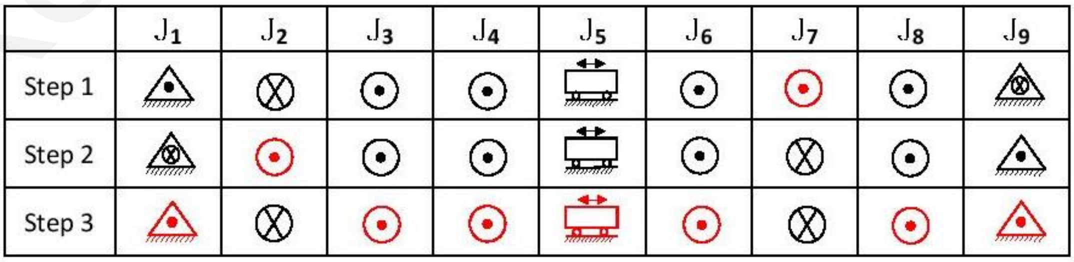

Konstantinos Petrou

Sequence 2t (S_{2t}):

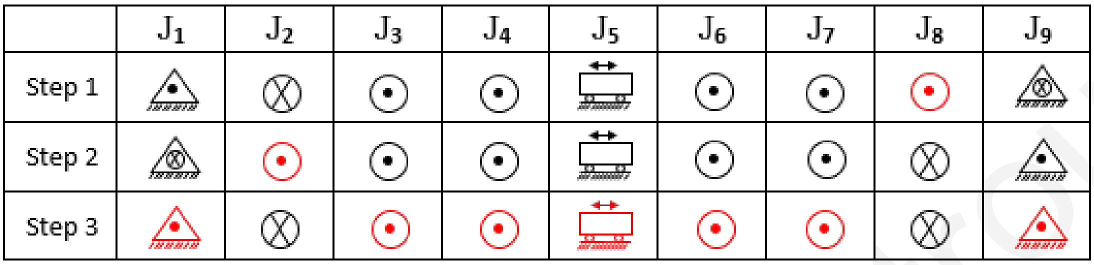

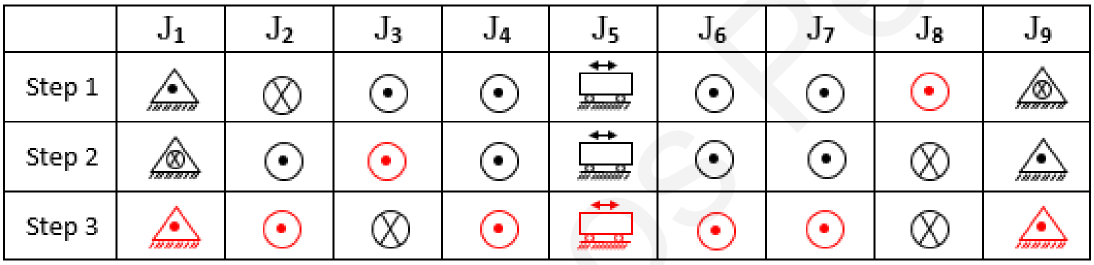

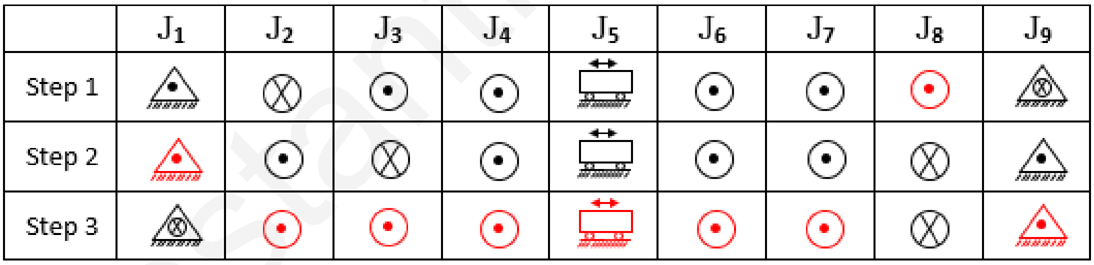

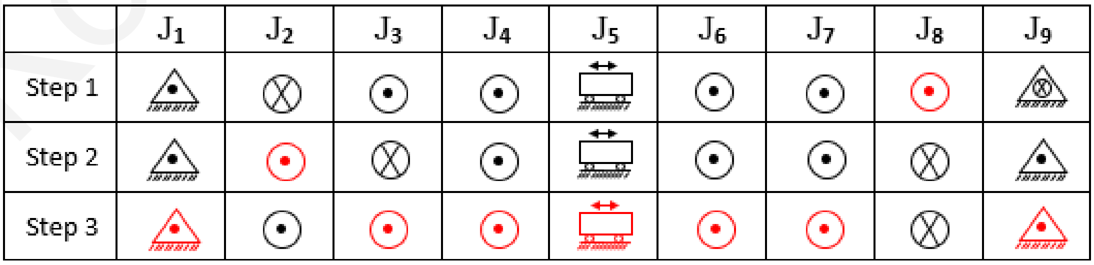

Konstantinos Petrou

Sequence 2u (S_{2u}):

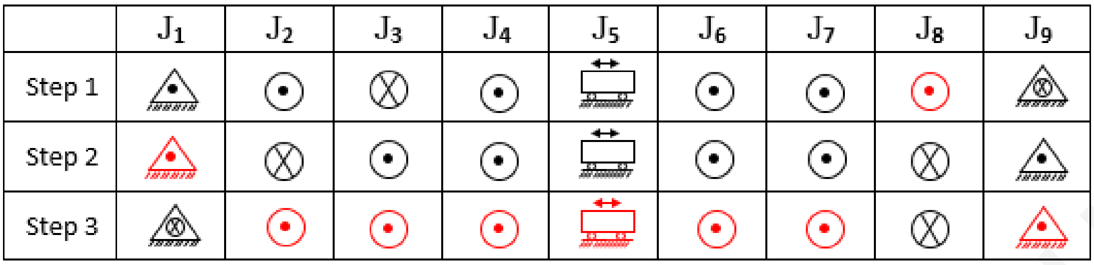

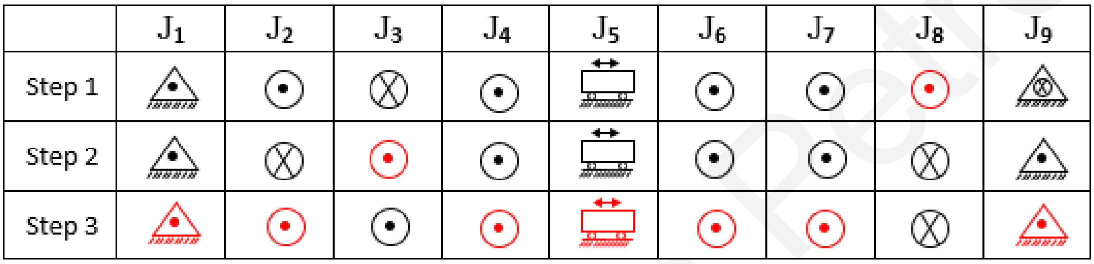

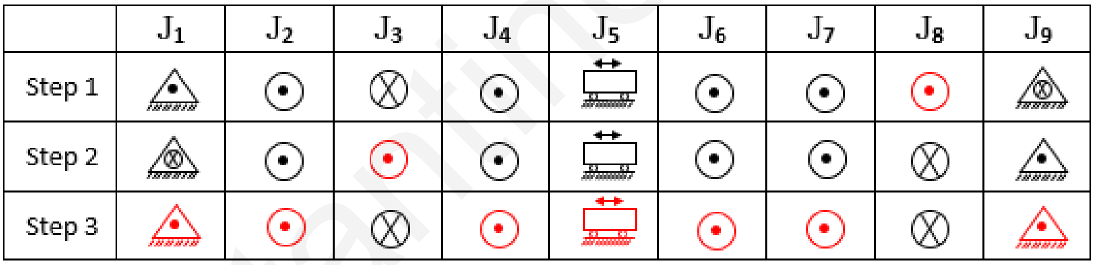

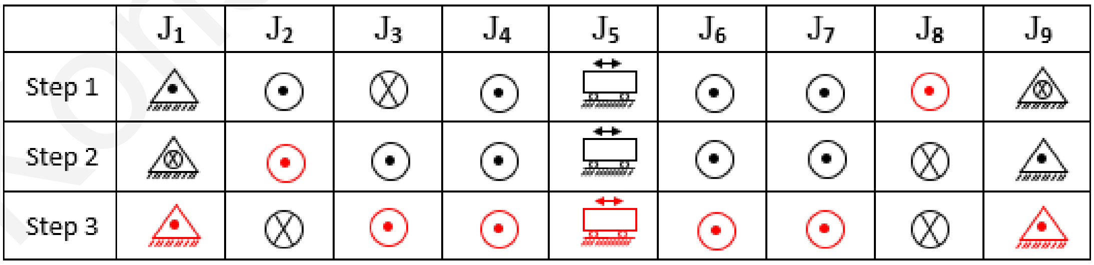

Konstantinos Petrou

Sequence 2v (S_{2v}):

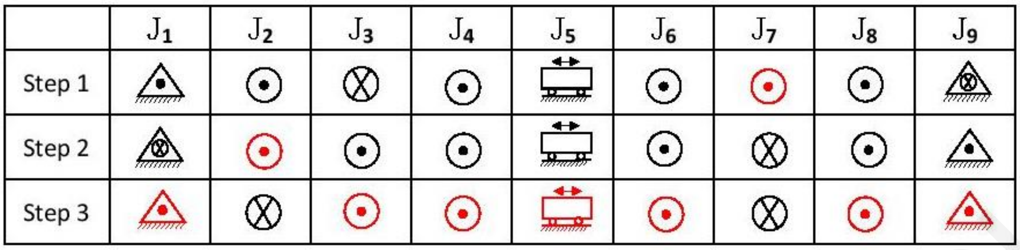

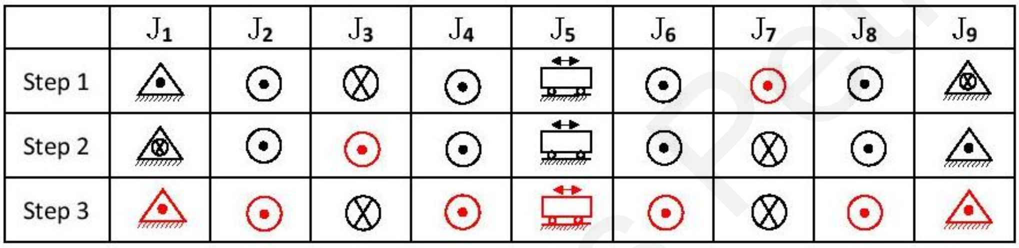

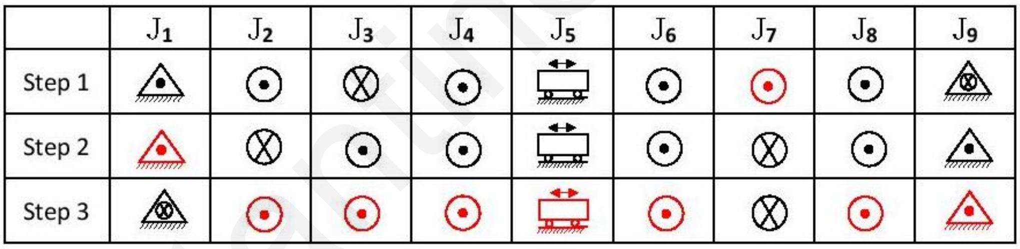

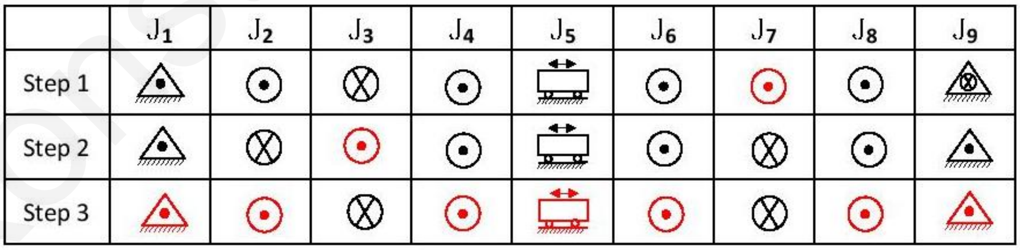

Konstantinos Petrou

Sequence 2w (S_{2w}):

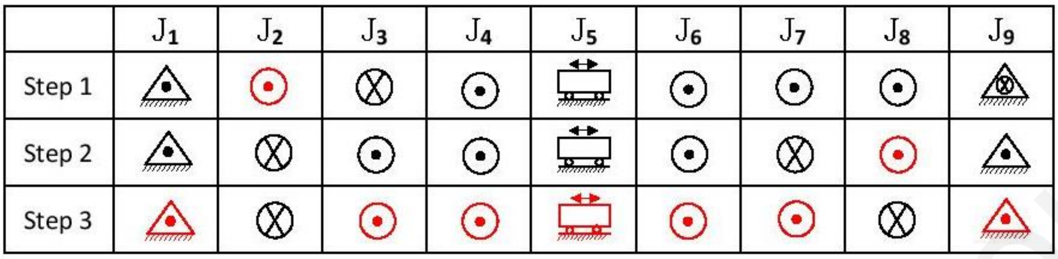

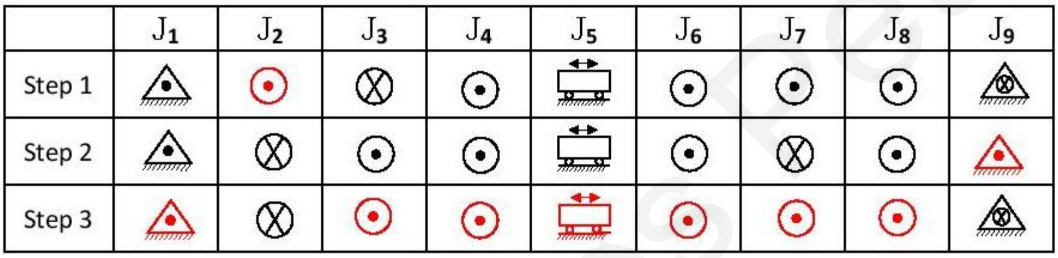

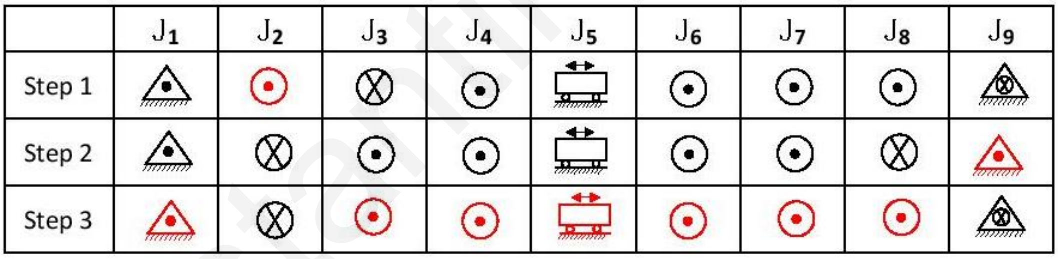

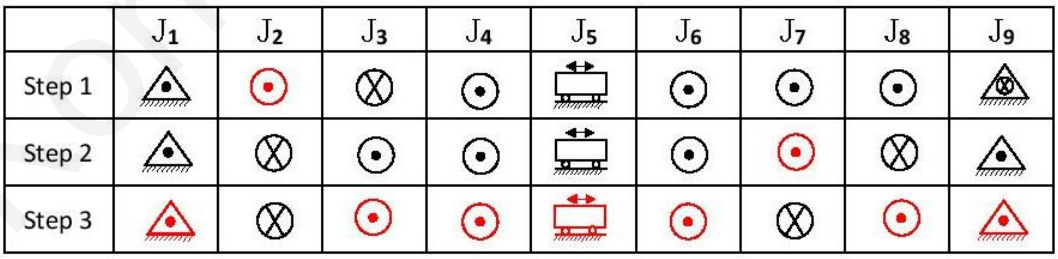

Sequence 2x (S_{2x}):

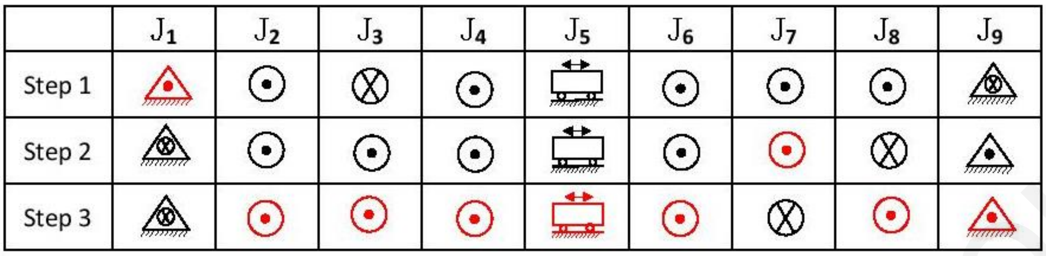

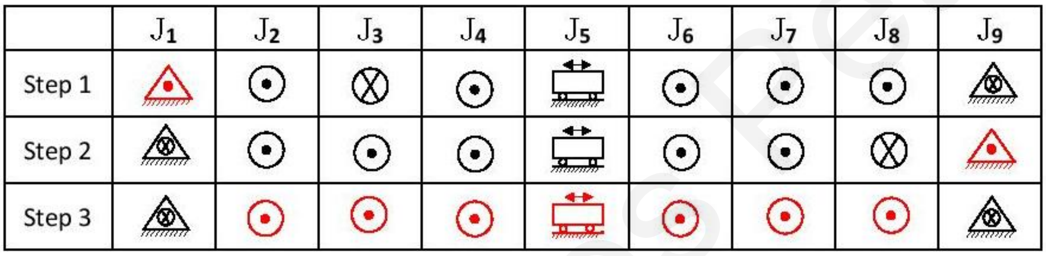

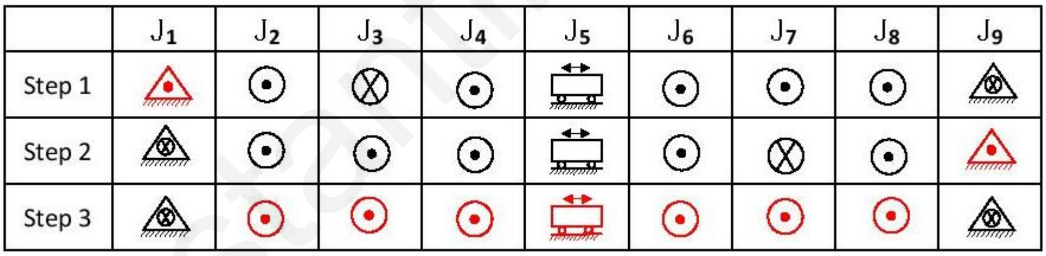

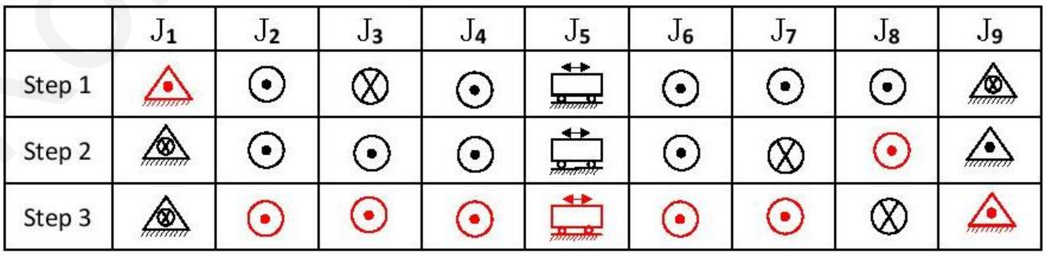

Konstantinos Petrou

Sequence 2y (S_{2y}):

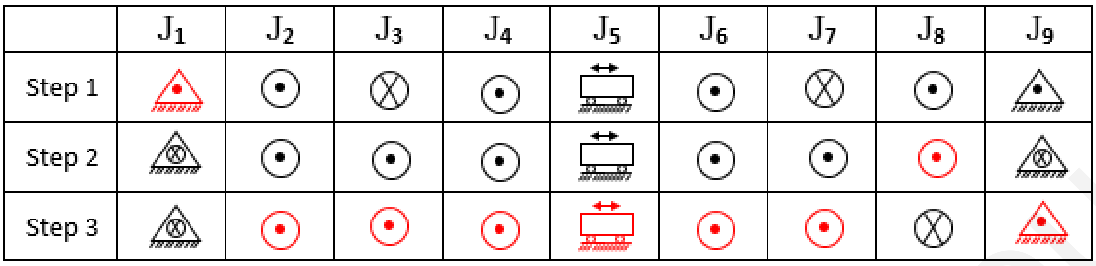

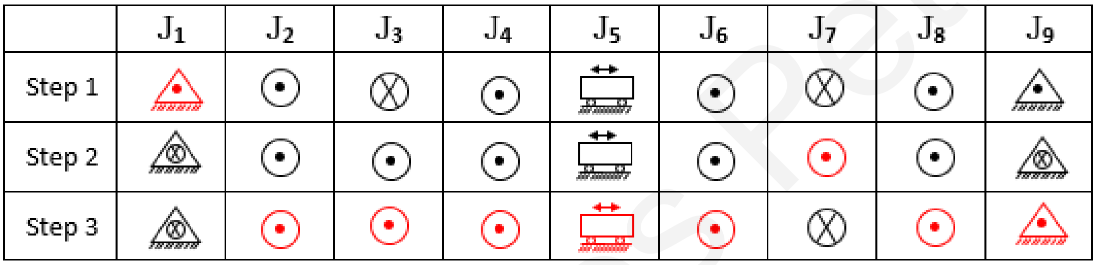

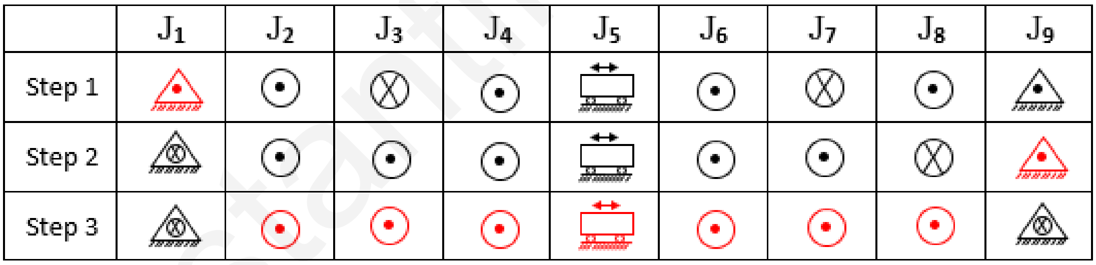

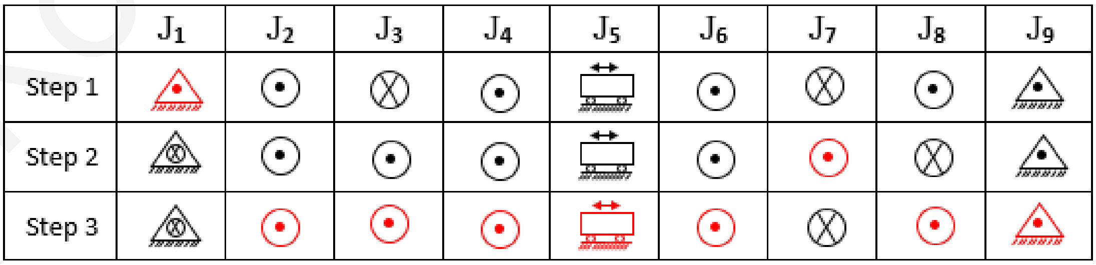

Konstantinos Petrou

Sequence 2z (S_{2z}):

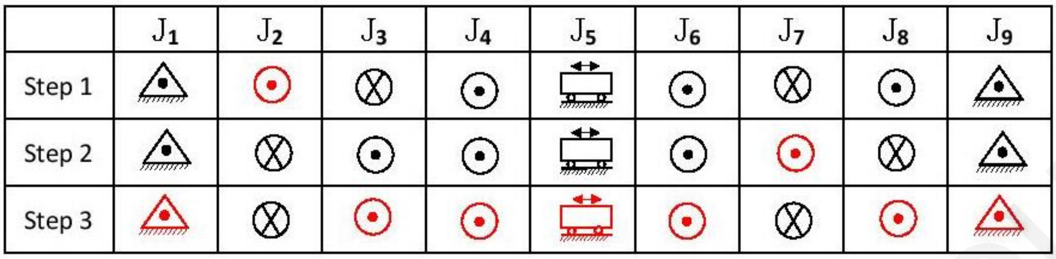

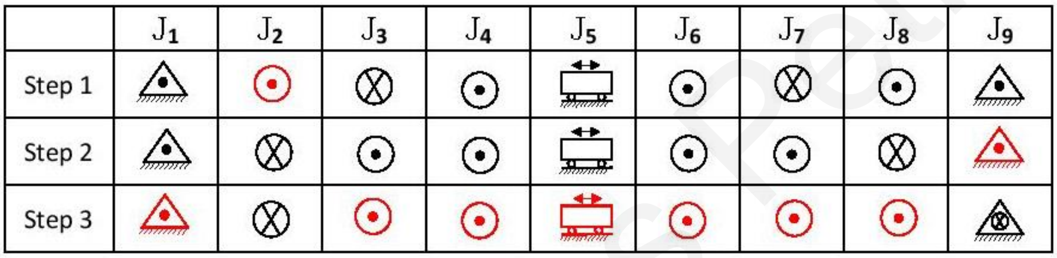

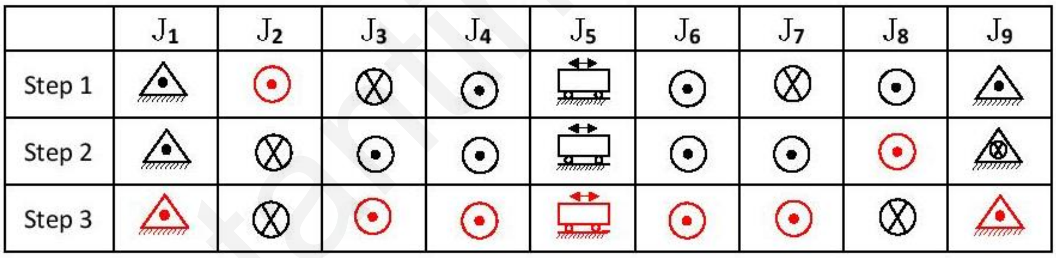

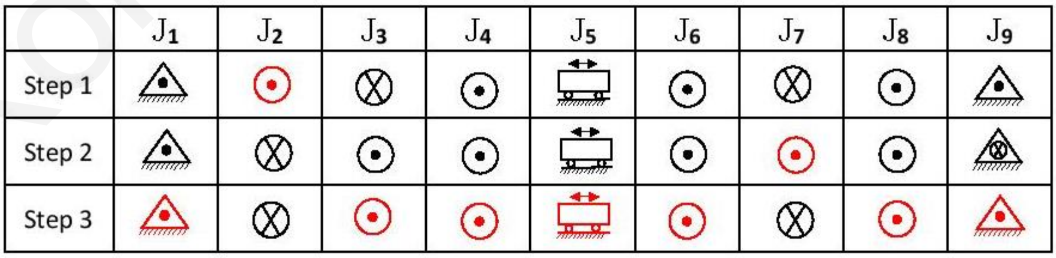

Sequence 2aa (S_{2aa}):

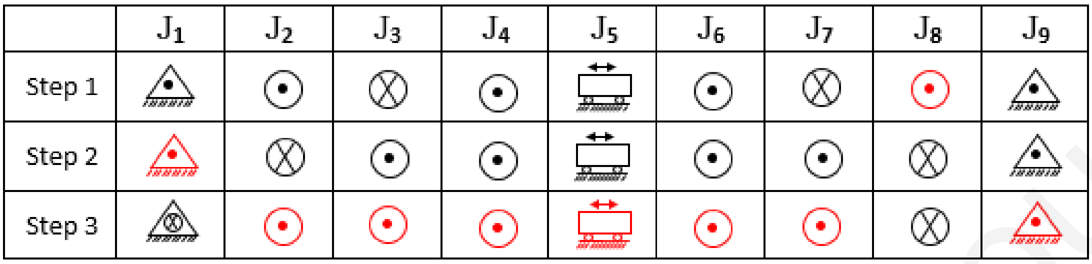

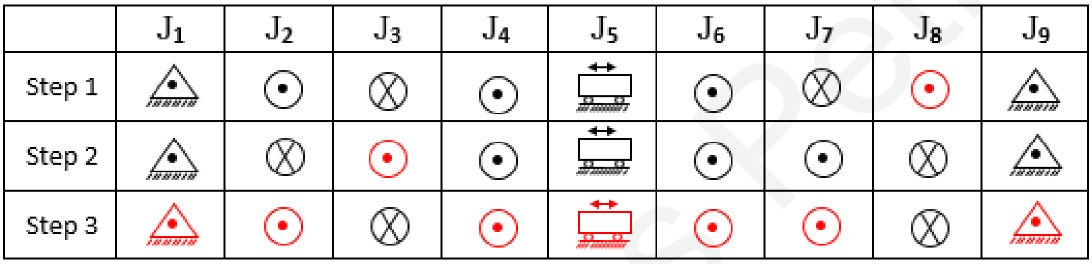

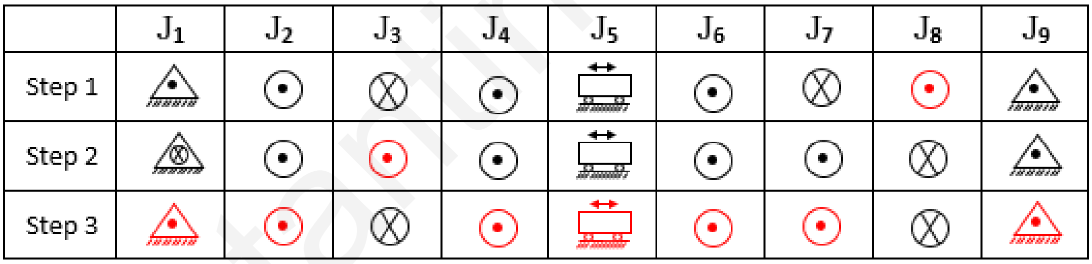

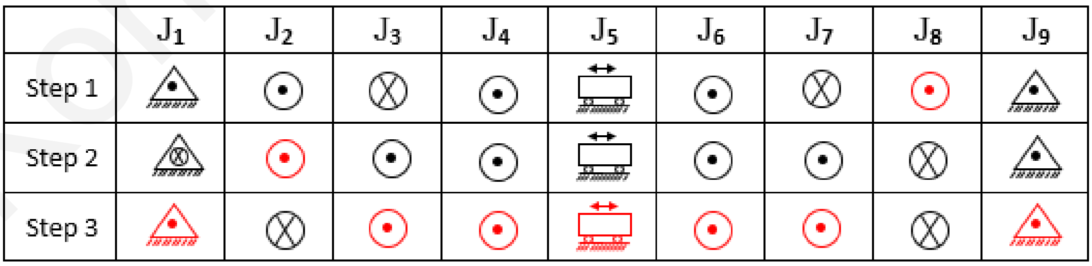

Sequence 2ab (S_{2ab}):

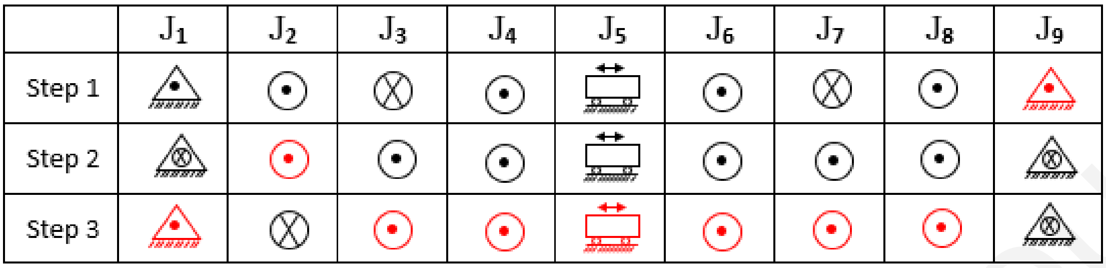

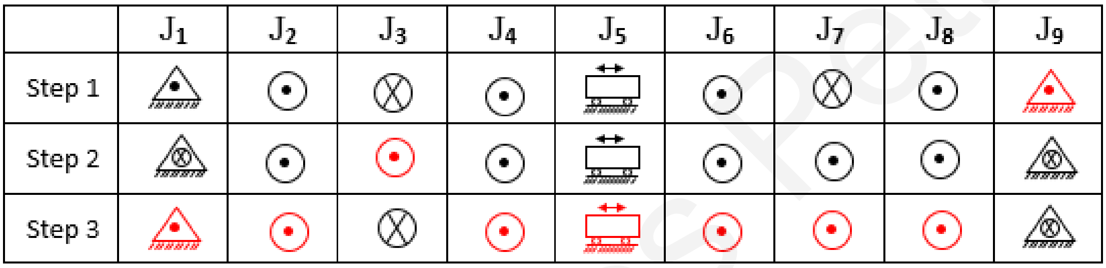

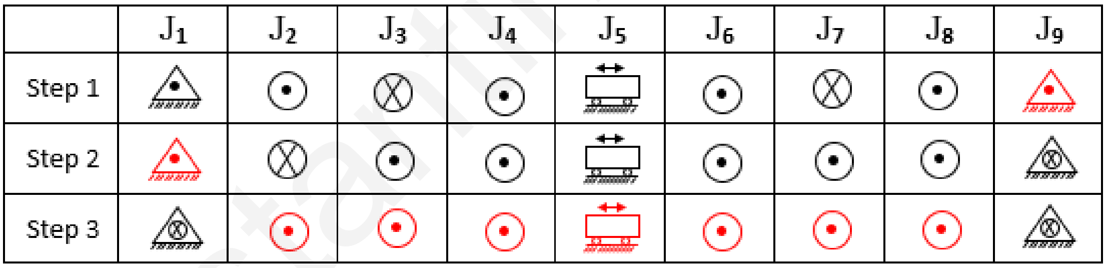

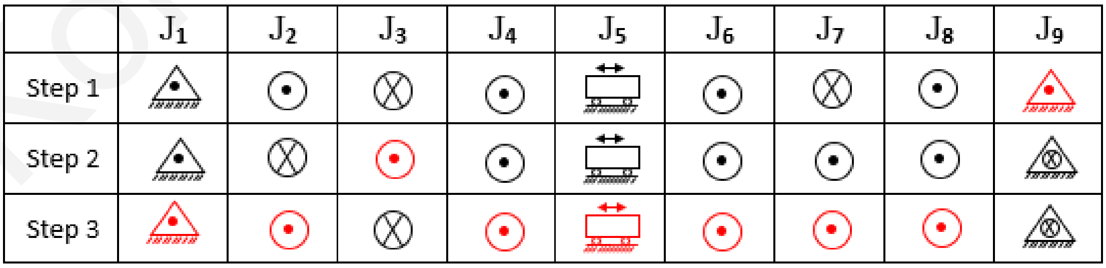

Konstantinos Petrou

Sequence 2ac (S_{2ac}):

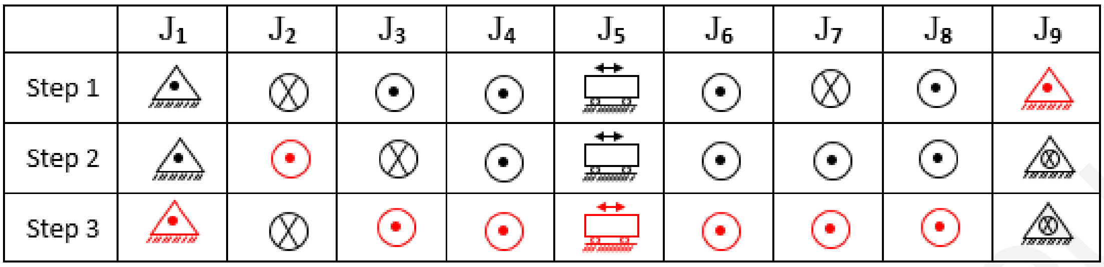

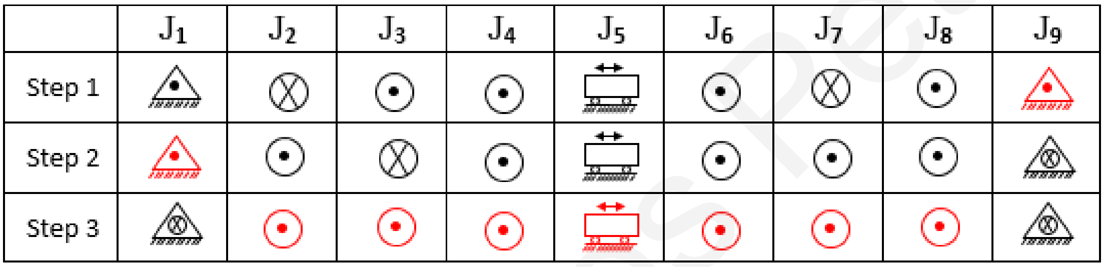

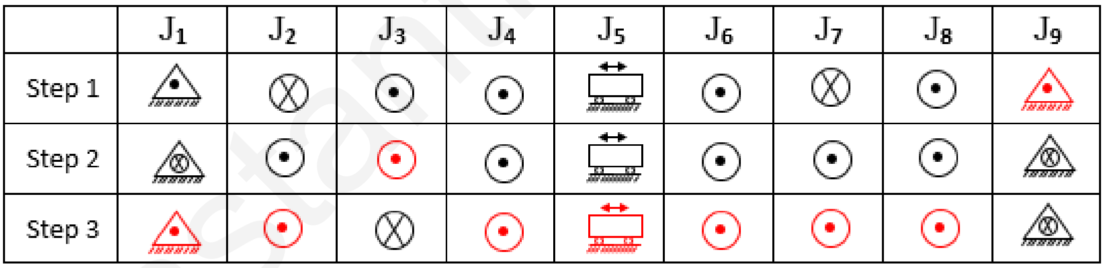

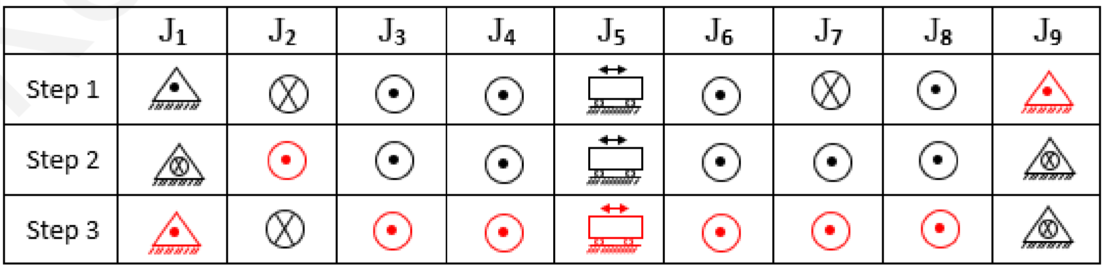

Konstantinos Petrou

Sequence 2ad (S_{2ad}):

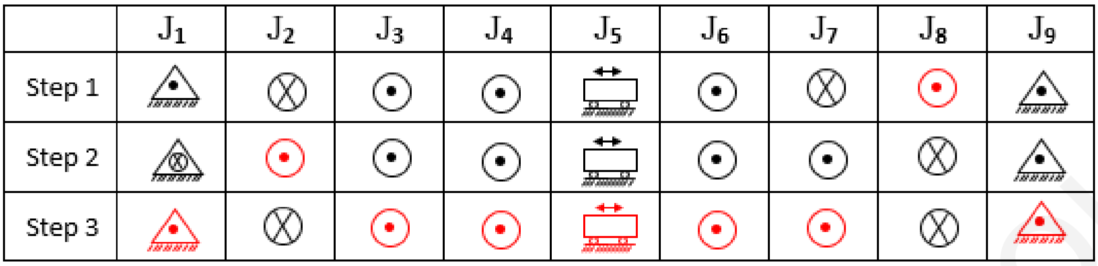

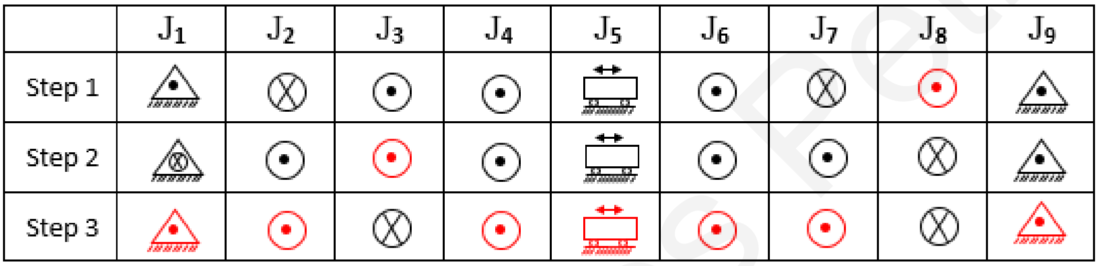

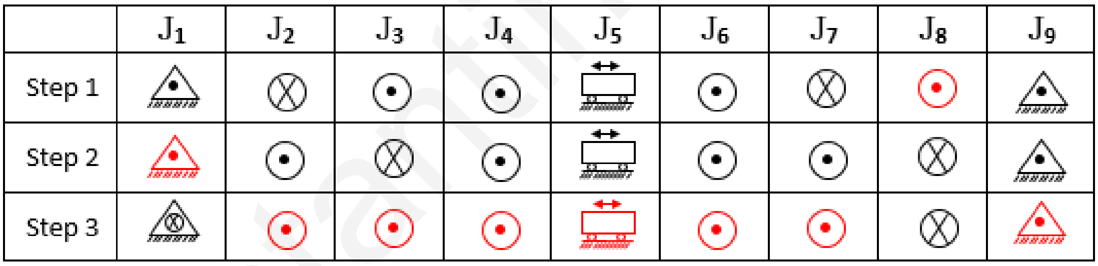

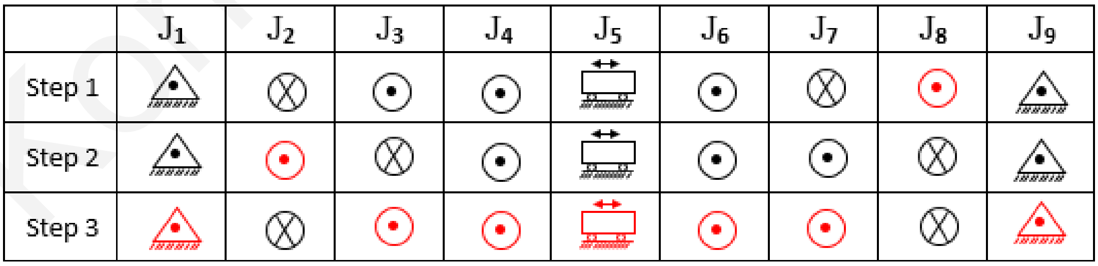

Konstantinos Petrou

Sequence 2ae (S_{2ae}):

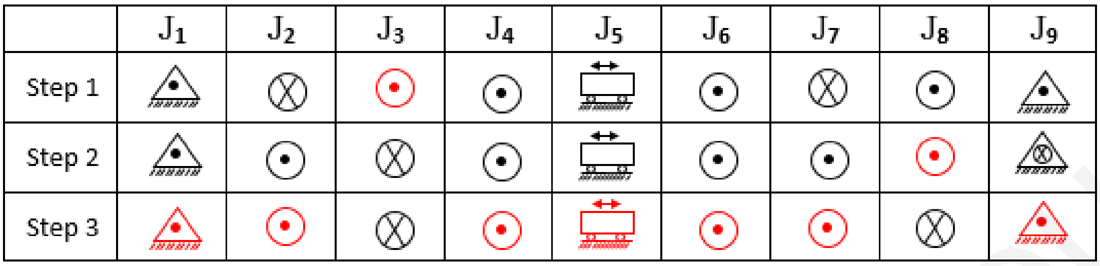

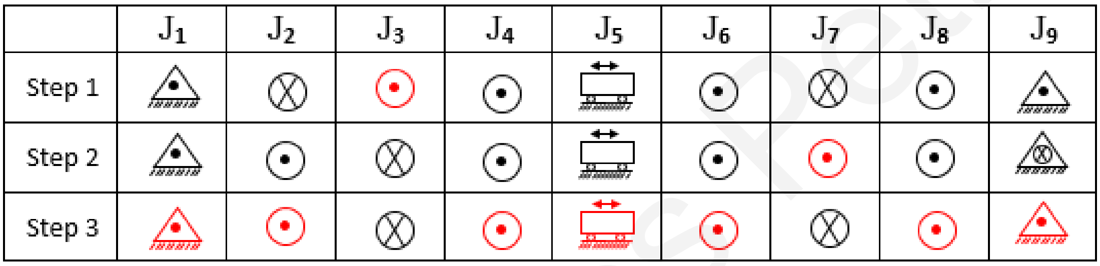

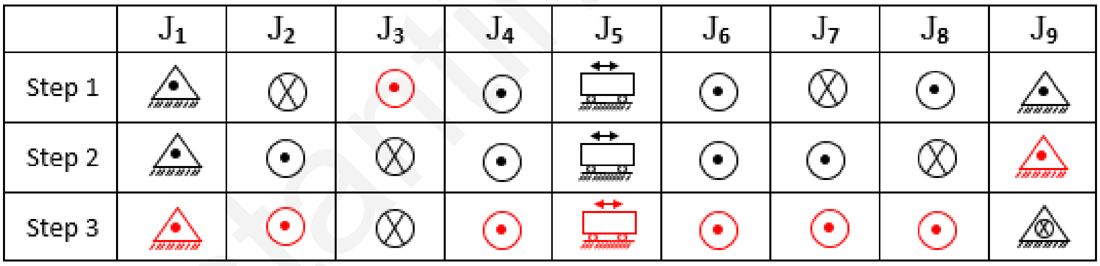

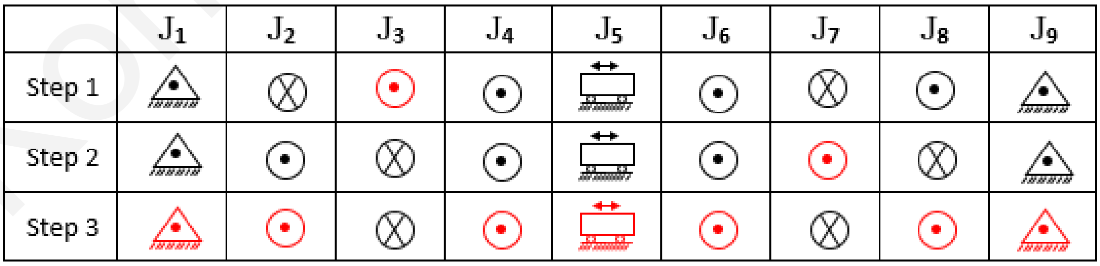

Konstantinos Petrou

Sequence 2af (S_{2af}):

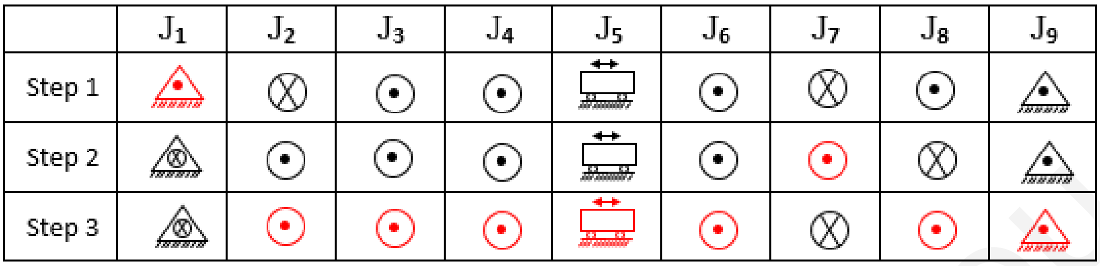

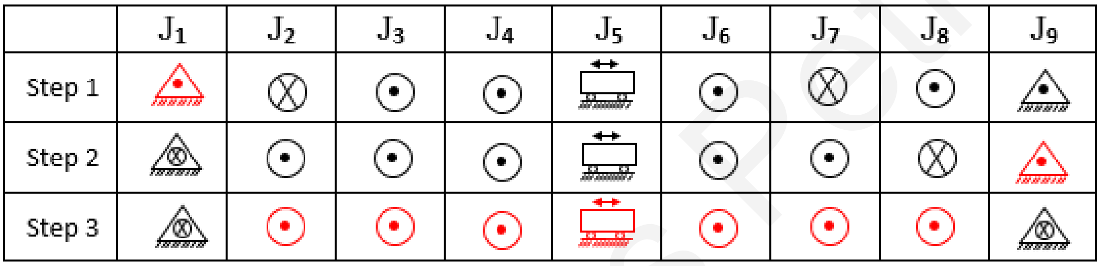

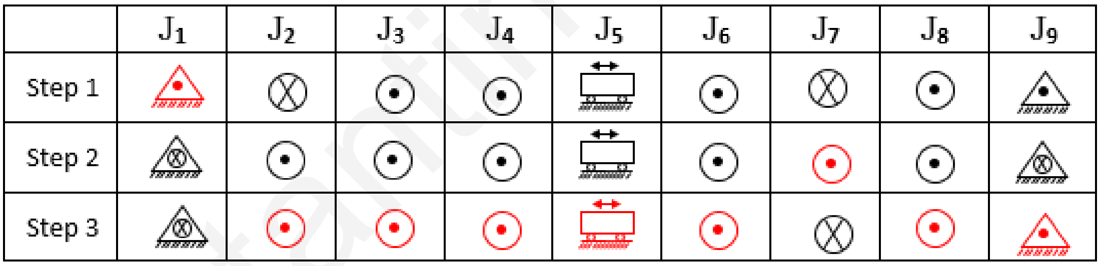

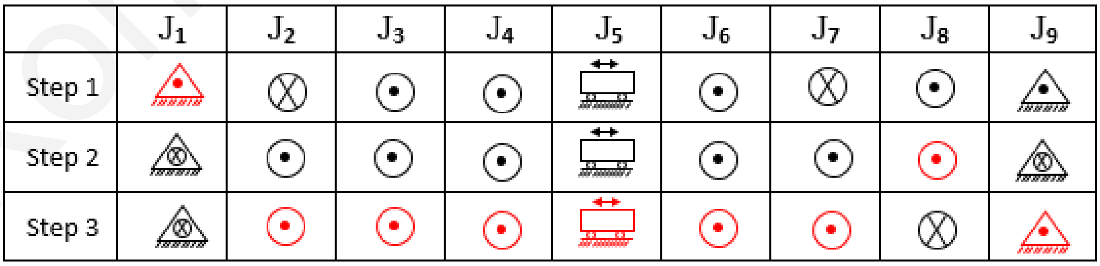

Konstantinos Petrou

Sequence 2ag (S_{2ag}):

	J_1	J_2	J_3	J_4	J_5	J_6	J_7	J_8	J_9
Step 1	△⊗	⊙	⊙	⊙	⇔	⊙	⊗	⊙	△•
Step 2	△•	⊗	⊙	⊙	⇔	⊙	⊙	⊙	△⊗
Step 3	△•	⊗	⊙	⊙	⇔	⊙	⊙	⊗	△•

	J_1	J_2	J_3	J_4	J_5	J_6	J_7	J_8	J_9
Step 1	△⊗	⊙	⊙	⊙	⇔	⊙	⊗	⊙	△•
Step 2	△•	⊗	⊙	⊙	⇔	⊙	⊙	⊙	△⊗
Step 3	△•	⊗	⊙	⊙	⇔	⊙	⊗	⊙	△•

	J_1	J_2	J_3	J_4	J_5	J_6	J_7	J_8	J_9
Step 1	△⊗	⊙	⊙	⊙	⇔	⊙	⊗	⊙	△•
Step 2	△•	⊗	⊙	⊙	⇔	⊙	⊙	⊗	△•
Step 3	△•	⊗	⊙	⊙	⇔	⊙	⊙	⊙	△⊗

	J_1	J_2	J_3	J_4	J_5	J_6	J_7	J_8	J_9
Step 1	△⊗	⊙	⊙	⊙	⇔	⊙	⊗	⊙	△•
Step 2	△•	⊗	⊙	⊙	⇔	⊙	⊙	⊗	△•
Step 3	△•	⊗	⊙	⊙	⇔	⊙	⊗	⊙	△•

Konstantinos Petrou

Sequence 2ah (S_{2ah}):

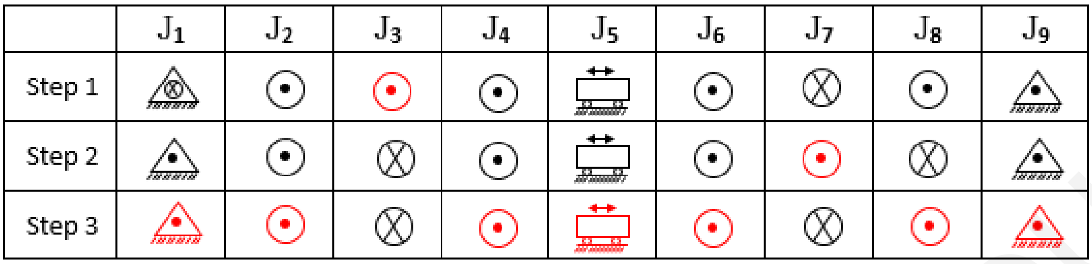

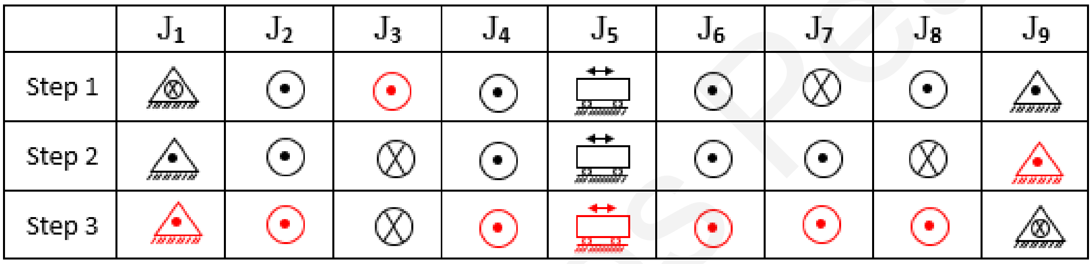

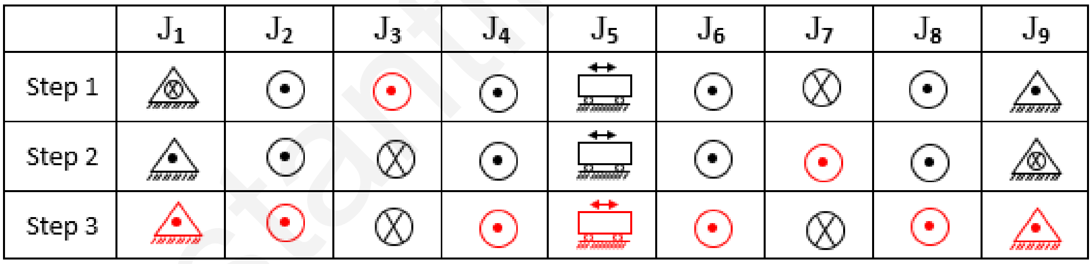

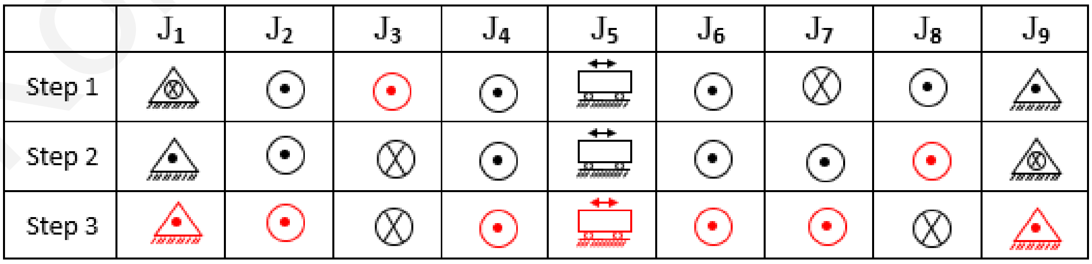

Sequence 2ai (S_{2ai}):

	J_1	J_2	J_3	J_4	J_5	J_6	J_7	J_8	J_9
Step 1	△⊗	⊙	⊙	⊙	⇄▭	⊙	⊗	⊙	△⊙
Step 2	△⊙	⊗	⊙	⊙	⇄▭	⊙	⊙	⊗	△⊙
Step 3	△⊙	⊙	⊗	⊙	⇄▭	⊙	⊙	⊗	△⊙

	J_1	J_2	J_3	J_4	J_5	J_6	J_7	J_8	J_9
Step 1	△⊗	⊙	⊙	⊙	⇄▭	⊙	⊗	⊙	△⊙
Step 2	△⊙	⊗	⊙	⊙	⇄▭	⊙	⊙	⊗	△⊙
Step 3	△⊗	⊙	⊙	⊙	⇄▭	⊙	⊙	⊗	△⊙

	J_1	J_2	J_3	J_4	J_5	J_6	J_7	J_8	J_9
Step 1	△⊗	⊙	⊙	⊙	⇄▭	⊙	⊗	⊙	△⊙
Step 2	△⊙	⊙	⊗	⊙	⇄▭	⊙	⊙	⊗	△⊙
Step 3	△⊗	⊙	⊙	⊙	⇄▭	⊙	⊙	⊗	△⊙

	J_1	J_2	J_3	J_4	J_5	J_6	J_7	J_8	J_9
Step 1	△⊗	⊙	⊙	⊙	⇄▭	⊙	⊗	⊙	△⊙
Step 2	△⊙	⊙	⊗	⊙	⇄▭	⊙	⊙	⊗	△⊙
Step 3	△⊙	⊗	⊙	⊙	⇄▭	⊙	⊙	⊗	△⊙

Konstantinos Petrou

Sequence 2aj (S_{2aj}):

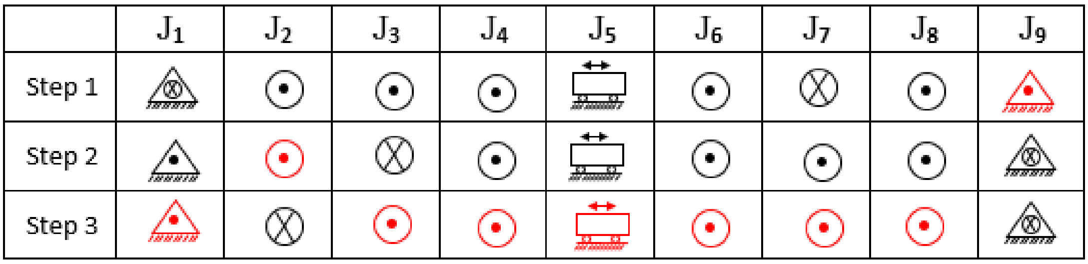

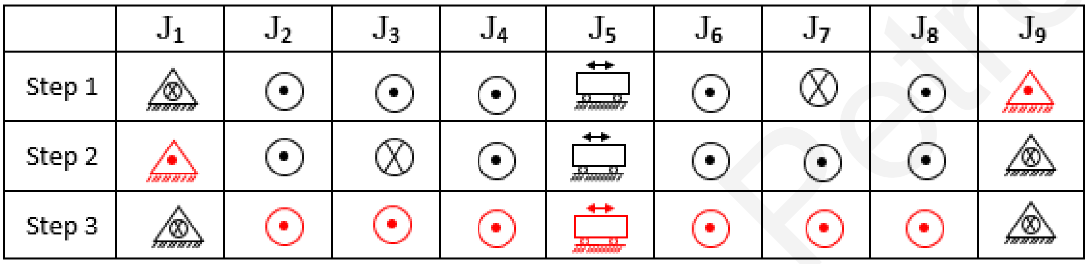

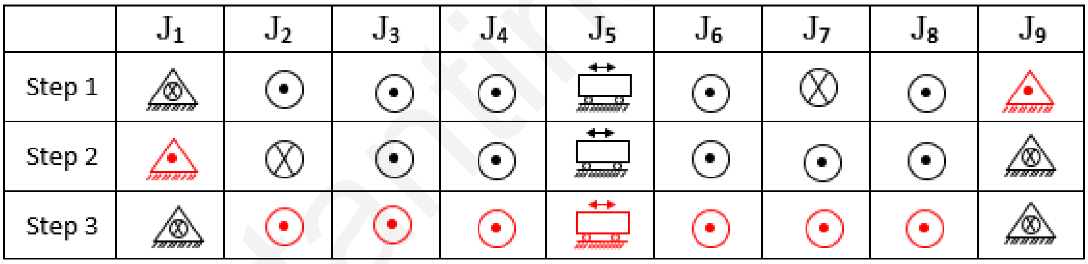

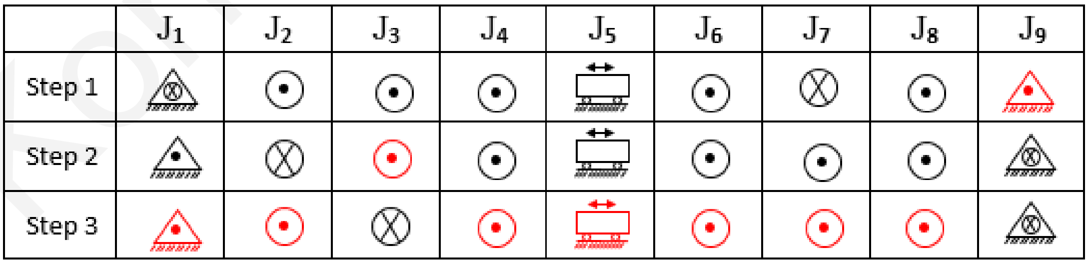

Konstantinos Petrou